CHALMERS

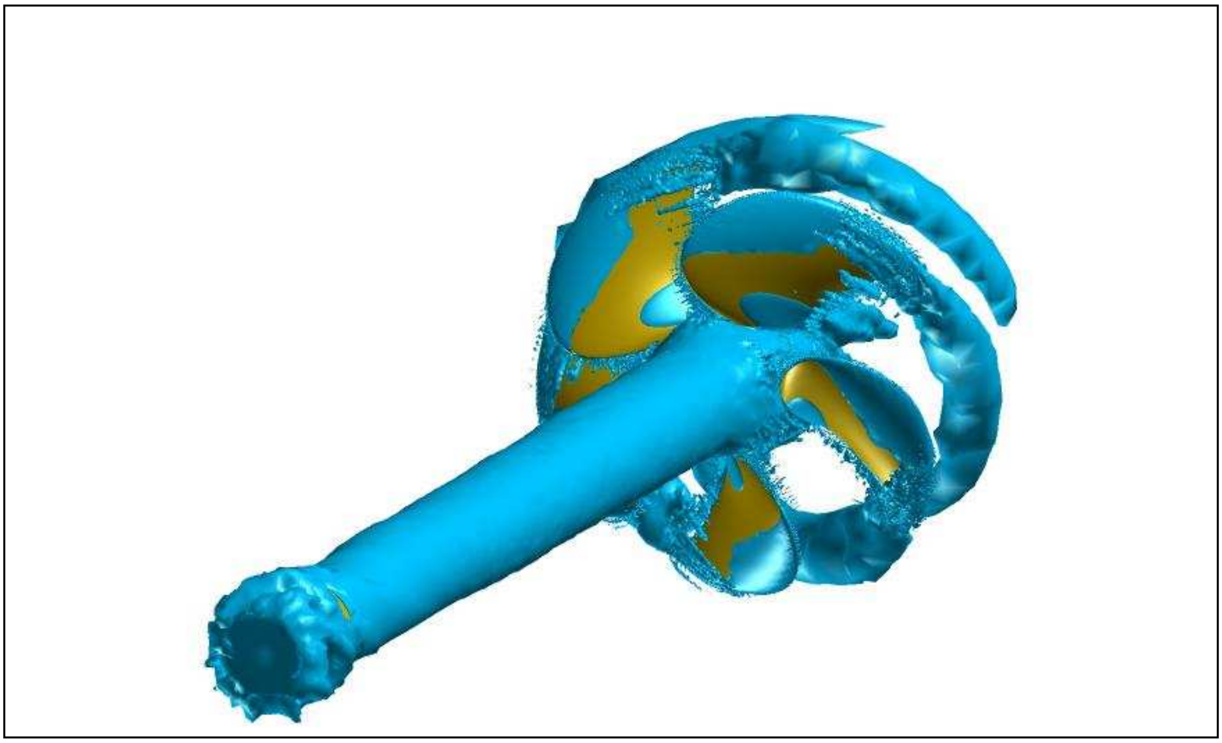

A Validation, Comparison and Automation of Different Computational Tools for Propeller Open Water Predictions

Master of Science Thesis

Olof Klerebrant Klasson

Department of Shipping and Marine Technology
Division of Sustainable Ship Propulsion
CHALMERS UNIVERSITY OF TECHNOLOGY
Göteborg, Sweden, 2011
Report No. X-11/264

A THESIS FOR THE DEGREE OF MASTER OF SCIENCE

A validation, comparison and automation of different computational tools for propeller open water predictions

Olof Klerebrant Klasson

Department of Shipping and Marine Technology
CHALMERS UNIVERSITY OF TECHNOLOGY
Göteborg, Sweden 2011

A Validation, Comparison and Automation of Different Computational Tools for Propeller Open Water Predictions

Olof Klerebrant Klasson

Report No. X-11/264

Department of Shipping and Marine Technology
Chalmers University of Technology
SE-412 96 Göteborg
Sweden
Telephone +46 (0)31-772 1000

Printed by Chalmers Reproservice
Göteborg, Sweden, 2011

A validation, comparison and automation of different computational tools for propeller open water predictions

OLOF KLEREBRANT KLASSON
Department of Shipping and Marine Technology
Chalmers University of Technology

Abstract

Open water behaviour of a propeller is an important indication of the propeller performance. This Master's Thesis report describes the procedure for computing open water characteristics using four different methods, how to measure velocity fields and how to predict cavitation for a propeller in uniform inflow. The four methods were Computational Fluid Dynamics (CFD), boundary element method, lifting line method and Wageningen Series. Further the report describes how the methods were automated in means of computing open water characteristics and how they compare to model test results. The objective with the project was to gain knowledge about when the methods are preferred to use, what limitations they have and how to minimize the work effort by means of automation of the tools. The benefit of setup automation is not solely the time savings, but also the security in standardized setup methods. This reduces the risk of setup errors in the results. Automatic post processing was developed to some extent for the tools as well.

For the project, three different propeller geometries were used; one designed to generate a tip vortex, one designed to reduce pressure pulses and one with a more conventional design. The propeller designed to generate a tip vortex was part of the SMP'11 Workshop on Cavitation and Propeller Performance. The SMP'11 Workshop was intended to give research groups the possibility to validate their computational tools against both model tests and other software, set up by different users. The workshop provided model test results of open water characteristics, velocity field measurements and cavitation patterns. These test results were predicted in this project and will also be included in the workshop. The other two propellers were used to automate the four methods and validate them against model test results.

The CFD analyses were performed with the open source CFD toolbox OpenFOAM. Steady Reynolds-Averaged Navier-Stokes (RANS) simulations with $k - \omega$ SST turbulence model and wall functions in combination with Multiple Reference Frames (MRF) were used for the CFD simulations. The grids and automatic CFD pre-processing were performed with the commercial meshing software ANSA. The boundary element method predictions and grid generation were performed in the CRS developed tool PROCAL. The lifting line method predictions were performed in an Excel workbook with macros. The Wageningen Series predictions came directly from the Wageningen polynomials. The three latter methods were automated using visual basic and Excel.

One important conclusion is that CFD gives the most accurate predictions, but requires many CPU-hours. When results are needed quickly, the boundary element method is useful and accurate enough. The lifting line method generates less accurate results than the other methods. The Wageningen Series is useful to give an indication of the predicted results validity. The automated codes save hours of work and results in consequent setups.

Keywords: *Open water characteristics; CFD; Boundary element method; Lifting line method; Wageningen Series; SMP'11 Workshop; Validation; Setup automation; Automatic post processing*

Preface

This thesis is a part of the requirements for the master's degree at Chalmers University of Technology, Göteborg, and has been carried out at Berg Propulsion Technology AB, Hönö.

I would like to acknowledge and thank my examiner, Associate Professor Rickard Bensow at the Department of Shipping and Marine Technology, and my supervisor, Ph.D. Tobias Huuva at Berg Propulsion Technology AB, for all help and support throughout the project. I would also like to show my gratitude to Magnus Pettersson at Berg Propulsion Technology AB for all help concerning both support in the use of the software and valuable theory discussions. Finally, I would like to thank Lars Lübke at SVA for the support with the SMP'11 test cases and Johan Bosschers at MARIN for all the PROCAL support.

Göteborg, June, 2011
Olof Klerebrant Klasson

Nomenclature

Glossary

Bollard pull = Low speed condition where the ship is towing
Dead top centre = The twelve O' clock position of the propeller disc
Design workbook = Excel workbook at Berg Propulsion containing the blade design
Rake = Angle that blades slant forward/aftward compared to a line perpendicular to the shaft line
Size box = Box drawn in ANSA, used to locally refine the mesh
Skew = Angle describing the asymmetry of the blade face
Thickness distribution = The thickness of the blade at different radial sections
Thrust identity = Load condition in model test stating equal Kt rather than velocity

Abbreviations

BEM = Boundary Element Method
CFD = Computational Fluid Dynamics
CP = Controllable Pitch
CPP1 = Berg propeller for a single screw vessel
CPP2 = Berg propeller for a twin screw vessel
EAR = Blade area ratio
ITTC = International Towing Tank Conferrence
LDV = Laser Doppler Velocimetry
LE = Leading Edge; foremost part of the blade
LEs = Leading Edge spacing
LLM = Lifting Line Method
MRF = Multiple Reference Frames
OW = Open Water
P/D = Non-dimensional Pitch
P0.7/D = Non-dimensional pitch at R0.7
PHIW = Wake panel distribution
PID = Property Identification
r/R = non-dimensional propeller radius
R0.7 = Propeller radial section at 0.7*propeller radius
RANS = Reynolds-Averaged Navier-Stokes
RPM = Revolutions Per Minute
RS = Root spacing
SMP'11 = Workshop for propellers, held in Potsdam
SW = Solid Works

TC = Tip chord fraction
TE = Trailing Edge; aftmost part of the blade
TEs = Trailing Edge spacing
VBA = Visual Basic
WS = Wageningen Series

Roman letters

c = Chord length
$c_{0.75}$ = Chord length at R0.75
C_D = Drag coefficient
C_L = Lift coefficient
D = Propeller diameter
F_x = Radial axial force
I = Turbulence intensity
J = Advance ratio
$J\ \eta_{Max}$ = Advance ratio at maximum efficiency
k = turbulent kinetic energy
k_p = Full scale propeller surface roughness
K_Q = Dimensionless torque
K_T = Dimensionless thrust
n = Revolutions per second
P = Pressure
Q = Torque
r = Radial coordinate
R = Propeller radius
R_{nco} = Local Reynolds number based on chord length
T = Thrust
t = blade thickness
U = Instantaneous velocity
$\bar{U}$ = Averaged velocity
u = Fluctuating velocity
w = Effective wake fraction
V_A = Advance velocity
V_{ref} = Reference velocity
x = Distance
y^+ = Dimensionless wall distance
Z = Number of blades

Contents

1 Introduction

1.1 Background

In propeller design there are a variety of tools to be used for early predictions of the performance. At Berg Propulsion AB (Berg) there are several alternatives among these tools, and it might be difficult to know when to use which tool. Some of the tools also have extensive setup times. The limitations of the tools are to some extent investigated, but no comparison between the tools has been performed at Berg. A better understanding of which open water calculation tool that has to be used for a given situation is therefore useful.

The accuracy of numerical tools such as the boundary element method and Reynolds-Averaged Navier-Stokes (RANS) methods are not solely dependent on the tools capabilities itself, but also on how they are set up by the user. There are an abundance of tools that performs the same calculations with only slight differences in layout and user friendliness. The SMP'11 Workshop was intended to give research groups the possibility to validate their computational tools against both model tests and other software, setup by different users. This is a very valuable reference when studying the accuracy of the computational tools.

The setup time for different tools might be very long. One example is CFD, which might have several days, and even weeks, as setup time. The result from a computational tool might also, as stated, depend on the user. A procedure that not only reduces the setup time significantly, but also standardizes the methods and rules out setup errors is for this reason desirable.

1.2 Objective with the Investigation

The objective of the thesis is to investigate and validate the computational tools for open water propeller predictions at hand at Berg and make a user environment that speed up pre- and post-processing for the tools.

1.3 Limitations

The tools to automate and compare are only the Wageningen Propeller Series Program [1], the boundary element method PROCAL [2], the lifting line method LiftLine [3] and the open source Computational Fluid Dynamics (CFD) toolbox OpenFOAM [4]. The tools will be compared to each other considering solely open water characteristics of propellers. PROCAL's ability to predict open water cavitation and OpenFOAM's ability to predict velocity fields forward the propeller disc will be compared to model test results.

The automation regards pre-processing and post processing for open water characteristics predictions. By post-processing, the generation of open water diagrams is regarded. Automatic pre-processing is intended as a way to from either a few user questions or by taking data directly from the blade design location, get a complete open water setup.

For the CFD, the analysis will be of steady, non-periodic RANS-type without resolving the wall. The choice of non-periodic boundary condition depended on that the periodic boundary condition was not applicable for ANSA [12] interacting with OpenFoam when the project was performed.

The model test results are seen as the reality in this project. It is known that this might be untrue, but it is the best data to use as reference.

1.4 Outline and Overall Methodology

To complete the objective, the methodology of this thesis project could be summarized in seven steps;

1. Explore the functionality of the four open water prediction tools
2. Find a standardized method that generate reliable results for each tool
3. Compare the results from each tool between the other tools and to model tests to see if the methodologies are correct
4. Automate each tool for open water characteristics predictions
5. Validate the automation
6. Compare all the open water results gained from the predictions to model tests for a complete benchmark of the tools
7. Develop recommendations based on the results from step 6

To understand how to use the tools and how to perform the setups, a literature study had to be performed. This study was partly from program theory manuals and partly from relevant theory literature.

Three propeller geometries were provided; one propeller for the SMP’11 Workshop (SMP’11), one propeller for a single screw vessel (CPP1) and one propeller for a twin screw vessel (CPP2). The SMP’11 propeller was used to complete step 1-3 above. This was since SMP’11 provided test cases for predictions of open water characteristics, open water velocity field measurements and open water cavitation measurements. These test cases were enough to cover the exploration of the program functionality. CPP1 was used to develop the open water characteristics automation scripts, constantly applying the methods that were found reliable when analyzing the SMP’11 test cases. CPP2 was used to validate the scripts.

The outline of this thesis is based on the working order described above. It is started with a theory section (section 2) to describe the theory behind the computational tools and the setup methodologies. After this a summary of the used propeller geometries is presented in the geometries and setup section (section 0). This is followed by one proceedings section for each of the methods (section 4-7) to avoid nomenclature related confusions. After this a combined result and discussion section (section 8) follows that compares all the results to find the final recommendations that are presented in the conclusions section (section 9). The subsections of section 8 are divided into results of each test case to attain comprehensive comparisons.

2 Theory

To clarify the nomenclature and level of approximation of the compared methods, a theory review is introduced in this chapter.

2.1 CFD Methods

CFD is the analysis of systems with fluid flow, heat transfer and similar phenomena using simulation by computer. The theory behind steady RANS with a low Reynolds number turbulence model, wall functions and multiple reference frames to model rotation will be reviewed in this section.

2.1.1 RANS equations

The propeller is a hydrodynamic construction. Water is an incompressible and a Newtonian fluid, hence the incompressible Navier-Stokes equations apply, see eq. 2.1. The continuity equation applies as well, see eq. 2.2.

$$\frac{\partial}{\partial x_j}\left(U_j U_i\right) = -\frac{1}{\rho}\frac{\partial P}{\partial x_i} + \nu\frac{\partial^2 U_i}{\partial x_j \partial x_j} \tag{2.1}$$

$$\frac{\partial U_j}{\partial x_j} = 0 \tag{2.2}$$

This set of equations requires extreme computer power to solve. Since the flow is turbulent, it is preferable to decompose the pressure and velocities into a mean and a fluctuating part, i.e. as in eq. 2.3. This is known as Reynolds decomposition.

$$\begin{aligned} U_i &= \overline{U}_i + u_i \\ P &= \overline{P} + p \end{aligned} \tag{2.3}$$

By inserting eq. 2.3 into eq. 2.1 and 2.2, the Reynolds-Averaged Navier-Stokes and continuity equation are obtained, see eq. 2.4 and 2.5. A closure problem appears; there are four equations and ten unknown variables. [5]

$$\frac{\partial}{\partial x_j}\left(\overline{U}_i \overline{U}_j\right) = -\frac{1}{\rho}\frac{\partial \overline{P}}{\partial x_i} + \nu\frac{\partial^2 U_i}{\partial x_j \partial x_j} - \frac{\partial \overline{u_i u_j}}{\partial x_j} \tag{2.4}$$

$$\frac{\partial \overline{U}_j}{\partial x_j} = 0 \tag{2.5}$$

2.1.2 Discretization Schemes

When an equation is discretized, a continuous differential equation is calculated into an algebraic discrete equation. In CFD, the domain can be divided into finite volume elements, each with known node, face and neighbour locations, see Fig. 2.1.

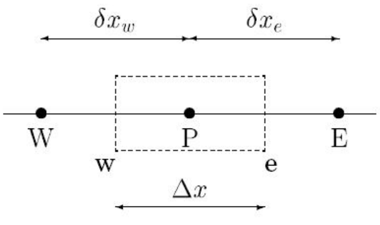

Fig. 2.1: A finite volume, where capital letters represent nodes, small letters represents faces, e stands for east, w stands for west and p stands for the current cell [6]

If one finite volume is studied, the continuous equation is integrated from face to face in each direction. This gives discretized equations telling how the current node is related to the cell faces using the studied differential equation. Since the studied quantity was integrated from face to face, the quantities are known at the faces.

The next step is to relate the nodes to the faces. This is done using a discretization scheme. One example is to assume that the faces are connected by a straight line and linear interpolation can be used to determine the quantity on the node lying between the faces. This is known as the central differencing scheme. If the discretized equation is Taylor expanded and compared to the continuous differential equation, it can be shown that terms of order x^2 will remain. This is known as second order accuracy. Since x is the cell length, this means that the error will be reduced by a factor 4 if the cell length is halved.

There are some problems with the central differencing scheme; it is neither bounded, nor transportive. If a scheme is conservative, it is meant that the flux leaving the cell should be the same as the flux entering the neighbouring cell. This is fulfilled by the central differencing scheme. A bounded scheme fulfils the requirement that the value at a face cannot be larger or smaller than the cell values used to compute the face value. With a transportive scheme it is meant that the information is transported in the correct way. Velocity, e.g., is transported from upstream to downstream. This means that the current cell should depend more on the cells upstream than the cells downstream to be transportive.

The first order upwind scheme takes the value from the node closest to west if the velocity in direction west to east is larger than zero. If the velocity is in the other direction, it takes the value from its eastern node. This scheme fulfils all the criterions; it is conservative, bounded and transportive. The drawback is that it is inaccurate due to the fact that it is only first order accurate. Since it is bounded, it is a very stable scheme.

To solve the problem with the inaccuracy of the first order upwind scheme, a second order upwind scheme could be used. It uses two nodes upstream and assumes that the gradient between them is the same as the gradient between the current face and the upstream neighbouring node. The scheme is transportive and conservative, but it is not bounded, making it less stable than the first order upwind scheme. On the other hand it is second order accurate. [6]

2.1.3 Pressure Velocity Coupling

If the pressure gradient in the Navier-Stokes equations is discretized over a control volume, the discretized equation will be computed without respect to the pressure in the current node. This results in a so called checker-board pressure field. It means that the equation is solved, but the result is a highly oscillating pressure field. This can be solved using Rhie-Chow interpolation and a correction algorithm such as SIMPLE.

The procedure of the SIMPLE algorithm is to:

(1) Guess the pressure
(2) Solve the Navier-Stokes equations using the old pressure
(3) Solve the pressure correction equation
(4) Correct the velocities and the pressures based on the computed pressure correction
(5) Repeat point (2)-(4) until convergence is reached

The pressure correction equation comes from discretizing the continuity equation and rewriting it so it contains one old velocity term and one correction term for each velocity direction and a term representing the continuity error. After this it is combined with the discretized Navier-Stokes equation so that a direct relation between a velocity correction and a pressure correction is achieved. When the continuity error in the continuity equation vanishes, the pressure correction is converged. [6] There are other ways to couple pressure and velocity, such as PISO. PISO is similar to SIMPLE, but has one further corrector step. [7]

2.1.4 Multiple Reference Frames

Multiple reference frames can be used to model rotating boundaries in a flow, such as a propeller. To derive the equations used for solving with multiple frames of reference in OpenFOAM, the steady Navier Stokes equations for incompressible flow are used. First the acceleration term of the rotating frame (Ω) is studied. It is related to the position vector, r. Note that cylindrical coordinates are used. After this the incompressible Navier-Stokes equations of the inertial frame is introduced. To get the relative velocity, the acceleration term is taken into account for the incompressible Navier Stokes equations. The equation for absolute velocity in the rotating frame comes from coupling the rotating frame with the inertial frame so that the convected velocity in the rotating frame is the velocity in the inertial frame. For the full derivation, see [8]

The incompressible Navier Stokes equations with multiple frames of reference can be written as eq. 2.6-2.8. The inertial frame of reference's absolute velocity is described by eq. 2.6. The relative and absolute velocities of the rotating frame of reference are described by eq. 2.7 and 2.8 respectively. Since the indexes might be confusing using tensor notation, the equations are written on vector notation.

$$\begin{cases} \nabla \cdot \left(\vec{U}_I \text{ x } \vec{U}_I\right) = -\nabla\left(\frac{p}{\rho}\right) + \nu\nabla \cdot \nabla\left(\vec{U}_I\right) \\ \nabla \cdot \vec{U}_I = 0 \end{cases} \tag{2.6}$$

$$\begin{cases} \nabla \cdot \left(\overrightarrow{U_R} \text{ x } \vec{U}_R\right) + 2\Omega \text{ x } \vec{U}_R + \Omega \text{ x } \Omega \text{ x } \vec{r} = -\nabla\left(\frac{p}{\rho}\right) + \nu\nabla \cdot \nabla\left(\vec{U}_R\right) \\ \nabla \cdot \vec{U}_R = 0 \end{cases} \tag{2.7}$$

$$\begin{cases} \nabla \cdot \left(\vec{U}_R \text{ x } \vec{U}_I\right) + \Omega \text{ x } \vec{U}_I = -\nabla\left(\frac{p}{\rho}\right) + \nu\nabla \cdot \nabla\left(\vec{U}_I\right) \\ \nabla \cdot \vec{U}_I = 0 \end{cases} \tag{2.8}$$

Where notation I=Inertial; notation R=rotating and U is the velocity vector in Cartesian coordinates. [8]

2.1.5 Turbulence Models

With the RANS equations there is still a closure problem. This is solved using a turbulence model. Turbulence is irregular, diffusive, three dimensional and dissipative. The better the turbulence model can represent these statements about turbulence, the more accurate it is. A common way to make a turbulence model is to divide the turbulence into one turbulent kinetic energy (k) and one dissipative (ϵ) part. If eq. 2.4 is subtracted from eq. 2.1 and the result is multiplied by u_i and time averaged, the exact k-equation is attained. An exact equation for ϵ can also be derived from the Navier-Stokes equations.

The number of unknown terms in both the exact k and ϵ model are large. Therefore the equations are modelled using physical reasoning. The result from this is the so called k-ϵ

model. [5] This model is unsatisfactory when predicting near wall behaviour, but good when predicting the free stream. To improve the near wall behaviour, the k-ω model could be applied instead. The specific dissipation (ω) is an equation derived from the ϵ-equation. It behaves more similar to the exact dissipation term near the wall. The k-ω SST-model is a hybrid between the k-ϵ and the k-ω model. It is using blending functions to be able to use the k-ω model near the wall and the k-ϵ in the free stream and to get a smooth transition between them. The energy and dissipation equation of k-ω SST can be seen in eq. 2.9 and 2.10. [7]

$$\frac{\partial u_j k}{\partial x_j} = \frac{p}{\rho} - \beta^* \omega k + \frac{\partial}{\partial x_j}\left[(\nu + \sigma_k \nu_t)\frac{\partial k}{\partial x_j}\right] \qquad (2.9)$$

$$\begin{aligned}\frac{\partial u_j \omega}{\partial x_j} = \frac{\gamma}{\mu_t \rho} p - \beta \omega^2 + \frac{\partial}{\partial x_j}\left[(\nu + \sigma_\omega \nu_t)\frac{\partial \omega}{\partial x_j}\right] \\ + 2(1 - F_1)\frac{\sigma}{\omega}\frac{\partial k}{\partial x_j}\frac{\partial \omega}{\partial x_j}\end{aligned} \qquad (2.10)$$

Where u=the velocity and ν_t*= the turbulent viscosity.* β^*, β, σ *and* σ_k *are constants.*

2.1.6 Wall Functions

The wall was modelled with wall functions to reduce the need for high mesh resolution near the wall. To apply wall functions means that the flow near the wall is assumed to behave as a fully developed turbulent boundary layer. The first cells are computed using the wall functions and are then inserted as boundary conditions into the cells computed by the RANS equations. The last cell of the wall functions should typically be in the interval $30 \leq y{+} \leq 100$ to get reliable results. The dissipation and production term are much larger than the other terms in the log-law region. Using analytical and empirical equations from the log law, an equation for the turbulent viscosity can be written, see eq. 2.11.[5]

$$\begin{cases} \nu_t = \dfrac{u_* \eta \kappa}{\ln(E\eta^+)} \\ \eta^+ = \dfrac{u_* \eta}{\nu} \end{cases} \qquad (2.11)$$

Where η *= the normal distance to the wall;* u_**=the friction velocity; E=constant and* κ*=the turbulent wave number.*

2.2 Boundary Element Method

The panel method, or boundary element method, is using the exact formulation of the potential flow problem on propellers. The direct formulation is used in PROCAL and will be described in this section. The direct formulation solves directly for the potential and then determines the velocities.

The Morino formulation, which is a direct formulation, is used in PROCAL. Assuming irrotational and incompressible flow, the velocity can be expressed as a potential, see eq. 2.12.

$$V = \nabla \phi \qquad (2.12)$$

The potential can be written as the sum of the potential of the undisturbed flow (φ_∞) and the disturbance potential to be solved (φ). By applying Green's second theorem, the 3D computational domain will be reduced to the unknowns at the boundaries only. The potential at the boundaries can be written as in eq. 2.13.

$$\varphi = \frac{1}{2\pi}\int_S \left[\varphi_q \frac{\partial}{\partial n_q}\left(\frac{1}{R_{p,q}}\right) - \frac{\partial \varphi_q}{\partial n_q}\frac{1}{R_{p,q}}\right] dS \qquad (2.13)$$

Where n=the normal to the surface; R= the vector connecting a point on the surface and the point p and p=the collocation point

Here, the potential interior of the surface S has the value zero. On the surface, the zero penetration boundary condition gives the source strengths, see eq. 2.14.

$$\sigma_q = \frac{\partial \varphi}{\partial n_q} = -V_\infty n_q \qquad (2.14)$$

Where σ=the monopole strength and V_∞=the undisturbed velocity

Blades, hub and part of the wake for each blade are represented by dipole panels. The Kutta condition makes the pressure difference between the face and the back go to zero. This condition couples the wake to the propeller. The condition is non-linear and therefore requires an iterative solution. A Jacobian disturbance value is used as a relaxation factor for the Kutta iterations. [9]

The boundary is divided into structured, quadrilateral panels. The sources and potentials are assumed to be constant over each panel. The Bernoulli equation is used to compute the pressure over each panel as in eq. 2.15. [10] [11]

$$p = p_\infty + 0.5\rho(|U_\infty + \omega \times x|^2 - |V|^2) - \rho\frac{\partial \varphi}{\partial t} + \rho g h \qquad (2.15)$$

2.3 Mesh Types

The boundary element method and the CFD method need to be meshed in proper ways to get reliable and converged results. Some grid generation theory is described below.

2.3.1 CFD Method

CFD is a very grid dependent technique. The largest errors occur where the largest gradients are. For this reason, the resolution should be increased in such regions. Only a restricted amount of cells can be used due to restrictions in computational power. Therefore it is beneficial to have a denser grid where e.g. the curvature of the surface is high and having larger cells closer to the middle of the surface. In ANSA there is a surface mesh type called CFD. This mesh becomes dense at high curvature and boundaries and coarser close to the middle of the surface. The mesh is consisting of triads, making the geometrical description good, but leads inevitable to triads and pyramids before the volume mesh can be hexahedral.

To mesh a complex geometry, such as a propeller, a structured grid is hard to apply. A structured grid has better numerical properties than an unstructured grid. An unstructured grid generally requires less time to apply than a structured grid. Unstructured grids are built from polyhedrons in the volume and commonly triads on the surface. Close to the wall, very large gradients occur. In this case, the optimal would be to have cells at 90° angles to the wall with equal edge lengths.[13] A mesh type that fulfils this criterion is the prism layer. A prism layer has a face almost identical to the surface mesh below and grows almost solely in the orthogonal direction to the wall. [14]

The structured mesh consists of hexahedrons in the volume and quadrilaterals on the surface. As said, these have imperious numerical properties compared to the unstructured elements and should therefore be used when possible. In ANSA there is a volume mesh type called hexa-interior. It uses as few tetrahedrons and pyramids as possible to quickly evolve into a fully hexahedral mesh. This gives a good combination of numerical stability and geometrical representation. [14]

To fit the geometry, the elements need to be squeezed in different ways. This might affect the results. High skewness of the cells might lead to instabilities and lower accuracy. In Fig. 2.2 the fluent definition of skew is shown

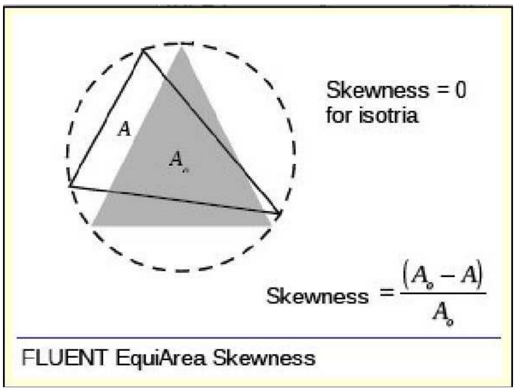

Fig. 2.2: The definition of skewness used for quality checking [14]

The numerical error will increase and convergence will be harder to achieve if adjacent cells are very different in size or if the ratio between cell height and cell area is high. This is known as aspect ratio. [13] There are an abundance of quality criterions for the mesh, but these two mentioned problems are the ones that have been considered extra carefully in this thesis work.

2.3.2 Boundary Element Method

For the boundary element method, a structured quadrilateral mesh is needed. The parameters for the user to change are usually on the surface mesh of the blade in PROCAL. The hub mesh may be changed as well, but this has small effect on the results.

The panels leading edge to trailing edge determine how many panels that should be placed in chord wise direction on each of the suction and pressure side of the blade. The panels root to tip determines the same, but in radial direction instead, see Fig. 2.3

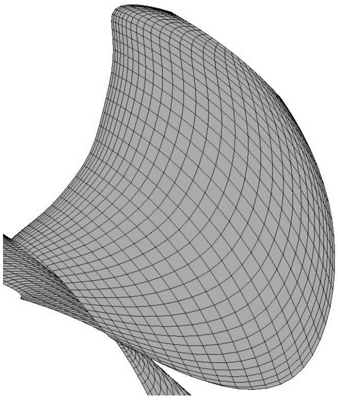

Fig. 2.3: The panelling leading edge to trailing edge and root to tip in PROCAL

The leading edge spacing determines the element length of the first panel at leading edge in chord wise direction. The trailing edge spacing is the same, but for the first panel at trailing edge, see Fig. 2.4

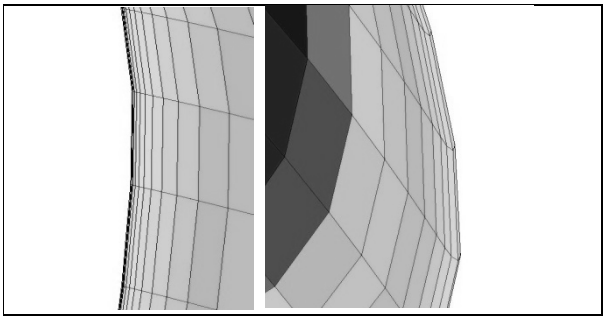

Fig. 2.4: The trailing edge spacing to the left and the leading edge spacing to the right, exaggerated to visualize the effect.

The tip spacing determines the first element length at the tip in radial direction, see Fig. 2.5. The root spacing is the same, but for the first panel at the root, see Fig. 2.6.

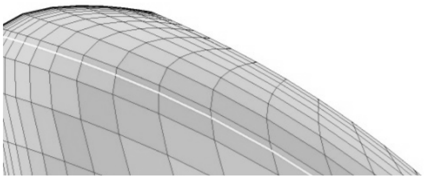

Fig. 2.5: PROCAL tip spacing, exaggerated to visualize the effect

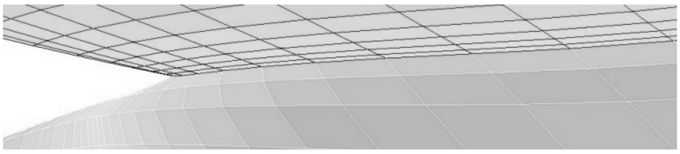

Fig. 2.6: PROCAL root spacing, exaggerated to visualize the effect

The two additional options to get good convergence and smooth reliable pressure distributions are the tip chord fraction and the hub smoothening. The tip chord fraction uses the fact that the tip length at the last radial section is finite. This allows the user to increase the chord fraction as a percentage of the length of the radial section before the tip section. The effect of changing the tip chord fraction is to reduce the skewness of the last element at trailing edge, see Fig. 2.7. The hub smoothening should be performed to avoid overlapping panels near leading and trailing edges. This is performed preferably using Thomas Middlecoff control functions.[15]

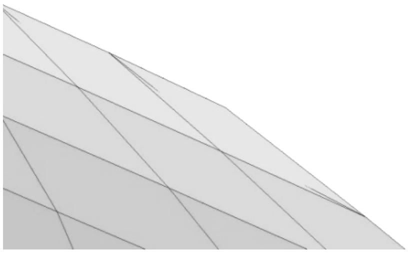

Fig. 2.7: Last trailing edge element, placed in the top right corner.

These are the parameters that are changed by the user. Some have more influence on the results and the convergence than the others. Gridding guidelines found by the developers of PROCAL and Lloyd's Registry of Shipping are presented below.

The number of panels should be set in accordance with the skew angle of the blade. Table 2.1 shows how the panel distribution should be.

Table 2.1: The panelling depending on skew as recommended by Lloyd's Registry of Shipping. [28]

Skew	Panels LE to TE*root to tip
0	20 x 20
15	25 x 25
30	30 x 30
45	35 x 35
50	40 x 40

The leading edge spacing (LEs) is also determined based on the skew angle of the blade. If the skew is larger than 35°, LEs should be 0.001. LEs should be 0.004 if the skew is smaller than 25°. Otherwise, the LEs should be 0.003.

Trailing edge spacing (TEs) is determined based on the skew angle in degrees and leading edge spacing, see eq. 2.16.

$$TEs = Skew * LEs * 0.15 \qquad (2.16)$$

The root spacing (RS) has upper and lower values, yielding an interval. The interval is determined based on TEs and LEs, see eq. 2.17. The value should preferably be as close to the minimum value as possible.

$$\frac{TEs + LEs}{2} \leq RS \leq TEs \qquad (2.17)$$

The tip spacing (TS) is determined from LEs, propeller diameter (D) hub ratio ($\frac{d_h}{D}$) panels root to tip and tip chord fraction (TC). Again an interval is prescribed, see eq. 2.18.

$$LEs * D\frac{d_h}{D} * TC \leq TS \leq \frac{D * \frac{d_h}{D} * TC}{\frac{D}{2} * panels\ LE\ to\ TE} \qquad (2.18)$$

Lloyds Registry recommends tip spacing in the interval $0.1 \leq TS \leq 0.2$, but this interval might be too narrow. The goal when meshing is to get the mesh as orthogonal as possible. Following these recommendations gives a good starting estimation of an orthogonal mesh. [16]

2.4 Lifting-line Theory

The lifting-line methods are common in propeller design as a first design step. They are then used to find an optimum geometric radial distribution of the propeller with respect to efficiency. Lifting-line methods are based on lifting-line theory, which will be explained below.

Assume that a foil has a line of vortices, see Fig. 2.8.

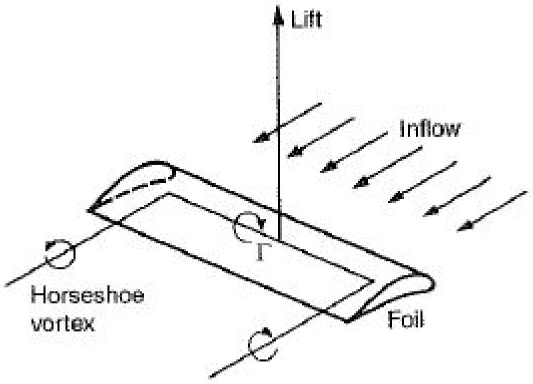

Fig. 2.8: A foil with a line of vortices from an inflow. [9]

These vortices create a lifting force perpendicular to the inflow velocity. Adapting Helmholtz's first and second law, i.e.

(1) The strength of a vortex line is constant along its length
(2) A Vortex line must be closed; it cannot end in the fluid

leads to the bending of the vortex line at the end of the foil. The vortex lines are closed again far downstream, in this context at infinity, resulting in an infinitely long horseshoe vortex line. In Fig. 2.9, one can see the vortex line following the foil, called "bound vortex". Together with this bound vortex there are vortex lines known as trailing vortices, which shapes the imaginary infinite horse shoe.

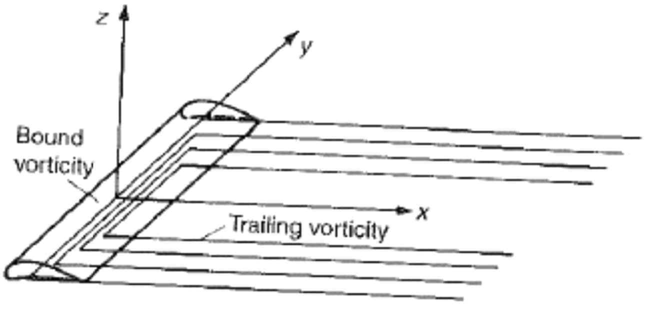

Fig. 2.9: The bound and trailing vorticity for a foil. [9]

Since the lift isn’t constant over the whole foil, the constant lift is divided into discrete piecewise constant vortex segments. Summing these vortex segments will form a lifting-line of varying vorticity. These vortex segments will now be referred to as elements (to keep the analogy in accordance with the panel and CFD methods).

The vortex strengths of the elements are determined at a number of collocation points, through which there is no flow. There will be one collocation point for each element so that the result is a linear system of equations that can be solved numerically. When the vortex strengths are determined, the velocities and pressures can be evaluated everywhere.

For a propeller, the blades are represented by one lifting line for each blade. The lifting line extends from the hub to the tip and ends with the horseshoe shape by trailing vortices. One major concern for the lifting-line methods is that it is unclear how the blade should end at the hub. It is usual to use the “hub less propeller assumption”, which means that the hub is neglected and that the vortices goes to zero at the tip. Usually the lifting-line methods result in unrealistic results near the surface of the hub and the blades. This is often corrected after the computations in the programs.

The benefit of the lifting line method is that it is well known and thereby validated to a large extent. Its limitations are well known and it takes rotative losses into account. The largest drawbacks are that it doesn’t yield the complete propeller geometry and has problems with high skew. [9]

2.5 The Wageningen B-Series

The Wageningen B-Series is a large series of model tested propellers with varying blade area ratio, pitch, number of blades and advance ratio. The propellers are based on designs that have been found effective. The series consists of about 130 propellers. All tests have been performed with a local Reynolds number at 0.75R of 2 million. Regression polynomials for K_T and K_Q has been derived for the four and five bladed propellers in the series. The regression polynomials, usually referred to as the Wageningen polynomials, are functions of advance ratio, pitch, blade area ratio and number of blades.

The B-Series is intended to use for predictions of open water characteristics. Rake, blade contour and thickness distribution has small effect on the performance characteristics. It mostly affects the cavitational behaviour. Therefore the tests are made as functions of blade area ratio, pitch and number of blades, which have major importance on the performance characteristics. The skew affects the radial loading distribution and thereby the efficiency. For this reason the B-Series has a small amount of skew. To conclude it could be said that the geometries in the Wageningen B-Series have reasonable cavitation performance, but far from optimized in this respect. On the other hand, the propellers of the series have very good open water performance. All the propellers have a hub ratio of 18%. [17]

2.6 The Open Water Test

The open water test is performed with the model scale propeller working in a uniform inflow. This could be done in a towing tank or in a cavitation tunnel. The test is usually performed altering the advance velocity (V_A) for a fix number of revolutions per second (n). The propeller thrust (T) and the propeller torque (Q) is measured during the test.

The fix RPM is altered to get the open water test at different Reynolds Numbers. The RPM must be sufficiently high to overcome the viscous effects when scaling. To get the same conditions in full scale as in model scale, the relationship between V_A and the velocity in tangential direction, yielding an indication of the angle of attack for the blade profiles, must be the same. This relationship is known as the advance ratio (J) and is defined as in eq. 2.19

$$J = \frac{V_A}{nD} \tag{2.19}$$

Where D=the propeller diameter

The non-dimensional quantities K_T, K_Q and $\eta_o$are defined as in eq. 2.20-2.22

$$K_T = \frac{T}{\rho n^2 D^5} \tag{2.20}$$

$$K_Q = \frac{Q}{\rho n^2 D^5} \tag{2.21}$$

$$\eta_o = \frac{J K_T}{2\pi K_Q} \tag{2.22}$$

Where K_T = dimensionless thrust; K_Q = dimensionless torque; ρ = the fluid density and η_o = the open water efficiency

K_T, K_Q and η_o are the values usually measured in the open water test and are known as open water characteristics. Plotting them against J gives the open water chart. These characteristics are of interest, since they ideally are the same in model as full scale. The difference is the viscous scale effects, which are dealt with in the ITTC recommendations in the Hague 1978, see section 2.7. [18]

2.7 Viscous Scale Effects

The values of K_T, K_Q and η_o obtained at the model test or from the Wageningen series are in model scale. These values would be identical in full scale if the lift and drag coefficient (C_D and C_L) would be the same at model scale. This is approximately true for C_L, but not for C_D. C_D is decreasing with increasing Reynolds number. This results in higher K_T, lower K_Q and, studying eq. 2.22, thereby higher η_o. According to the ITTC-78 recommendations, the scale effects should be taken into account as described below.

First the local Reynolds number at model scale is defined as in eq. 2.23.

$$R_{nco} = \frac{V_A c_{0.75}}{\nu} \tag{2.23}$$

Where $c_{0.75}$=the model scale chord length at 0.75R and ν is the viscosity at the model test.

C_D in model and full scale are defined as in eq. 2.24 and 2.25 respectively. [18]

$$C_{DM} = 2\left(1 + 2\frac{t}{c}\right)\left(\frac{0.044}{R_{nco}^{\frac{1}{6}}} - \frac{5}{R_{nco}^{\frac{2}{3}}}\right) \tag{2.24}$$

$$C_{DS} = 2\left(1 + 2\frac{t}{c}\right)\left(1.89 + 1.62\log_{10}\left(\frac{c}{k_p}\right)\right)^{-2.5} \qquad (2.25)$$

Where t=the full scale thickness at R0.75; c=the full scale chord length at R0.75 and k_p=the full scale propeller surface roughness (standard value=$30 * 10^{-6}$m) [17]

The difference in profile resistance between the model and ship propeller, ΔC_D, is computed using eq. 2.26.

$$\Delta C_D = C_{DM} - C_{DS} \qquad (2.26)$$

Finally, the coefficients in full scale, K_{TS} and K_{QS} can be calculated using eq. 2.27 and 2.28.

$$K_{TS} = K_{TM} + \Delta C_D * 0.3\frac{P}{D} * \frac{cZ}{D} \qquad (2.27)$$

$$K_{QS} = K_{QM} - \Delta C_D * 0.25 * \frac{cZ}{D} \qquad (2.28)$$

Where D=the propeller diameter at full scale; P= the full scale pitch at R0.75 and Z=the number of blades. [18]

2.8 Pitch Setting

In the CFD setups for Controllable Pitch (CP) propellers it is commonly necessary to adjust the pitch. This might be to match e.g. a model test or to change from free running to bollard pull. The pitch is usually changed with the pitch at R0.7 as reference. The pitch is defined as the axial distance every blade section screws itself during one rotation, see Fig. 2.10.

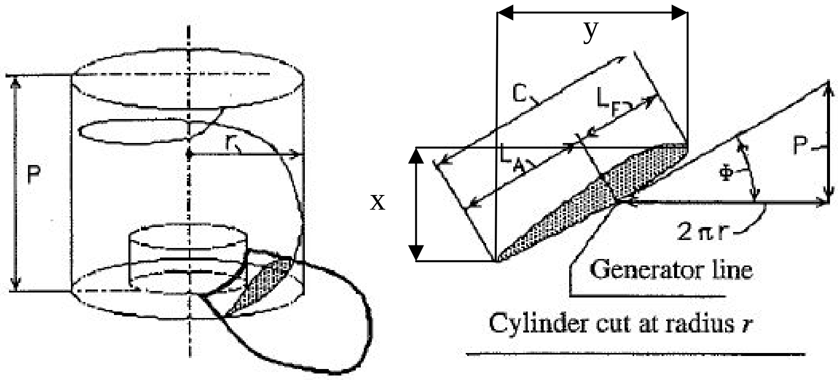

Fig. 2.10: The definition of pitch for a propeller. [18]

Since the blade section at R0.7 is of interest, a cylindrical cut must be performed. The reason for this is to present the radial coordinates in a Cartesian plane. The radius of such a cut can be described by eq. 2.29.

$$r_{cut} = 0.7 * \frac{D}{2} \qquad (2.29)$$

The distance between the intersection of the cutting plane and the leading and trailing edge respectively describes a distance in the lateral (y) and axial (x) direction. The pitch angle (ϕ) see Fig. 2.10, can then be described by the relationship in eq. 2.30

$$\phi = \arctan\left(\frac{x}{y}\right) \tag{2.30}$$

From Fig. 2.10 it is evident that the pitch (P) can be described by eq. 2.31 [18]

$$\begin{aligned} \tan\phi\,(x) &= \frac{P(x)}{\pi 2R\left(\frac{r}{R}\right)} = \{at\ R0.7\} \\ &= \frac{\frac{P0.7}{D}D}{2\pi * 0.7 * \frac{D}{2}} = \frac{\frac{P0.7}{D}}{\pi * 0.7} \end{aligned} \tag{2.31}$$

(This page is intentionally left blank)

3 Propeller Geometries, Test Setups and Resources

Three different propellers and five different setups were used for the validation and automation of the computational tools. The first propeller and three first setups were from the SMP’11 case 2, which provided a CP propeller with different hub caps for push and pull configuration. Further a CP-propeller for a single screw vessel (CPP1) and a CP-propeller for a twin screw vessel (CPP2) were provided from Berg Propulsion. In order to protect the commercial value of the two last mentioned propellers, the exact data of them cannot be provided in this report.

3.1 The SMP’11 Propeller and Test Setups

The SMP’11 case 2 contained three setups; one open water characteristics measurement, one velocity field measurement and one cavitation test setup. These setups where performed at different test points and for different inflow conditions.

The propeller was a five bladed CP-propeller. One of the design criterions for the propeller was to generate a tip vortex. The propeller design was provided with different hub caps for push and pull arrangement. [19]

Some propeller characteristics can be seen in Table 3.1. A picture of the propeller can be seen in Fig. 3.1. The propeller drawing and detailed propeller characteristics can be seen in Appendix A.

Table 3.1: Some propeller characteristics of the SMP’11 propeller

D	[m]	0.25
RPM	[rev/min]	900
P07/D	[-]	1.635
Z	[-]	5
EAR	[-]	0.77896

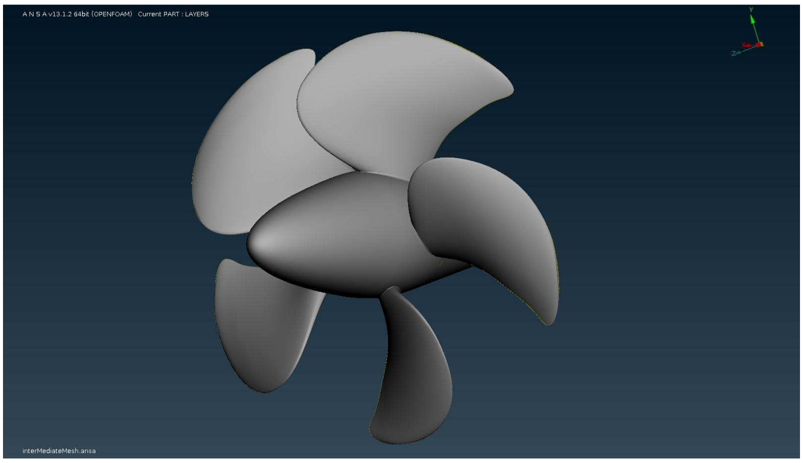

Fig. 3.1: The SMP’11 propeller geometry in 3D representation.

3.1.1 Case 2.1: Open Water Test

The open water test was carried out in a pull configuration. The hub was designed to avoid a pressure build up, see Fig. 3.2.

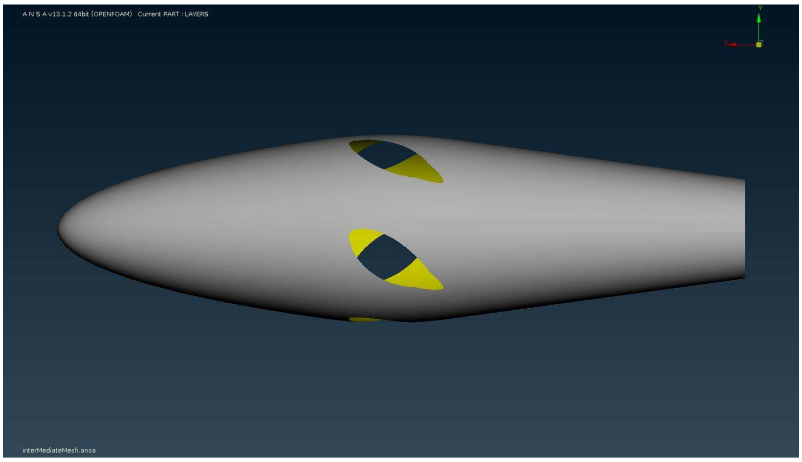

Fig. 3.2: The open water hub with a design that avoids a pressure build-up

The test was performed in the SVA towing tank. The tank had a breadth of 9 m, the depth was 4.5 meters and the shaft was submerged with 0.375 m. The propeller was placed in the lateral centre of the tank. A slide test was performed. A principal sketch of the slide with propeller, shaft, blades and hub is show in Fig. 3.3.

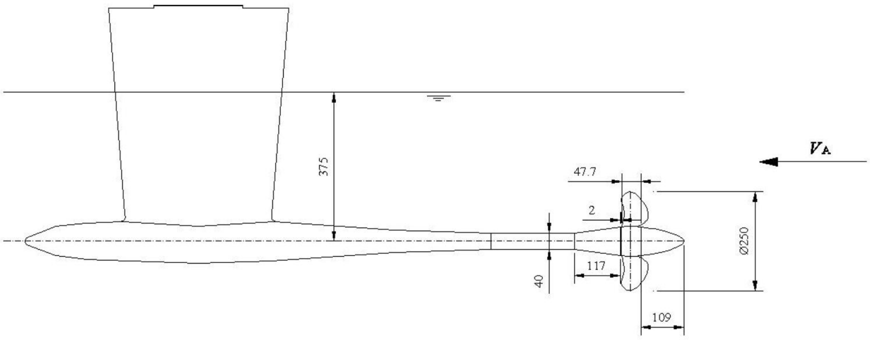

Fig. 3.3: The sled with propeller, shaft blades and hub

Before the open water test, the pressure probes were calibrated using only the rotating hub and the nose cap. Hence the results are considered to be solely generated by the propeller blades. Table 3.2 shows the operating conditions of the open water test.

Table 3.2: The operating conditions for the SMP'11 open water test

Water density (for T = 17.5°C)	ρ	[kg/m³]	998.67
Kinematic viscosity of water (for T = 17.5°C)	ν	[m²/s]	1.07E-06
Rate of revolutions	n	[1/s]	15
Advance Velocity	V_A	[m/s]	2.25-5.25

The results for comparison were K_T and K_Q at J=0.6-1.4 with an interval of 0.2. [20]

3.1.2 Case 2.2: Velocity Field Measurements

The velocity field measurement was performed in the SVA Potsdam cavitation tunnel K15A. The tunnel had a cross section of 600*600 mm and a length of 2600 mm. The propeller was positioned in the vertical and lateral centre of the tunnel. The longitudinal position was 570 mm from the beginning of the test section, see Fig. 3.4. The test setup was a push configuration. Another type of hub was used for the test to match the push configuration better, see Fig. 3.5.

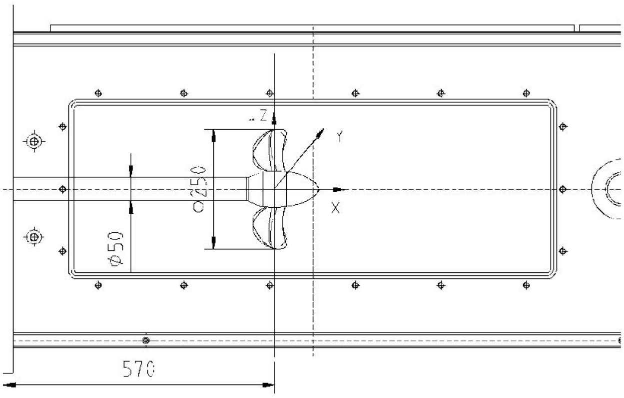

Fig. 3.4: The lateral and longitudinal propeller position for cavitation tests and velocity field measurement

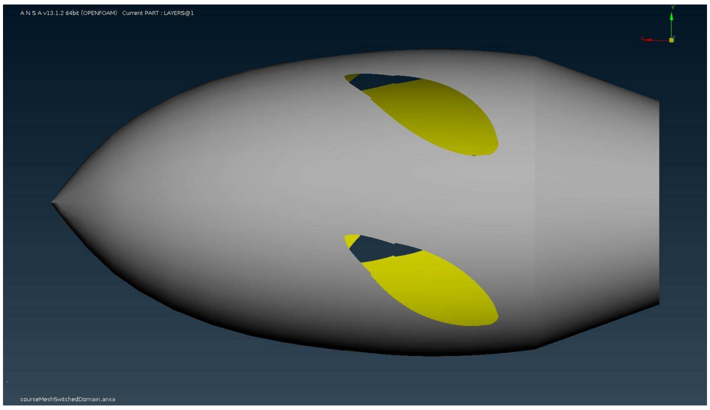

Fig. 3.5: The hub used in the cavitation tests and the velocity field measurement

The velocity field was measured using Laser Doppler Velocimetry (LDV). The inflow was homogenous and the LDV measurements were performed in the planes 0.1D and 0.2 D in front of the propeller disc, see Fig. 3.6.

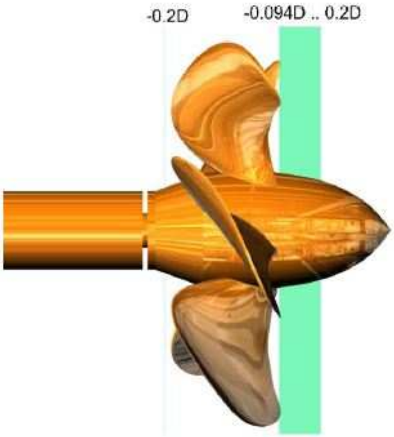

Fig. 3.6: The measuring planes for the velocity field measurement [21]

The measurements were angular based with the zero degree position defined as the 12 o' clock position. The velocities in all directions were measured at every 0.25° step. The measurements were performed along a constant line at angular position $\Phi = 225°$ and then related to the zero degree position. The blade position was recorded at every time step, making the velocity field relating to the zero degree position possible.

The test was performed with a non-cavitating propeller. The operating condition is presented in Table 3.3.

Table 3.3: The operating conditions for the SMP'11 velocity field measurement

Water density (for t_w=24.7°C)	[kg/m3]	997.1
Kinematic viscosity of water(for t_w=24.7°C)	[m²/s]	9.03E-07
Number of revolutions	[1/s]	23
Velocity	[m/s]	7.204
Advance coefficient	[-]	1.253
Thrust coefficient	[-]	0.250
Torque coefficient	[-]	0.725

The velocities were positive in the following directions: Axial velocities in the flow direction, radial velocities for increasing radii and tangential velocities in the direction of rotation.

The data provided was firstly axial, tangential and radial velocities for the angular interval $-50° \leq \Phi \leq 22°$ at 0.25° step size for the two planes in front of the propeller disc at radial positions R0.7, R0.97 and R1.0

The tip vortex at x/D=0.1 was also given as velocities in the Cartesian directions at Φ in the interval $-40° \leq \Phi \leq 0°$ and r/R in the interval $0.4 \leq r/R \leq 1.1$ [21]

3.1.3 Case 2.3: Cavitation Tests

The cavitation tests were performed in the same tunnel and at the same position as in the velocity field measurement, see section 3.1.2. The test was performed at three different conditions. The first and third cases (case 2.3.1 and 2.3.3) were off-design conditions. Case two (case 2.3.2) was the design condition. For these conditions the cavitation patterns were analyzed using high speed camera observations and the cavitating thrust was measured. The operating conditions for case 2.3.1-2.3.3 are presented in Table 3.4 [22]

Table 3.4: The operating conditions for the SMP'11 cavitation test

Case:		[#]	**2.3.1**	**2.3.2**	**2.3.3**
Advanced coefficient	J	[-]	1.019	1.269	1.408
Cavitation number based on n	σ_n	[-]	2.024	1.424	2.000
Thrust coefficient (non-cavitating!)	K_T	[-]	0.387	0.245	0.167
Number of revolutions	n	[1/s]	24.987	24.986	25.014
Water density	ρ	[kg/m$_3$]	997.44	997.44	997.37
Kinematic viscosity of water	ν	[m²/s]	9.34E-07	9.34E-07	9.34E-07
Vapour pressure	p_v	[Pa]	2818	2818	2869
Air content	α/α_s	[%]	53.5	53.5	58.5

3.2 The Propeller for the Single Screw Vessel (CPP1)

CPP1 is a large, low RPM propeller with moderate pitch. It is a four bladed CP propeller. The design is very smooth and it is reasonably unloaded at the tip. Some propeller characteristics can be seen in Table 3.5.

Table 3.5: Some propeller characteristics of CPP1

D	[m]	5.16
RPM	[rev/min]	136
P07/D	[-]	0.774
Z	[-]	4
EAR	[-]	0.523

Open water tests at two different pitch settings, 0.752 and 0.788, for J=0.1 to J=0.8 were available. A picture of the propeller can be seen in Fig. 3.7 .

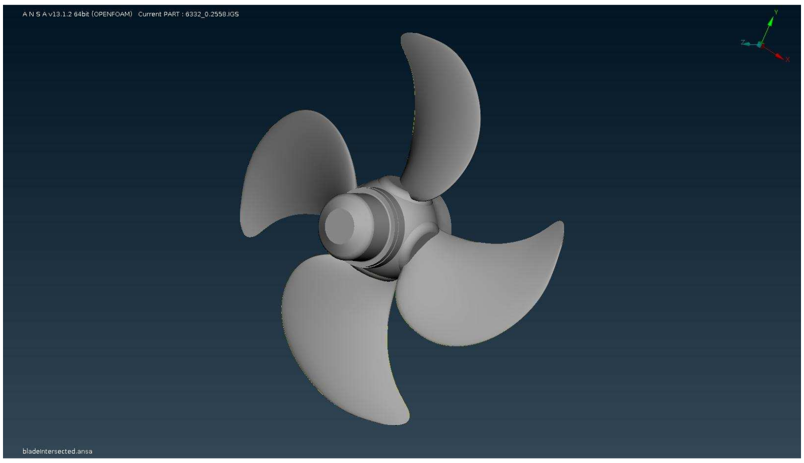

Fig. 3.7: The propeller geometry of CPP1

3.3 The Propeller for the Twin Screw Vessel (CPP2)

CPP2 is a medium sized, medium RPM propeller with moderate pitch. It is a four bladed CP propeller. The design is heavily unloaded and has high skew to reduce pressure pulses. Some propeller characteristics can be seen in Table 3.6.

Table 3.6: Some propeller characteristics of CPP2

D	[m]	2
RPM	[rev/min]	350
P07/D	[-]	1.088
Z	[-]	4
EAR	[-]	0.6904

An open water test with the pitch setting 1.088 at J= 0.0726 to J=1.0201 were available. A picture of the propeller can be seen in Fig. 3.8.

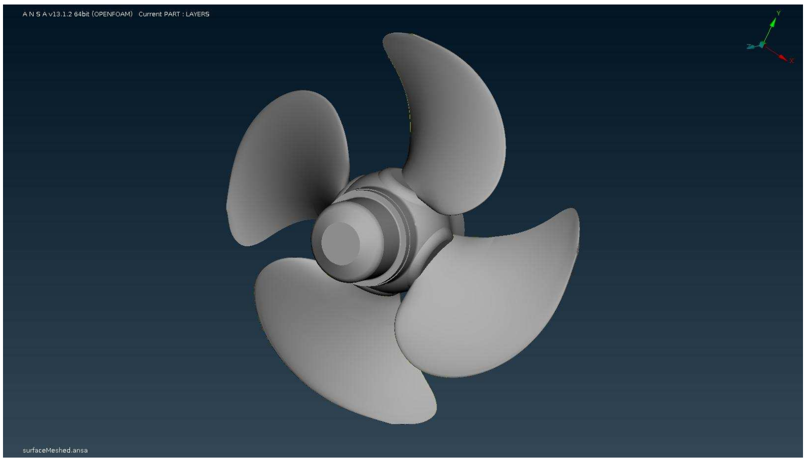

Fig. 3.8: The propeller geometry of CPP2

3.4 Computer Resources

The CFD simulations were performed on eight cores with a clock frequency of 3.4 GHz each. The RAM was 24 GB. The boundary element method simulations were performed on two cores with a clock frequency of 2.13 GHz each. The RAM was 4 GB.

4 Proceedings of CFD

This section describes how the CFD-setups were made, how the results were post processed and how the pre processing automation was performed. In section 4.1-4.3 the proceedings of SMP’11 are described, since these were used to develop the automation method. In section 4.4 the proceedings of the automation using CPP1 is described. Finally in section 4.5-4.6 the proceedings of the actual open water tests of CPP1 and CPP2 are described, since more steps than performed by the automated script were needed to match the model test descriptions for these propellers.

4.1 Open Water Test of the SMP’11 Propeller

The meshing tool used for the open water test of the SMP’11 propeller was ANSA. The original geometry of the SMP’11 propeller had some deficiencies from the beginning. Firstly there was a small play between the blade and the hub, see Fig. 4.1.

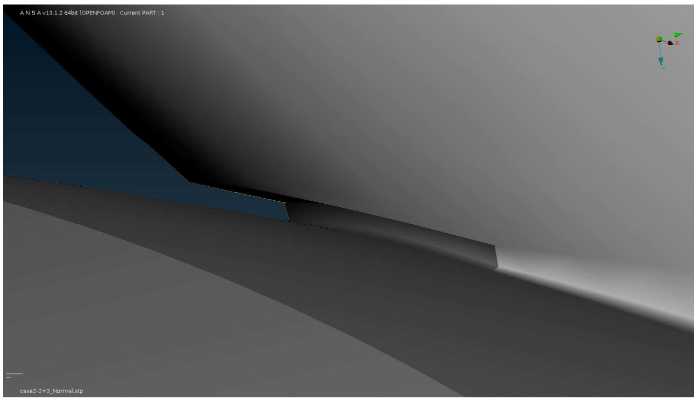

Fig. 4.1: The small play between the blade and the hub.

The intention was to use prism layers. Since they would grow into each other in the play, it was filled by projecting the blade downwards and intersect the blade with the hub fillet, see Fig. 4.2. This should make negligible difference, since almost no work is performed near the blade root; see pitch distribution in Appendix A.

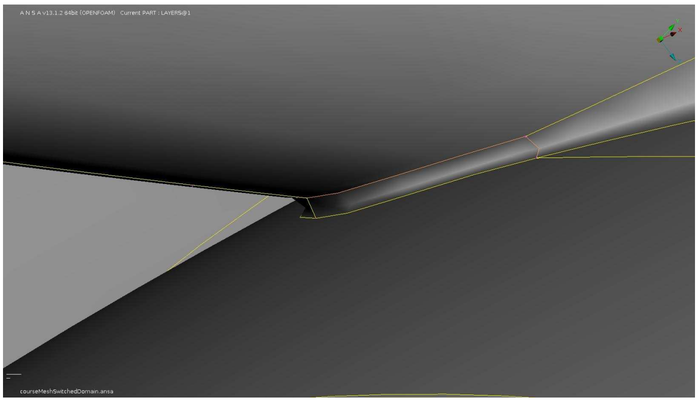

Fig. 4.2: The small play between the blade and the hub removed.

The same prism layer related problem would occur for the play in the intersection between shaft and hub, see Fig. 4.3.

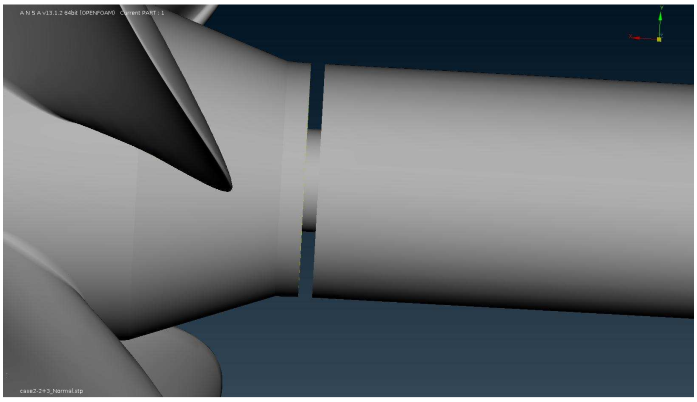

Fig. 4.3: The gap between the shaft and the hub

The geometry was simplified by removing this gap, see Fig. 4.4.

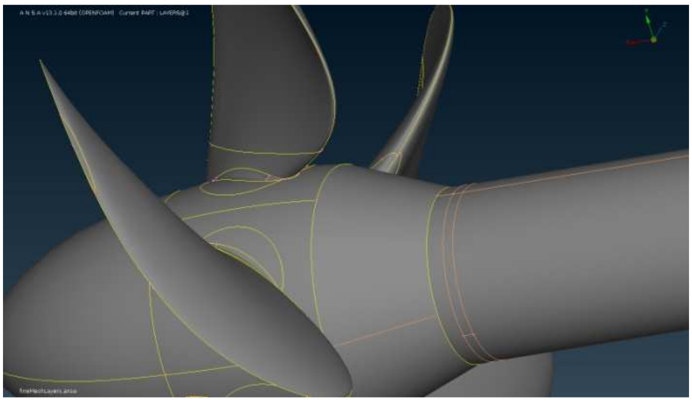

Fig. 4.4: The gap between shaft and hub removed

Lines with no connections was pasted together and the tip length at r/R=1.0 was smoothened by a small cut yielding better geometrical representation, see Fig. 4.5.

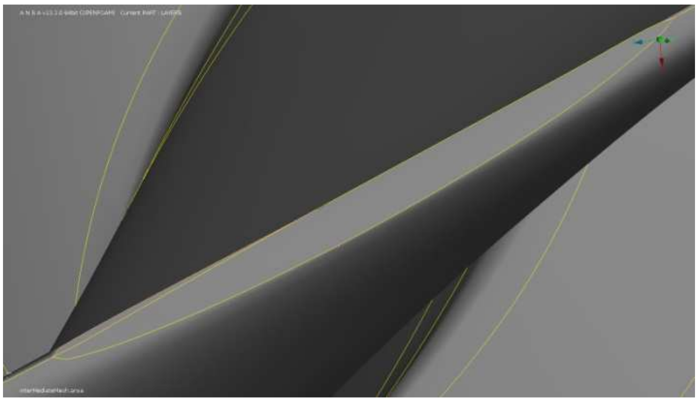

Fig. 4.5: The modification of the tip, where the sharp line shows the new representation and the thinner one the old representation.

To make the blade meshing more efficient and above all symmetrical, only one blade was meshed and then the completed mesh was copied to the remaining four blades.

The blade, hub and shaft were surface meshed with triads. The triads were smaller at high curvature and larger near mid surface sections. This is since the large gradients from the flow occur at the sharp edges. For the coarse mesh, the smallest element length on the surface was 1 mm and the largest 10 mm, see Fig. 4.6.

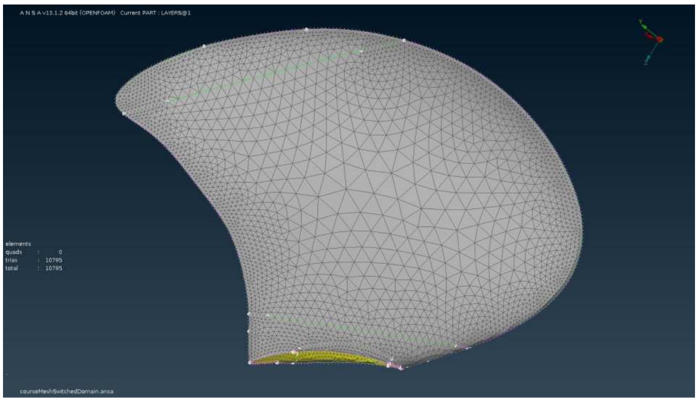

Fig. 4.6: The triad surface mesh on one blade.

As turbulence model, the K-omega SST model was applied. To model the boundary layer, wall functions were needed. Five prism layers with 1.2 as growth ratio and a starting length of 0.5 mm were applied to get the gradients close to the wall resolved.

The rotation was modeled with MRF. To make use of MRF, a volume surrounding the rotating parts was needed. This volume was made cylindrical with a radius 59 mm larger than the propeller radius. The length of the volume was 69 mm upstream and 2442 mm downstream. Within this volume, all parts were set to rotate. The propeller inside this volume is shown in Fig. 4.7. The motive for the distances was based on experience and assumptions. A slip stream of approximately ten diameters length is appropriate. The diameter of the cylinder was based on experiments; increasing this parameter by a factor 1.5 made no difference on the results, see section 8.2.

Fig. 4.7: The propeller inside the MRF-zone

As domain, a larger cylinder was used. This cylinder was made with 1261 mm upstream, 3000 mm downstream and 1261 mm diameter. These distances were based on experience; five propeller diameters as upstream length and as domain diameter and twelve propeller diameters as downstream length has proven accurate and giving a reasonable amount of cells before. [29] The inner volume is, except for being the MRF zone, representing the slipstream.

The settings of the final coarse mesh can be seen in Table 4.1. It should be noted that the maximum computational power at hand allowed about thirteen million cells. This was the reason for the cell length choice; the aim was to have high resolution near the propeller, a maximum growth ratio of 1.2 and not cells of a size that completely dissolves the gradients.

Table 4.1: The meshing parameters of the coarse mesh for the open water test

	Perimeter length [mm]	Surface mesh type	Surface mesh size [mm]
Blades	1	CFD	1 to 10
Hub	1	CFD	2 to 10
Shaft	5	CFD	3 to 10
Interface	10	CFD	1 to 10
Domain	50	CFD	10 to 50

As interpolation schemes, first order accurate schemes were used for the turbulent quantities kinetic energy, inverse turbulent time scale and the turbulent viscosity. The computation was started with a first order upwind scheme for the velocity. When the computation was stabilized, a second order upwind scheme was applied instead.

To indicate grid independence for the results, the mesh was refined at regions with large gradients. The mesh was made larger around shaft and hub, but refined with a factor of two at blade corners and blade tip. The maximum volume element length in the slip stream was also reduced by a factor two. The contingent difference between the coarse and the fine mesh should depend on the discretization error. Since a second order accurate scheme was used, the error would reduce in the order of x^2, if x is the cell length and the mesh was structured. In this case the error would reduce, but not necessarily in the exact order of x^2. [7] The mesh settings of the fine mesh can be seen in Table 4.2. The resulting number of cells for the fine and the coarse mesh can be seen in Table 4.3.

Table 4.2: The meshing parameters of the fine mesh for the open water test

	Perimeter length [mm]	Surface mesh type	Surface mesh size [mm]
Blades	0.6	CFD	0.6 to 6
Hub	0.6	CFD	0.6 to 6
Shaft	5	CFD	0.6 to 6
Interface	5	CFD	0.6 to 6
Domain	60	CFD	5 to 60

Table 4.3: The resulting number of cells for the coarse and the fine mesh for the open water test.

SMP'11	OW coarse	OW fine
Surface mesh elements	100000	150000
Prism layer elements	502920	600000
Total elements	4500000	11000000

As boundary conditions, the no-slip condition was applied for velocity on the surface. The outlet was set as pressure outlet with zero gradients for the remaining quantities.
The inlet was set up with uniform velocity inlet and the remaining quantities calculated in accordance with eq. 4.1-4.4 and set as Dirichlet conditions. [5].

Table 4.4 and Table 4.5 summarizes the boundary conditions for the surface and the outer domain respectively

$$k = \frac{3}{2} V_A^2 * I \qquad (4.1)$$

Where k = the turbulent kinetic energy; V_A *= the advance velocity and I = the turbulent intensity*

$$\epsilon = \frac{0.09\rho k^2}{\frac{\mu_t}{\mu}\mu} \qquad (4.2)$$

Where μ_t *= the turbulent viscosity;* μ *= the fluid viscosity;* ϵ *= the turbulent dissipation and* ρ *= the density of the fluid*

$$\omega = \frac{\epsilon}{k} \qquad (4.3)$$

Where ω *= the specific dissipation.*

$$\frac{\mu_t}{\mu} = 10 \qquad (4.4)$$

Table 4.4: The boundary conditions for the surface boundaries

Boundary:	**Blades**	**Hub**	**Shaft**
Velocity	no-slip	no-slip	no-slip
Turbulent kinetic energy	Wall function	Wall function	Wall function
Specific dissipation	Wall function	Wall function	Wall function
Pressure	Homogenous Neumann	Homogenous Neumann	Homogenous Neumann

Table 4.5: The boundary conditions for the outer boundaries

Boundary:	**Domain**	**Inlet**	**Outlet**
Velocity	slip	Dirichlet	Homogenous Neumann
Turbulent kinetic energy	Wall function	Dirichlet	Wall function
Specific dissipation	Wall function	Dirichlet	Wall function
Pressure	Homogenous Neumann	Homogenous Neumann	Homogenous Dirichlet

For the domain, wall functions were used and the pressure was of zero gradient type here.

The CFD package used for the simulations was OpenFOAM with the solver MRFSimpleFoam. The simulation was of steady RANS type. The forces and moments were computed on the blades only.

4.2 Velocity Field Measurement of the SMP’11 Propeller

The velocity field computation of the SMP’11 propeller was performed in the same way as for the open water test and for the same propeller, but with a different hubcap, see section 4.1. The domain and inner volume were rotated and elongated to fit the new arrangement and the longer shaft. The final fine and coarse mesh settings and number of cells can be seen in Table 4.6 and Table 4.7. The final number of cells for the coarse and fine mesh can be seen in Table

4.8. A square size box was used due to a bug in ANSA, making the preferred cylindrical size box unusable.

Table 4.6: The settings of the coarse mesh for the velocity field measurement

	Perimeter length [mm]	**Surface mesh type**	**Surface mesh size [mm]**
Blades	1	CFD	1 to 10
Hub	1	CFD	1 to 10
Shaft	5	CFD	1 to 10
Interface	10	CFD	1 to 10
Domain	50	CFD	10 to 50

Table 4.7: The settings of the fine mesh for the velocity field measurement

	Perimeter length [mm]	**Surface mesh type**	**Surface mesh size [mm]**
Blades	0.3	CFD	0.3 to 5
Hub	1 to 5	CFD	1 to 10
Shaft	5	CFD	0.3 to 10
Interface	5.25	CFD	0.3 to 5.25
Domain	100	CFD	5.25 to 100

Table 4.8: The final number of cells for the coarse and fine mesh of the velocity field measurement

SMP'11	**Velocity field coarse**	**Velocity field fine**
Surface mesh elements	290000	200000
Prism layer elements	410000	1000000
Total elements	4600000	13600000

To comply with the thrust identity, the speed had to be lowered somewhat. Two different speeds were tested and then the linear relationship between J and K_T was used to find the proper velocity yielding the correct thrust.

4.3 Post Processing of the SMP’11 Propeller

When the CFD-computations had reached final convergence, they were stopped. Final convergence was considered to be achieved when all residuals of velocity and turbulent quantities were below 10^{-5} and all residuals of pressure were below 10^{-4}.

The open water diagram was made from the integrated forces along (T) and moments around (Q) the x-axis. Eq. 2.20-2.22 were used to compute the open water characteristics.

The RANS results were post processed in FieldView [23]. The velocity field was extracted using the sampleDict in OpenFOAM. A cloud of points were picked from the input file demands of SMP’11. The input file requested the tangential, radial and axial velocity at a given ϕ and r/R. ϕ is defined as the angle between the dead top centre and the current blade tip position. It is positive in clockwise direction. Hence it can be described by the relationship in eq. 4.5. The given radial section can be described in terms of Cartesian coordinates as in eq. 4.6. This is since the equation will yield a cylinder cutting through the given radial section.

$$\tan(\phi) = \frac{y}{z} \tag{4.5}$$

$$\frac{r}{R} = \sqrt{\left(\frac{y}{R}\right)^2 + \left(\frac{z}{R}\right)^2} \tag{4.6}$$

Where r = the radial coordinate and R = the propeller radius

Rewriting gives the Cartesian coordinates as in eq. 4.7 and 4.8

$$y = tan(\phi) * z \tag{4.7}$$

$$z = \frac{r}{\sqrt{tan(\phi)^2 + 1}} \tag{4.8}$$

By sampling the requested points, results of velocity in x, y and z direction were attained. To convert y- and z-direction into radial and tangential velocities, the relationship described by eq. 4.9 and 4.10 were used.

$$V_r = cos(\phi)\, V_z + sin(\phi)\, V_y \tag{4.9}$$

$$V_t = cos(\phi)\, V_y - sin(\phi)\, V_z \tag{4.10}$$

Where V_r *= the radial velocity;* V_t *= the tangential velocity;* V_z *= the velocity in z-direction and* V_y *is the velocity in y-direction*

4.4 Automation of the Pre-processing

CPP1 was used to make the script for automatic CFD pre-processing. In short terms it could be said that the methodology found to be efficient when analysing the open water characteristics of the SMP’11 propeller, see section 4.1, was automated.

The script was made in three parts; one geometrical cleanup and domain defining part, one surface meshing part and one volume meshing part. This was since the meshing needs two natural breakpoints. Firstly the pitch needs to be controlled and set and secondly the surface mesh needs to be checked. These two points naturally determines the quality and accuracy of the calculation. Therefore it is essential with breakpoints to let the user control the setup. The entire pre-processing code was programmed in a C++-like scripting language included in ANSA. Below an explanation of what the code performs step by step is described. For a more detailed description, including records used and the actual code, see Appendix B.

4.4.1 Geometrical Cleanup and Domain Definition

The first part of the script; cleanBladeUntilPitchSetting, which makes a geometrical cleanup and domain definition, starts with cleaning the blade. The blade is generated by a script linked with solid works, so all blades need to be cleaned in the same way. This script will be referred to as Solid Works (SW) to avoid confusion. First there are five excessive faces that need to be removed for the mesh to be generated, see Fig 4.8.

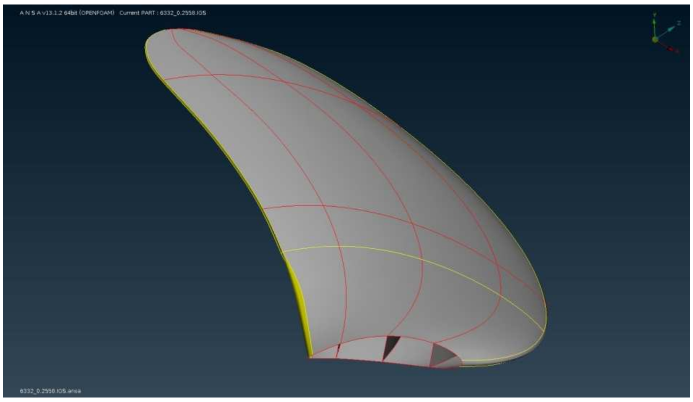

Fig. 4.8: The uncleaned blade as extracted from SW

If the SW generated blade is studied, it is obvious that the smallest area of all the faces occur at the blade. The ANSA script (script) searches for the smallest face, makes it and its neighbours visible and saves it in a temporary file and loads the file. This makes the five excessive faces in the middle of the blade to disappear. After this, the solution is compressed, which means that parts, property identification (PID) and points that have no use will be erased.

A finite tip length is applied at the uppermost radial section to close the leading and the trailing edge in SW. This hole needs to be filled. By searching for holes smaller than the sum of 10mm and 3% of the propeller diameter and fill them, the script gets rid of this hole. The resulting cleaned blade can be seen in Fig. 4.9.

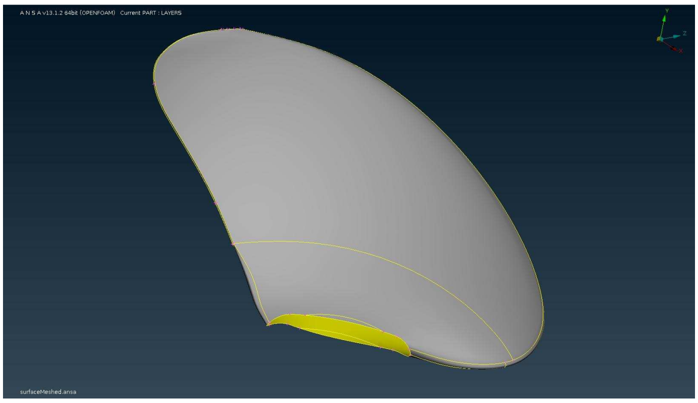

Fig. 4.9: The cleaned blade as a result of the cleanup algorithm.

The best way to get a proper computational domain definition is to use a template. From the methodology used when analysing the SMP’11 propeller, see section 4.1, a good setup could be made. The methodology of how the template was made can be seen in section 4.4.2. The template contains among more things a domain, a MRF-zone, a shaft, a hub, different size boxes and an empty PID named blades, all made to fit a propeller with a diameter of 2760 mm and a hub with diameter 690 mm.

In the script this template file is merged to the cleaned blade. The blade is put in the PID blades. Two input dialogs asking for the hub and propeller diameter shows up. When the inputs are typed in, they are recomputed into scale factors, which are based on the template hub and propeller diameter. The two scale factors, α_{hub} and α_{prop} are given by eq. 4.11 and 4.12.

$$\alpha_{prop} = \frac{input_{prop}}{2760} \tag{4.11}$$

$$\alpha_{hub} = \frac{input_{hub}}{690} \tag{4.12}$$

The shaft and the hub are scaled with α_{hub} and the rest of the parts except for the blades are scaled with α_{prop}. The code has now reached its first breakpoint; the domain is defined, the geometry is clean and all the parts have proper PIDs. The next step is for the user to set up the pitch, which can be done in many ways. A recommended procedure for this is the procedure presented in section 4.5.

4.4.2 The meshing template

The template mentioned in section 4.4.1 is described in this section. From the methodology used when analysing the SMP’11 propeller, see section 4.1, a good setup could be made. The only difference between the SMP’11 procedure and this template was that the domain was surface meshed with a uniform surface mesh in the template. This was because a size varying mesh is unnecessary so far from the propeller and the large cylinder is not a complex geometry.

The template was made as a regular ANSA-file. One of the Berg Propulsion’s standard hubs with a diameter of 690 mm was used. Based on this hub, a propeller diameter (D) four times the hub diameter, i.e. 25% hub ratio and thereby D=2760 mm, was assumed. Based on this diameter and the proceedings of the SMP’11 propeller, the template could be set up with properties as in Table 4.9 and Table 4.10. Note that the volume mesh and surface mesh parameters in the template will scale in accordance with the scale factors mentioned in section 4.4.1.

The standard hub was cleaned and made to an intact surface for simple intersection with the blade foot. A shaft was connected to the hub. Fig 4.10 shows the computational domain in the template.

Fig. 4.10: The domain template, where the shaft is the small structure in the middle, the thick lines are the size boxes and the thinner lines are the interface and the domain.

To conclude the most accurate open water setup template a study of some different possible open water setup techniques was performed. The first decision to make was whether the shaft should be long or short to yield accurate results. The propeller was set in a push configuration. The shaft was altered from 1*D to 2*D length and the results of K_T and K_Q was compared to the model test results. Further, a comparison between the results when using a spherical and a straight end cap was performed. This was tested with a long shaft. The difference when increasing the size of the MRF-zone by a factor 1.5 was tested. This was only performed for the short shaft with a spherical end cap.

The difference between the setups pointed toward one conclusion; the most accurate ones generated a high load near the blade root. Therefore the setup was switched into a pull configuration, which yielded the most accurate results. This was expected, since the open water tests usually are carried out in this way. The spherical end cap did not affect the results at all, but made the convergence faster. As a consequence a pull configuration using a long shaft with spherical end cap in a MRF-Zone with slightly larger diameter than the propeller diameter was used for the open water configuration template.

All parts were named after representation to make the OpenFOAM setup understandable. The PID names were set to blades, hub, shaft, domain, inlet, outlet and interface, where interface is representing the MRF-zone. To simplify the meshing function in the script, a batch mesh scenario was added to the template. A batch mesh scenario is a tool where one adds a filter finding a PID with a certain name, e.g. blades, and then meshes this blades PID automatically in accordance with the quality criterion, mesh size requirements and geometrical representation requirements.

The size boxes were set behind the propeller disc to have a good resolution in the slip stream. This was both for the computational accuracy and for the visualization; it is beneficial to have high resolution when e.g. rendering including a velocity field is performed. The size boxes were set with a maximum volume element length of 100 mm and 200 mm for the box closest to and the one more downstream respectively.

Table 4.9: The dimensions of the template file

Domain diameter	5D	**MRF-zone length**	7D
Domain length upstream	5D	**Size boxes length, each**	5D
Domain length downstream	10D	**Size boxes diameter, each**	D+0.25D
MRF-zone diameter	D+0.25D	**Propeller diameter, D**	2760 mm

Table 4.10: The mesh settings from the batch mesh scenario in the template file

	Perimeter length [mm]	**Surface mesh type**	**Surface mesh size [mm]**
Blades	5 to 50	CFD	5 to 50
Hub	5 to 50	CFD	5 to 50
Shaft	50 to 200	CFD	50 to 200
Interface	100	CFD	5 to 100
Domain	1000	ADV. FR.	1000

4.4.3 Surface Mesh

This section describes the second part of the script; makeSurfaceMesh, which performs a surface mesh on blades hub and shaft. When this script is started, the blade, hub and shaft are copy linked 360° to form a full propeller. The link option was chosen to guarantee symmetrical and faster meshing. Linking means that every change made on the original blade is automatically done on the link blades, so if the mesh should be manually improved, this only needs to be done at one blade. After this an automatic topology to get rid of single cons followed by an automatic geometry cleanup, fixing cracks, overlaps, needle faces, collapsed cons and unchecked faces is performed. This is since a clean geometry is demanded to make a complete surface mesh.

The script sets the perimeter length with automatic CFD spacing that should be used prior to CFD-meshing. This is done making each of the entities hub, shaft and blades visible one at a time. A call for the batch mesh scenario predefined in the template, resulting in a triad surface CFD mesh follows after this.

The last breakpoint of the code is now reached. This gives the user the opportunity to inspect and fix parts of the surface mesh that is found unsatisfactory. Usually ANSA has problems with meshing the leading edge. A recommended procedure for this is presented in Appendix C.

4.4.4 Layers and Volume Mesh

This section describes the third and last part of the script; layersAndVolumeMesh, which makes prism layers on the surface and meshes the volume. The script starts by reading a preset quality criterion with fluent skewness of 0.8 and maximum volume element skewness of 0.85 from a predefined file. These criterions have proven accurate before and allow ANSA to make a good geometrical description. Everything is made visible and the surface meshes for all macros are frozen. The setup is merged with another template that is preset with a layers batch mesh scenario. The settings of this scenario can be seen in Appendix B. Since the mesh was frozen, only layers will be generated when the batch mesh scenario is started.

For the open water setup, three volume definitions are needed. The first one is the inner volume, which is the volume occupied between the top cap fluid layers (top cap) and the interface. The top cap is a surface mesh lying on top of the prism layers. The second volume to define is the outer volume, which is the volume occupying the space between the domain and the interface. These volumes are defined in the script by first making the top cap and the interface being visible and make an auto detection of the volumes. The same thing is performed for the outer volume, but with only domain and interface visible instead.

Since all the size boxes and element lengths on the surfaces are set, the only thing needed is to apply a volume mesh with a maximum element length large enough to give stable volume meshing. A maximum size of twice the domain element length has proven sufficiently large to give a stable meshing session. The defined volumes are set up with the hexa interior mesh set to a maximum fluent skewness of 0.85 and a growth ratio of 1.2. The defined volumes are meshed with these settings.

The file is merged with a template only containing the PID names innerVolume and outerVolume. The fluid layers and the inner volume are put in PID innerVolume and the outer volume is put in outerVolume. The solution is compressed to remove excessive parts and PIDs. Finally the mesh quality is improved by allowing a node movement of maximum 0.2 times the local element length.

4.5 Open Water Test of CPP1

As stated, CPP1 was used to make the CFD ANSA script, see section 4.4. The resulting mesh after using the script can be seen in Table 4.11.

Table 4.11: The number of cells for the open water test of CPP1

Element type:	# Cells
Surface mesh elements	270000
Prism layer elements	1350000
Total elements	8125000

The propeller was analysed in a pull-configuration for the points J=0.1 to J=0.8 with the standard configuration presented in section 4.1, but with viscosity and density matching the ITTC-78 defaults in PROCAL, see Table 5.1.

The pitch was adjusted to yield accordance with the model test. A cylinder with radius 1806 mm, computed using eq. 2.29, was made. The distance from trailing to leading edge on the cutting plane was measured, yielding a lateral and an axial distance between the two points. In eq. 2.30 the axial coordinate (x) should be measured in Cartesian coordinates, but the lateral distance (y) should be measured in cylindrical coordinates, i.e. the y-distance is the arc length described on the cutting cylinder. The problem was solved by moving the aft most point of the blade section forward the axial distance measured. The angle (ϕ) between the shaft line centre, the axially moved aft most point and the foremost point of the blade section was measured, see Fig. 4.11.

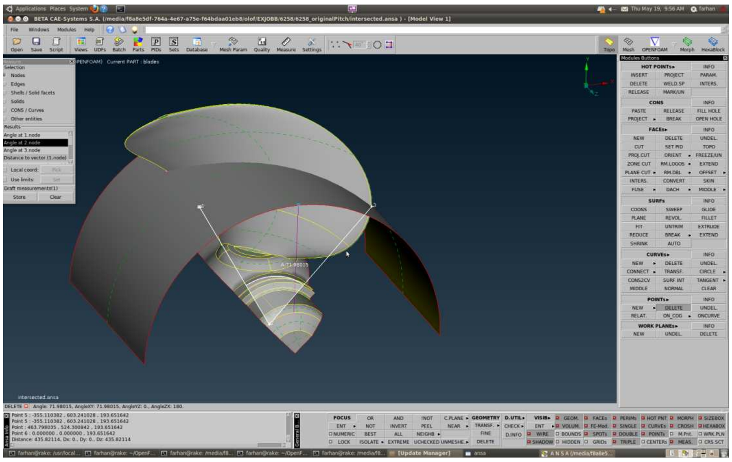

```
DELETE  Angle: 71.98015, AngleXY: 71.98015, AngleYZ: 0., AngleZX: 180.
Point 5 : -355.110382 , 603.241028 , 193.651642
Point 5 : -355.110382 , 603.241028 , 193.651642
Point : 463.798035 , 524.300842 , 193.651642
Point 6 : 0.000000 , 0.000000 , 193.651642
Distance: 435.82114, Dx: 0., Dy: 0., Dz: 435.82114
```

Fig. 4.11: The angle, **ϕ**, is measured between the two white lines, leftmost line goes from the axially moved aft most section point to shaft centre and the rightmost white line goes from the shaft centre to the fore most point.

This angle was used to compute the arc length (L_{arc}) as in eq. 4.13.

$$L_{arc} = \phi r \qquad (4.13)$$

Where ϕ= the measured angle in radians and r is the radius of the cutting cylinder

Since $y = L_{arc}$ in eq. 2.30, eq. 2.30 and 2.31 gave the current pitch. The pitch before adjustment was 0.774 and the required pitch for the model test was 0.788. Eq. 2.31 gave the required pitch angle, $\phi_{req} = 19.7139°$. The current angle was computed using eq. 2.30 from the measurement. It resulted in the current pitch angle, $\phi_o = 20.83°$. The blade hence had to be rotated 1.1161° around the y-axis.

4.6 Open Water Test of CPP2

CPP2 was used to validate the script and standard configuration presented in section 4.4. The script worked very well. First the clean blade button was pushed. The blade was intersected with the blade foot using the procedure described in Appendix D. The pitch was changed in the same way as for CPP1. The blade foot was intersected to the hub in accordance with Appendix D. After this, the makeSurfaceMesh-button was pushed. Everything except the surface mesh at leading edge was meshed. This was fixed in accordance with the procedure described in Appendix C. Finally the layersAndVolumeMesh-button was pushed, resulting in a complete volume mesh with the proper PID-names.

One problem was that since the propeller was smaller than the propeller used to write the script and the surface mesh resolution was static, the number of cells was fewer for this propeller. This rises, as stated, no significant impact on the results. Therefore the propeller was tested with the smaller mesh size to save some CPU hours. The pitch was checked in accordance with the method in section 4.5 and it matched the model test pitch setting. The propeller was tested at J=0.0726 to J=0.9461 with a step size of 0.1452. The resulting mesh can be seen in Table 4.12.

Table 4.12: The number of cells for the open water test of CPP2

Element type:	**# Cells**
Surface mesh elements	117000
Prism layer elements	584000
Total elements	4849000

(This page is intentionally left blank)

5 Proceedings of the Boundary Element Method

This section describes the proceedings of the boundary element method. Section 5.1 starts with describing how the open water test was performed for all propellers together, since this is the first step that has to be done for all analyses with the boundary element method. Section 5.2 continues with a description of how the cavitation test for the SMP’11 was performed, which was a part of exploring the functionality of the boundary element method. A description of how the open water test was automated considering both pre- and post-processing is described in section 5.3.

5.1 Open Water Tests of the Analysed Propellers

The open water test for all the propellers using the boundary element method PROCAL was performed in the same way, but of course with different parameters. First the geometry-file was extracted using a pre-calculated Excel sheet with all the parameters given from the blade design workbook. A new control file was made in PROCAL.

The operation conditions were set to full scale defaults in accordance with ITTC-78 for CPP1 and CPP2, see Table 5.1. The SMP’11 propeller was setup in accordance with the operating conditions in Table 3.2.

Table 5.1: Default full scale operating conditions in PROCAL

Water density	[kg/m$_3$]	1025
Kinematic viscosity of water	[m^2/s]	1.14E-06
Atmospheric pressure	[Pa]	102500
Vapour pressure	[Pa]	1700
Surface roughness	[µm]	0.00003

The propellers were meshed in accordance with Lloyd’s and PROCAL developer’s recommendations, see section 2.3.2. The tip spacing was set to 0.3 and the TE-spacing to 0.06 times the recommended value. This was since experience and previous validation studies have shown to give good results with these settings.

The velocity was set to match the reasonably high load $0.5 * J_{\eta_{Max}}$. A steady analysis was performed and the wake panel and axial force radial distribution were studied. If the curves showed reasonably smooth distributions and the Kutta-condition was converged, the solution was considered trustworthy. The Kutta condition was set to 0.001 and the jacobian disturbance value was set to 0.0001 for all cases. If the solution wasn’t trustworthy, the trailing edge spacing, tip spacing and tip chord fraction were altered. Great care was laid on getting the last trailing edge element skew angle to be sufficient. This angle should be in the interval $5^\circ < \beta < 30^\circ$ and preferably as close to 30° as possible. This angle is mostly affected by changing the tip chord fraction.

When the mesh was good enough the open water test could be performed by simply inserting the proper speeds matching the model test, i.e. $V_A = JnD$. If the solution was trustworthy for all advance velocities, the solution was considered converged.
Table 5.**2** shows the final open water mesh setups for the SMP’11 propeller, CPP1 and CPP2.

Table 5.2: The open water mesh setups in PROCAL for the SMP’11 propeller, CPP1 and CPP2.

Propeller	**SMP'11**	**CPP1**	**CPP2**
Panels LE to TE	30	30	30
Panels Root to Tip	30	30	30
Spacing at LE	0.003	0.003	0.003
Spacing at TE	0.00126	0.00305	0.00400
Spacing at Root	0.00780	0.00302	0.00299
Spacing at Tip	0.003	0.003	0.005
Tip Chord Fraction	0.6	0.4	0.57

5.2 Cavitation Measurement of the SMP’11 Propeller

For the cavitation analysis of the SMP’11 propeller, PROCAL was used. The cavitation prediction had to be preceded by an unsteady non-cavitating prediction to determine the non-cavitating K_T, which was governing for the design point in accordance with Table 3.4. The mesh setup for the cavitation free analysis was the same as presented in Table 5.2. The analyzed number of revolutions was six and the number of steps between blades was twelve.

The speeds had to be altered to match the thrust identity. This was done in the same way as for the velocity field measurement, i.e. the linear relationship between J and K_T was used.

The atmospheric pressure was computed from the cavitation number using eq. 5.1. [18]

$$p_a = 0.5\rho(nD)^2\sigma_n + p_v - \rho g H \qquad (5.1)$$

Where p_a *= the atmospheric pressure;* ρ *= the fluid density; n = number of revolutions per second; D = the propeller diameter;* σ *= the cavitation number;* p_v *= the vapor pressure; g = 9.81* m/s^2 *and H = the propeller submergence*

Finally, a cavitation mesh was set up. When cavitation should be solved in a boundary element method, the solution is very leading edge sensitive. [11] For this reason, the number of panels leading edge to trailing edge was increased to 70 panels and the leading edge spacing was reduced to 0.001. The number of panels root to tip was decreased to 20 to save some computation time.

5.3 Automation of the Pre-and Post-processing

This section describes how the pre- and post-processing of PROCAL was automated. All scripting were programmed in Visual Basic [26] (VBA). For a more detailed description, example of a PROCAL control file and the VBA code, see Appendix E.

5.3.1 The Pre-processing

PROCAL needs a control file and a geometry file to perform an analysis. By having those two files preset with the open water proceedings found in section 5.1 and exported to a location where the analysis should be performed, the pre processing could be considered automated. A grid dependence study needs to be performed before the open water characteristics can be analyzed. Therefore one regular control file with one speed and one control file with many ship speeds were programmed separately.

The geometry file was already pre-set in the design workbook when the automation work started. Only the lines containing operating conditions and meshing parameters needs to be changed in the control file. In PROCAL, both files are read in the free format, i.e. spaces are ignored. For this reason, the generation of the control file was decided to take place in Excel. By simply copying a control file from PROCAL, put it in an Excel sheet and letting commas be separators for new cells, the lines in the control file could be manipulated. The recommendations in section 2.3.2 were applied for the meshing parameters. The operating conditions in the regular control file were set to be in accordance with the operating conditions specified in the blade design sheet. V_A, RPM and reference velocity (V_{ref}) were set in accordance with eq. 5.2-5.4

$$V_A = V_S * (1 - w) \tag{5.2}$$

$$n = \frac{RPM}{60} \tag{5.3}$$

$$V_{ref} = n * D \tag{5.4}$$

Where V_S=the ship speed and w=the effective wake fraction

A new sheet for combined pre- and post processing was made in the design workbook; the openWaterResults-sheet. This sheet was given the three input cells Jmin, Jmax and Jstep. The names are quite self explanatory; the minimum and maximum value of the advance ratio and the step size to be analyzed between these points should be given. From this the number of advance ratio steps is calculated by eq. 5.5.

$$nj = \frac{J_{Max} - J_{Min}}{J_{Step}} + 1 \tag{5.5}$$

A code developed to generate the open water control file reads these four inputs, calculates the ship speeds and puts them in order in the control file in accordance with the demanded PROCAL format.

To continue the analysis with the defined geometry and control file, some kind of export from Excel to text files was needed. A script was made that reads the cells in the Excel sheets and saves them in a text file in a specified location with a format supported by PROCAL.

Three sub routines; one for exporting the geometry, one for exporting the regular control file and one for exporting the open water control file, was made. These subroutines were linked to one button each in the geometry file sheet in the design workbook, see Fig. 8.59. The pre-processing could now be considered automated, since only opening PROCAL, hit the “mesh” and the “perform analysis” button needs to be pressed to get a completed analysis. This is either for the design speed or for the complete open water diagram.

5.3.2 The Post-processing

With the pre-processing automated, it was time to make automatic post-processing. The PROCAL result files always have the same file names. The location of the files is known, since the control and geometry file are put there from the automatic pre-processing.

A script for reading the results was made. First it opens the results file. It loads it into Excel and cleans it to get the values free from text and number separators. It searches for the cell in the beginning and the end of the open water results section in the file and gets the cell’s addresses. An interval between these addresses is specified. Every line of open water data, i.e. K_T, K_Q and η_o, ends with a right curly bracket in the result file. If-cases determine whether the cell in the interval is a value or not. If it is a value, the value is outputted in the PROCAL results table in the openWaterResults-sheet. When a right curly bracket is found, it switches column and continues to print values. When three of those signs are found, the code stops. Every if-case has a row counter that defines at which row the new value should be put. The rows were set to run from 1 to nj.

By recording a macro that plots the results, sets a Berg Propulsion diagram template and puts the plot in the openWaterResults-sheet in Excel, a plotting sub-routine was made. The sub routine was declared as public and can thereby be called for the other result tables, i.e. Wageningen Series, lifting line method and CFD. Since the open water results predicted by PROCAL are read, put in a table and plotted in the design sheet at a button-click, the post processing can be considered automated.

6 Proceedings of the Lifting Line Method

This section describes how the lifting line method was used. It was automated directly, so the same procedure was used for all propellers. Therefore no sub sections are needed in this section.

There were not many parameters to change in the lift line code. The developers strongly recommended that the parameters shouldn’t be changed, so it was decided to let the defaults be trustworthy. [24] Only geometrical aspects needed to be changed to predict the open water behavior of a propeller.

The lifting line software was provided as an Excel workbook with macros. To call the macros, the sheet had to be open and propeller geometry inputs had to be put at certain cells in the workbook. The solution was to link the blade design workbook to the lifting line workbook. Pitch, rake, skew etc. were called as functions from the values presented in the blade design sheet. With the proper values inserted in the lift line workbook and the J_{Max}, J_{Min} and J_{Step} values from the openWaterResults-sheet inserted as well, the user only has to open the lift line workbook and press the OW calculation-button.

The results from the lift line workbook are put in a Results-sheet. A VBA code was made that reads the values from the known starting row and column and ends at the known end column and end row of the lift line results sheet. A staggered for-loop running through first columns and then rows was used to extract data at a specified row and column in the lift line workbook and put at a specified row and column in the openWaterResults-sheet. The code for data extraction can be seen in Appendix F. The result extracting code was linked to a button in the openWaterResults. Consequently only two buttons need to be pushed to perform an open water analysis with the lifting line method and the code could thereby be considered automated.

(This page is intentionally left blank)

7 Proceedings of the Wageningen Series

This section describes how the Wageningen Series was used for open water predictions and how it was automated. Section 7.1 describes how the Wageningen Propeller Series Program was used on the SMP'11 propeller, since this was the first step in the exploration of the program functionality. Section 7.2 describes how the results of the predictions were scaled to full scale, since this was necessary for the predictions of CPP1 and CPP2. The final sections, section 7.3 and section 7.4, describe how the automation of the Wageningen Series and the full scale extrapolation was performed.

7.1 Open Water Prediction of the SMP'11 Propeller

The Wageningen series program Wageningen Propeller Series Program was used for the SMP'11 propeller. The propeller has a P07/D of 1.635 and a blade area ratio of 0.77896. Four open water characteristics tables were extracted, since neither the blade area ratio, nor the P07/D could be calculated directly in the program. The contains of the generated tables is summarized in Table 7.1

Table 7.1: A summary of the tables used for the Wageningen interpolations

Table:	**1**	**2**	**3**	**4**
EAR	0.75	0.9	0.75	0.9
P07/D	1.55	1.55	1.6	1.6

One table was interpolated between table 1 and table 2, yielding results at the proper blade area ratio, but at too low pitch. Table 3 and 4 was also interpolated to yield another table with the proper blade area ratio, but at another too low pitch. These two new tables with the too low pitches were extrapolated into one table with the correct pitch.

7.2 Viscous Scale Effects Correction

Since the Wageningen results are given in model scale, the results needed to be scaled to full scale to be compared to the CFD and the lifting line method results. This was performed using the equations described in section 2.7, where the full scale values were taken from the propeller to be analyzed and the model values from the model test reports. This had to be done for CPP1 and CPP2.

7.3 Automation of the Pre-and Post-processing

This section describes how the pre- and post-processing of the Wageningen series was automated. The VBA code that was made is presented in Appendix G.

The Wageningen method consists, as mentioned, of a lot of charts from which results can be withdrawn as a function of pitch, blade area ratio, number of blades and advance ratio. Since the Wageningen Propeller Series Program uses the polynomials, the easiest way to automate would be to program the polynomials directly into VBA. The polynomials are divided in two; one for K_T and one for K_Q. These polynomials were already at hand at Berg Propulsion, so they were programmed into separate VBA-functions.

The polynomials were programmed so that pitch, blade area ratio and number of blades were picked in the design-sheet. The remains were K_T and K_Q as function of advance ratio. These functions were called getKt and getKq in the code. The advance ratios were computed using eq. 5.5. They were programmed to be inserted in order in the leftmost column of the Wageningen table.

The VBA script loops through the given number of steps of J and in each step it gets the J-values from the column defined for the Wageningen table. K_T and K_Q are calculated from getKt and getKq. The open water efficiency is calculated from eq. 2.22. Since π, which is used in this equation, wasn't declared in VBA, it was hardcoded as in eq. 5.6.

$$\pi = 4 * \arctan(1) \tag{5.6}$$

At each step in the loop, the results are inserted in the proper columns of a table in the openWaterResults-sheet in the design workbook. This script was linked to a button in the openWaterResults-sheet. The open water characteristics according to the Wageningen Series are hence both calculated and inserted in the design workbook at a button click. Consequently the pre- and post-processing were automated.

7.4 Automation of Extrapolation to Full Scale

The extrapolation to full scale was automated by first programming a public sub routine containing the equations in section 2.7. First the variables P075/D, c075 and t075 in full scale were needed. The values are only given at radial sections R0.7 and R0.8 in the design workbook. To get the values at R0.75 a linear interpolation was made, where the sum of the properties at each of the above mentioned radial sections were divided by two. The diameter and number of blades were also picked from the design sheet. k_p was set to 30 μm. To get the chord length at model scale, the c075 was divided by the model scale factor. The open water efficiency was calculated as in section 7.3.

The function was programmed to get the values to be scaled, i.e. K_T and K_Q, as inputs together with strings containing the places at which the table with the scaled values should be placed.

The subroutine starts by inserting the input J-values in the leftmost column of a table in the openWaterResults-sheet. The script then loops through the declared number of steps of J. The corrections are made. The corrected K_{TS} and K_{QS} are inserted in the columns specified when calling the sub routine.

8 Results

This section discusses and presents all results from the project. Section 8.1 reviews the results from the SMP'11 Workshop test cases. Section 8.2 and 8.3 reviews the open water characteristics results of CPP1 and CPP2 respectively. An overlay discussion of the four methods can be read in section 8.4. Section 8.5 to 8.7 describes what happens when the automation scripts are used.

8.1 Results from the SMP'11 Propeller

This section is divided into three sub sections, each describing the results of one of the three cases of the SMP'11 workshop. It should be noted that all analyses of SMP'11 was performed as blind tests, i.e. no model test data was available when the tests were performed.

8.1.1 Case 2.1: The Open Water Test

The first part of this section is describing the resulting CFD grid and the results of the grid dependence study for the SMP'11 open water prediction. After this the validity of the CFD and boundary element method setups are discussed, since they yield more setup sensitive results than the other methods. Finally the results of CFD, boundary element method, lifting line method and Wageningen Series predictions are presented.

The final coarse and fine mesh for the open water test of the SMP'11 propeller are visualized with a centre plane cut in Fig. 8.1 and
Fig. 8.2. As can be seen the most significant difference is the cell distribution. The resolution close to the propeller and in the slip stream is significantly refined for the fine mesh. The cells in the domain region are slightly larger for the fine mesh as well. The cells close to the domain walls are slightly smaller than the free stream cells for both meshes. This depends on the transition from the triads on the domain surface mesh to the hexahedrons in the free stream volume; polyhedrons are usually smaller than structured hexahedrons.

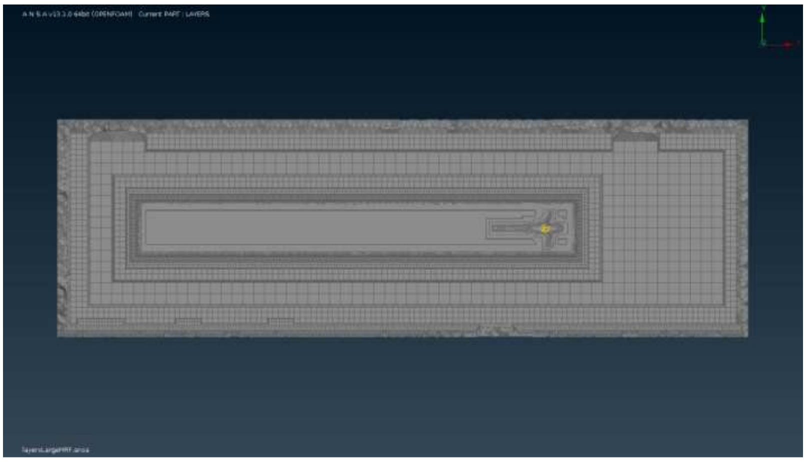

Fig. 8.1: The coarse mesh for the open water test

Fig. 8.2: The fine mesh for the open water test

The grid dependence comparison from J=0.6 to J=1.2 is presented in Table 8.1. The results are also plotted in Fig. 8.3. The grid dependence is very small; the result is almost unchanged between the two meshes. The difference should depend on the discretization error and the resolution of the gradients in the slip stream. The region around the propeller was also refined more in the fine mesh. The gradients in this region should also affect the results to some extent.

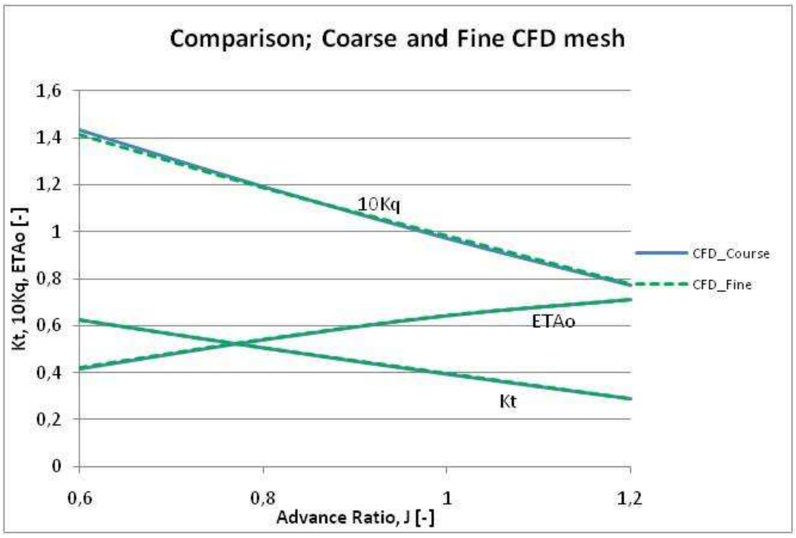

Fig. 8.3: A comparison between the coarse and the fine mesh for the CFD simulation of the SMP'11 propeller

Table 8.1: A comparison between the coarse and the fine mesh for the open water simulation of the SMP'11 propeller

J	**Kt coarse**	**Kt fine**	**Kq coarse**	**Kq fine**	**η_o coarse**	**η_o fine**
0.6	0.624	0.623	1.431	1.415	0.416	0.421
0.8	0.504	0.505	1.190	1.189	0.540	0.541
1	0.392	0.397	0.970	0.984	0.643	0.643
1.2	0.287	0.289	0.770	0.778	0.712	0.710

The y^+ values at the blades for the coarse and the fine mesh is presented in Table 8.2. They differ more between the fine and the coarse mesh than the forces. The prism layers were of the same size in orthogonal direction to the wall for both meshes. On the other hand, the surface mesh resolution on the blades was higher for the fine mesh. y^+ is proportional to the rate of change in normal direction to the wall of the velocity parallel to the wall, i.e.

$$y^+ \sim \sqrt{\frac{\partial u}{\partial y}}$$

[25] With more points to measure the gradients at the wall, the difference might be explained.

Table 8.2: The y^+-values at the blades for the coarse and fine mesh at corresponding advance ratios

J	**y^+ coarse**	**y^+ fine**
0.6	34	30
0.8	26	31
1	25	34
1.2	25	34

The axial velocity distribution of the open water test at J=0.6 is visualized in Fig. 8.6. J=0.6 was the lowest advance ratio tested for the SMP’11 propeller. As can be seen, quite an amount of water is sucked in front of the propeller. The velocity field looks reasonable; the velocity is accelerated in the direction of the inflow velocity. A separation zone is developed behind the shaft. This could be avoided if the slide in Fig. 3.3 was modeled. It affects the velocity field behind the propeller disc and thereby the forces on the propeller, which to some extent might affect the results. The separation could be reduced by replacing the flat end of the shaft with a sphere. On the other hand the forces were computed over the blades only, so the impact of the separation zone should be of small significance.

The radial wake strength (PHIW) and radial axial force (F_x) distributions of the SMP’11 propeller at $0.5J_{\eta Max}$ in the PROCAL open water prediction can be seen in Fig. 8.4. As can be seen they are smooth and the maximum load appears at the sections were most work should be performed, vouching for reliable results.

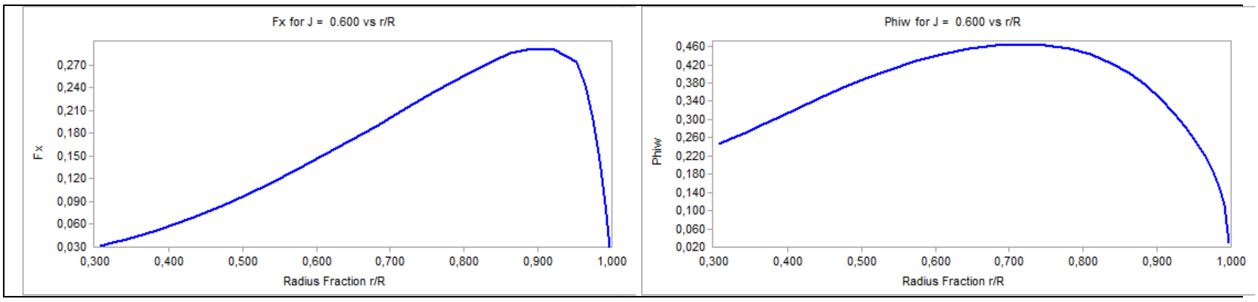

Fig. 8.4: F_x distribution to the left and PHIW to the right at $0.5J_{\eta Max}$ for CPP1

The results from the CFD simulations compared to the model test results can be seen in Fig. 8.5. As can be seen the prediction is very accurate until J=1.4. Note again that this prediction was performed as a blind test.

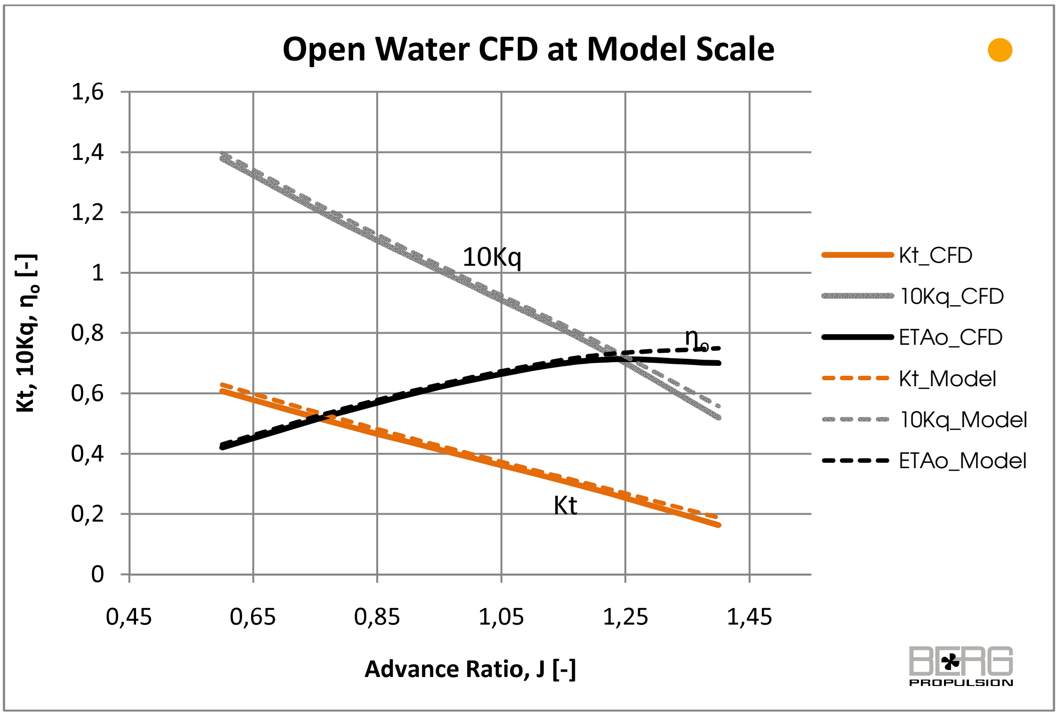

Fig. 8.5: The open water chart predicted by CFD compared to model test results for the SMP'11 propeller

The pressure distribution on the pressure side of the blades and hub in the open water test at J=0.8 and J=1.4 is visualized in Fig. 8.7 and Fig. 8.8 respectively. As can be seen in Fig. 8.8, separation occurs at J=1.4 and not for a speed before $J_{\eta_{Max}}$, as in Fig. 8.7. The separation after $J_{\eta_{Max}}$ might be over predicted due to the fact that wall functions are used and that the flow is assumed steady. This is not true for turbulence and especially not in model scale, where the turbulent flow isn't fully developed everywhere as the wall functions state. The over predicted separation results in lower thrust, hence explaining the $J_{\eta_{Max}}$ in the last point.

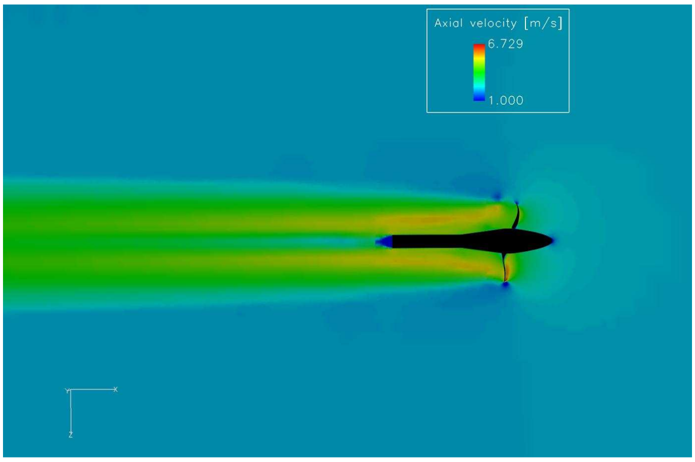

Fig. 8.6: The axial velocity distribution for the open water test at J=0.6

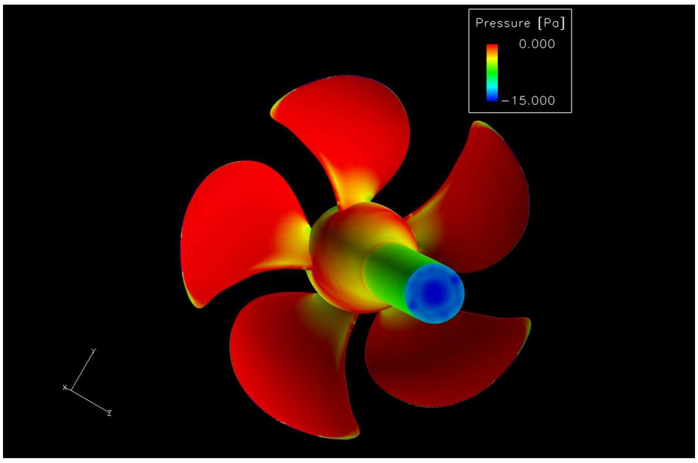

Fig. 8.7: Pressure distribution of the pressure side from the open water test at J=0.8 Note the overall high pressure distribution.

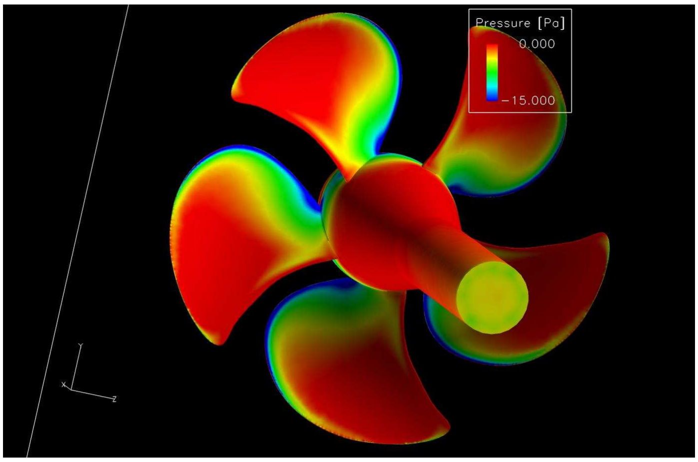

Fig. 8.8: Pressure distribution of the pressure side from the open water test at J=1.4. Note the low pressure region at leading edge, indicating separation on the pressure side.

The open water prediction of the SMP’11 propeller by PROCAL compared to the model test results can be seen in Fig. 8.9. The prediction is quite accurate. K_Q is slightly higher in the prediction, resulting in a little lower efficiency. This is reasonable since the hub is present in the PROCAL computation.

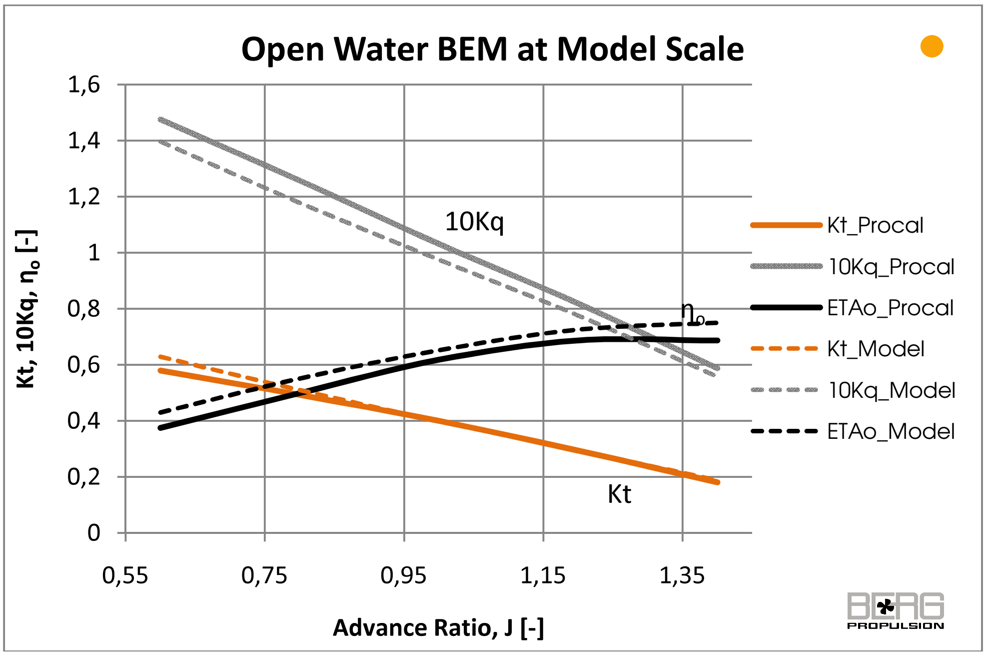

Fig. 8.9: The open water chart predicted by the boundary element method compared to model test results for the SMP'11 propeller

The open water prediction of the SMP'11 propeller by the lifting line method compared to the model test results can be seen in Fig. 8.10. The propeller predicted by the lifting line method seems to be too heavy. It should be noted that the effect from the hub is excluded in the model test force measurement. This should of course result in higher K_T than if the hub was present, since the hub would work in the counter direction of the thrust. The lifting line results, on the other hand, points in the opposite direction. The skew of the propeller is below 20°, which should benefit the lifting line calculation.

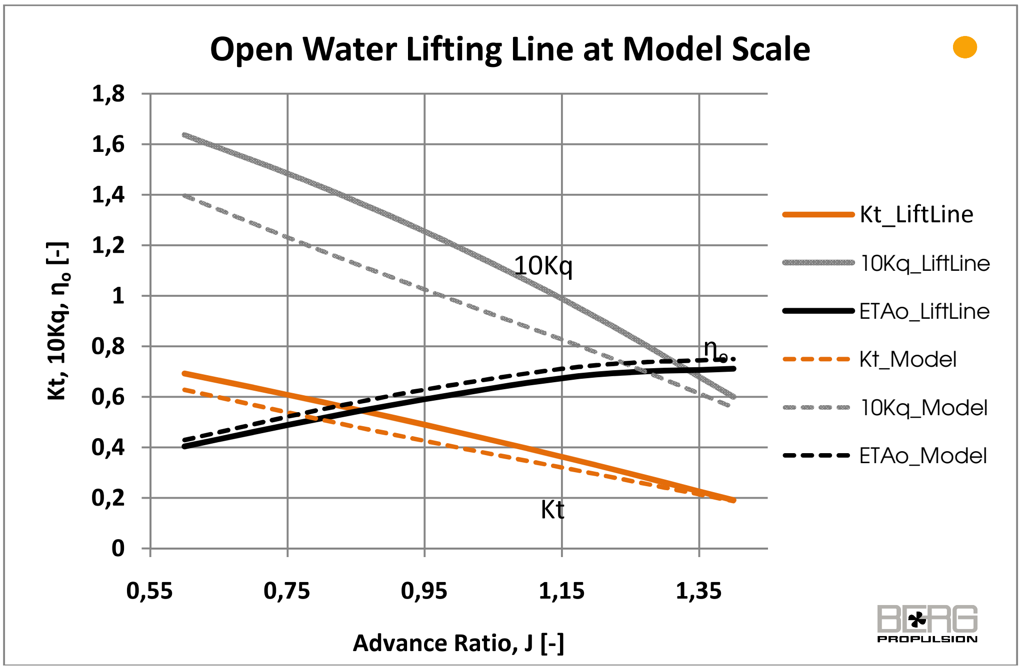

Fig. 8.10: The open water chart predicted by the lifting line method compared to model test results for the SMP'11 propeller

The open water prediction of the SMP'11 propeller by the Wageningen series compared to the model test results can be seen in Fig. 8.11. In this prediction the propeller is too light, but the efficiency until the design point is well predicted. The lightness of the propeller is expected, since the pitch wasn't corrected for camber in the Wageningen prediction. The camber results in a higher virtual pitch. No blade area correction was applied either. These corrections could result in more accurate predictions.

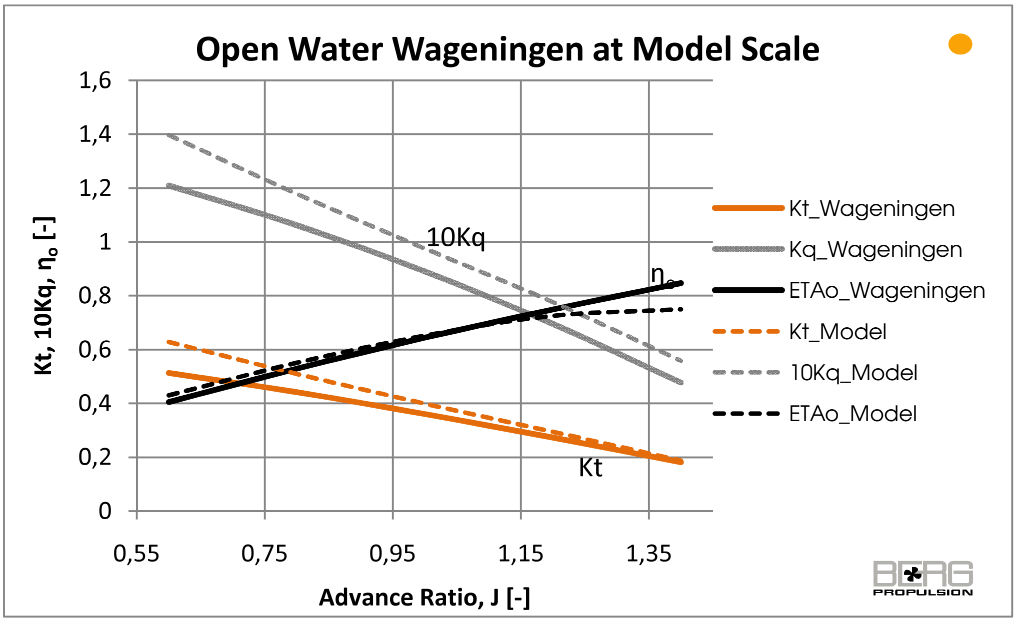

Fig. 8.11: The open water chart predicted by the Wageningen series compared to model test results for the SMP'11 propeller

8.1.2 Case 2.2: Velocity Field Measurement

This section first describes the resulting fine mesh for the velocity field measurement of the SMP'11 propeller. After this the validity of the setup is discussed. The last part of the section presents the results of the SMP'11 velocity field measurement and compares them to the CFD predictions.

The fine mesh used in the velocity field measurement is shown in Fig. 8.12. As can be seen, the mesh is very refined in the slip stream region. This is for the velocity gradients close to the propeller disc to be resolved and thereby preserving the tip vortex.

Fig. 8.12: The fine mesh used for the velocity field measurement

The velocity, corresponding K_T and corresponding y^+ for the fine mesh are tabulated in Table 8.3. y^+ tend to be higher than compared to the open water results, c.f. Table 8.2. This depends on that the inflow condition was changed to a push configuration with higher RPS and inlet velocity than for the open water test.

Table 8.3: Velocities and corresponding J, K_T and y^+ for the fine mesh of the velocity field measurement.

Va	**J**	**Kt**	**y^+**
7.204	1.25	0.2476	89
7.1867	1.25	0.2492	89

$V_A = 7.1867$ was chosen as working point, since it was closest to the thrust identity; $K_T = 0.250$. In Fig. 8.13 an iso-surface with helicity of 150 m^2/s^2 is shown to visualize the generated tip vortex. Helicity is the tendency of a particle to perform cork screw motions, which is exactly what happens to the particles in a tip vortex. The tip vortex is evident from this figure. If the cell resolution would be higher further downstream, the vortex would probably continue a bit further.

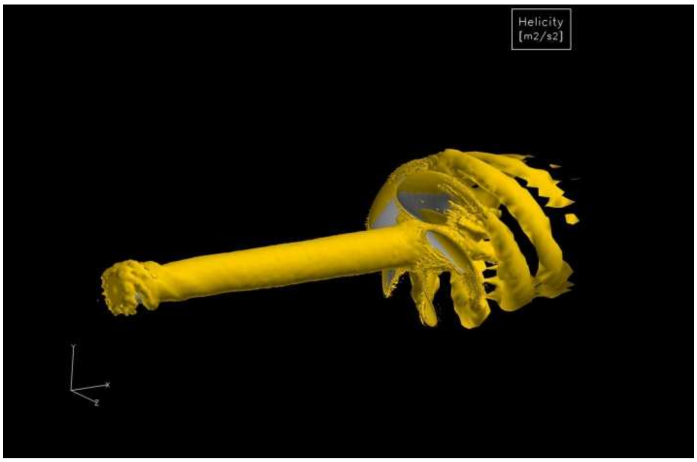

Fig. 8.13: Tip vortex with helicity of 150 $\mathbf{m^2/s^2}$ at the working point

For a better understanding of the results, the axial velocity field is shown in Fig. 8.14, and the pressure distribution of the propeller suction side is visualized in Fig. 8.15. As can be seen, no odd separation occurs at the blades and the velocity field looks stable. The boundary layer on the shaft looks stable too. The low pressure zone on the shaft indicates separation, which could have been avoided by setting the inlet at the beginning of the shaft. This small separation zone should not affect the results, though, since it is sufficiently far upstream, as can be seen on the boundary layer in Fig. 8.14.

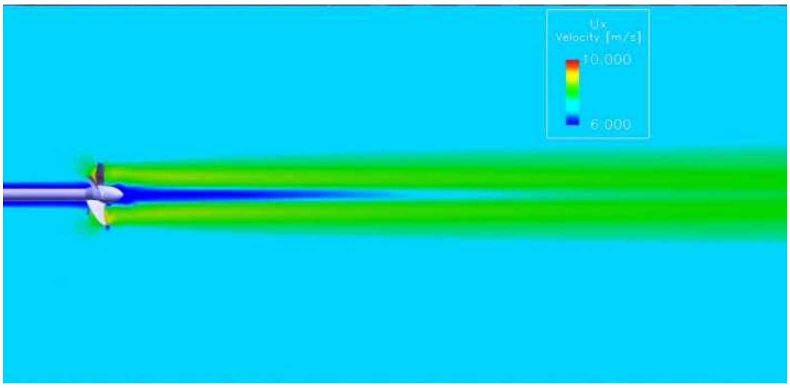

Fig. 8.14: The axial velocity field at the working point for the velocity field measurement

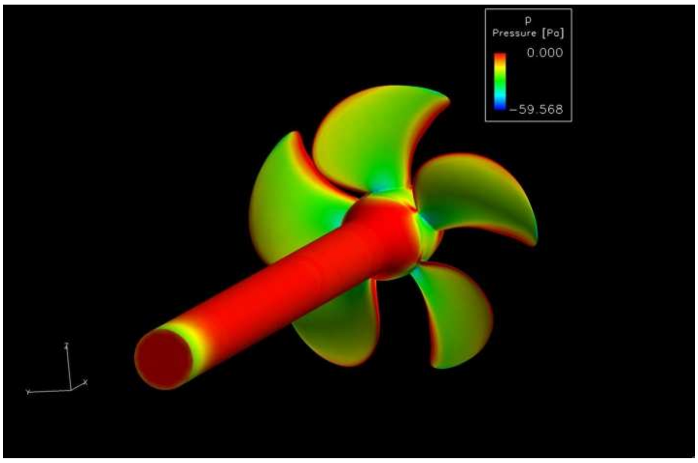

Fig. 8.15: Pressure distribution of the suction side at the working point for the velocity field measurement

The velocity field measurement at radius R0.7 in plane x/D=0.1 downstream the propeller disc is plotted in Fig. 8.16. The calculation is smooth, which is an effect of the averaged simulation (RANS). The prediction is quite good, as can be seen. The fluctuations in the model test depends on that the measured turbulence is real, and turbulence is fluctuating. The tendency of the velocity field is definitely caught by the calculations.

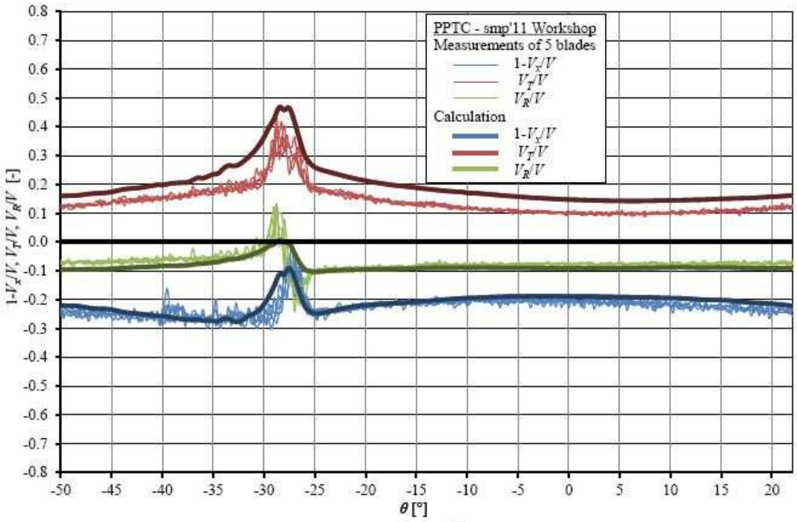

Fig. 8.16: The velocity field measurement results at R0.7 in plane x/D=0.1 for the SMP'11 propeller with non-dimensional axial, tangential and radial velocities from the prediction plotted against the model test. The thick line represents the calculation and the thin, fluctuating line represents the model test.

The velocity field measurement at radius R0.7 in plane x/D=0.2 is plotted in Fig. 8.17. The tendency is captured, but it should be noted that the tip vortex in the interval $-50^\circ \leq \theta \leq -45^\circ$ is not captured at all.

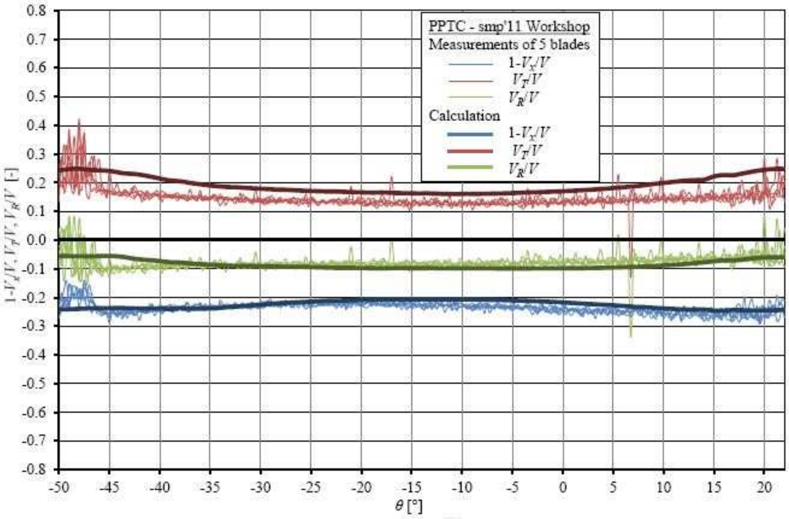

Fig. 8.17: The velocity field measurement results at R0.7 in plane x/D=0.2 for the SMP'11 propeller with non-dimensional axial, tangential and radial velocities from the prediction plotted against the model test. The thick line represents the calculation and the thin, fluctuating line represents the model test.

The velocity field measurement at radius R0.97 in plane x/D=0.1 is plotted in Fig. 8.18. The tip vortex is well captured. The axial field seems to be a little under predicted. The fluctuating behavior of the prediction should depend on that the solution wasn't entirely converged in this region. To achieve convergence there is hard.

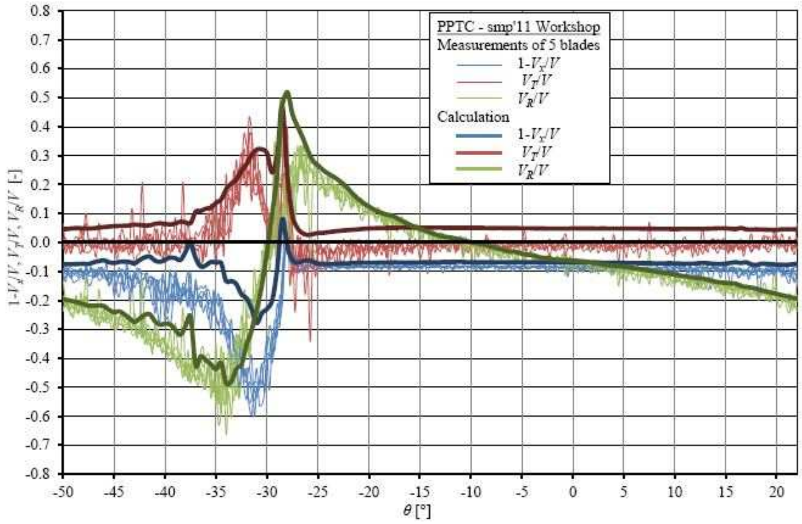

Fig. 8.18: The velocity field measurement results at R0.97 in plane x/D=0.1 for the SMP’11 propeller with non-dimensional axial, tangential and radial velocities from the prediction plotted against the model test. The thick line represents the calculation and the thin, fluctuating line represents the model test.

The velocity field measurement at radius R0.97 in plane x/D=0.2 is plotted in Fig. 8.19. Here it is more evident that the tip vortex is dissolved at plane x/D=0.2. The tendency of the velocities is captured until the vortex. The reason for the unresolved tip vortex will be explained later in this section.

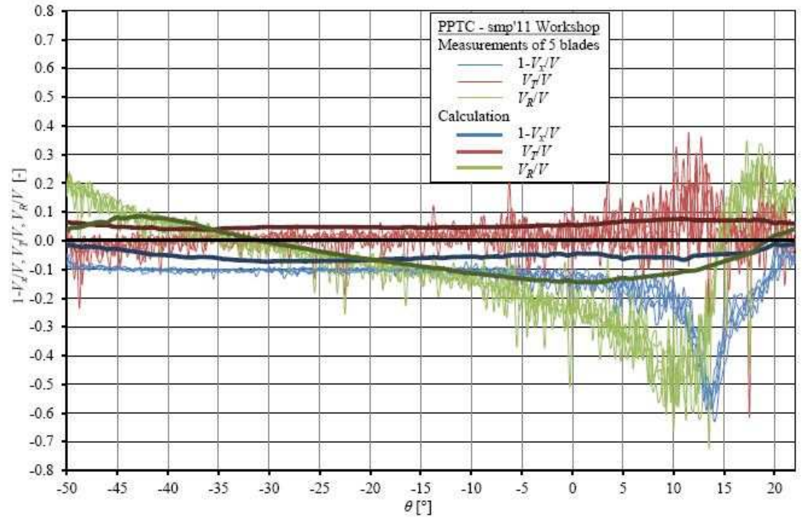

Fig. 8.19: The velocity field measurement results at R0.97 in plane x/D=0.2 for the SMP’11 propeller with non-dimensional axial, tangential and radial velocities from the prediction plotted against the model test. The thick line represents the calculation and the thin, fluctuating line represents the model test.

The velocity field measurement at radius R1.0 in plane x/D=0.1 is plotted in Fig. 8.20. This time all velocities seem well predicted. The fluctuations appear here as well as in Fig. 8.18. This should also depend on the convergence.

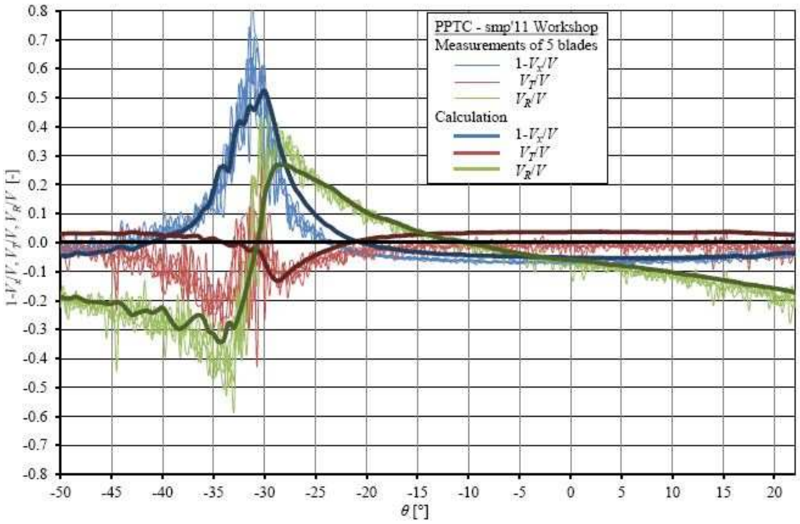

Fig. 8.20: The velocity field measurement results at R1.0 in plane x/D=0.1 for the SMP'11 propeller with non-dimensional axial, tangential and radial velocities from the prediction plotted against the model test. The thick line represents the calculation and the thin, fluctuating line represents the model test.

The velocity field measurement at radius R1.0 in plane x/D=0.2 is plotted in Fig. 8.21. As for the other measurements at x/D=0.2 the tendency is caught, but the tip vortex is dissolved.

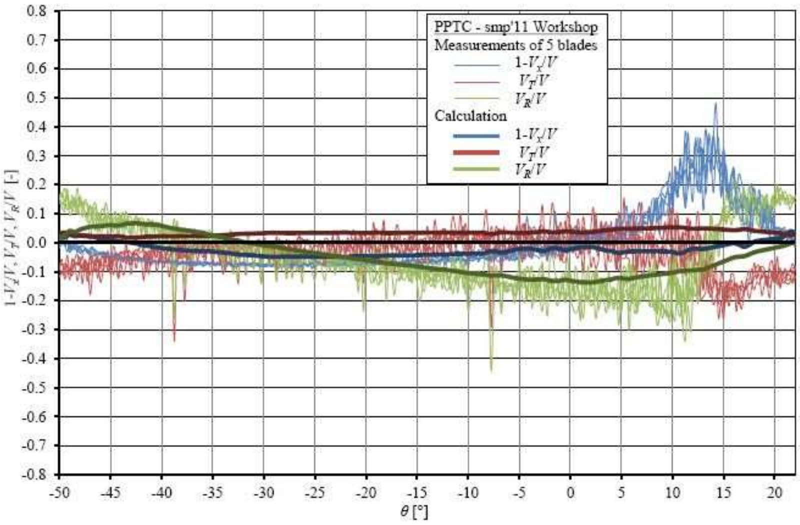

Fig. 8.21: The velocity field measurement results at R1.0 in plane x/D=0.2 for the SMP'11 propeller with non-dimensional axial, tangential and radial velocities from the prediction plotted against the model test. The thick line represents the calculation and the thin, fluctuating line represents the model test.

The axial velocity field downstream the propeller disc with the mesh visible is visualized at x/D=0.1 in Fig. 8.22. As can be seen, the mesh resolution is high near the blades. The convergence could have been disturbed by the large cells occurring between the blades. This issue could have been solved by using a stricter setting for the size box. Unfortunately this problem was not noted when the results were submitted to the SMP'11 workshop.

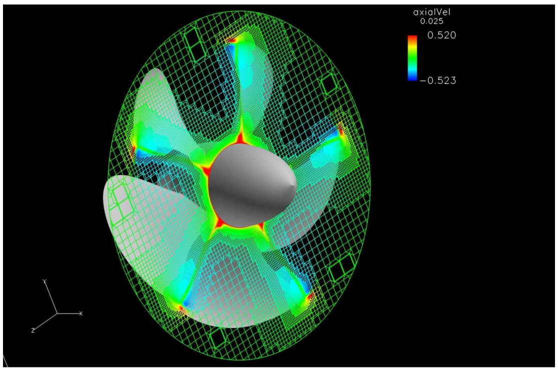

Fig. 8.22: The velocity field at x/D=0.1 downstream the SMP’11 propeller disc with the mesh visible and results of $\mathbf{1 - V_X/V}$.

The velocity field downstream the propeller disc with the mesh visible is visualized at x/D=0.2 in Fig. 8.23. It is evident that the mesh is coarser in this region, being the reason for the dissolved the tip vortex. Again a size box with stricter mesh settings should be used to avoid this.

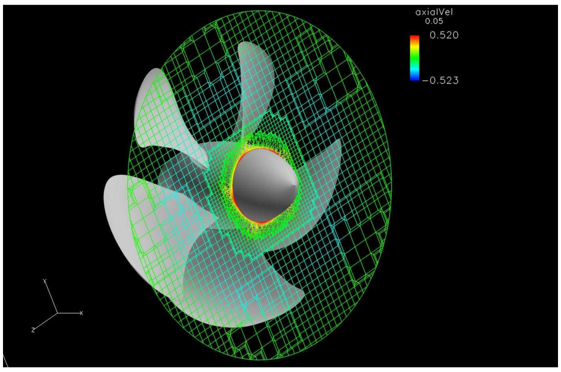

Fig. 8.23: The velocity field at x/D=0.2 downstream the SMP’11 propeller disc with the mesh visible and results of $\mathbf{1 - V_X/V}$.

The velocity field at x/D=0.1 downstream with smoothed shading can be seen in Fig. 8.24 to visualize the velocity field with resolved tip vortex. From this picture it can be seen that the results from Fig. 8.16, Fig. 8.18 and Fig. 8.20 are reasonable and that the gradients seem to be dissolved near the large cells in Fig. 8.22.

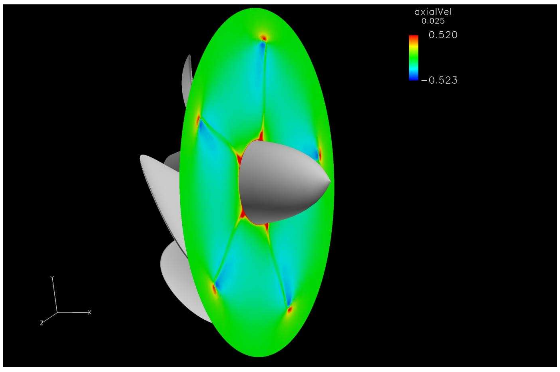

Fig. 8.24: The velocity field at x/D=0.1 downstream the SMP’11 propeller disc and results of $\mathbf{1 - V_X/V}$.

8.1.3 Case 2.2: Cavitation Tests

This section starts by showing the resulting non-cavitating and cavitating mesh of the SMP'11 propeller. It continues with discussing the validity of the setup and finally the results are shown.

The non-cavitating mesh used for finding the thrust identity is shown in Fig. 8.25. As can be seen, the mesh is rather orthogonal everywhere, which should yield reliable results. The trailing edge spacing is reduced to capture the shape of the sharp knuckle at trailing edge.

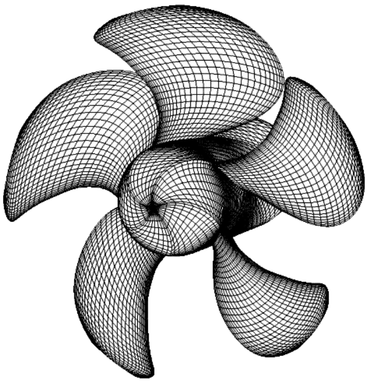

Fig. 8.25: The non cavitating mesh for the cavitational analysis

The cavitation mesh is shown in Fig. 8.26. This mesh is the same as the non-cavitating mesh, but with increased number of panels trailing edge to leading edge and decreased leading edge spacing.

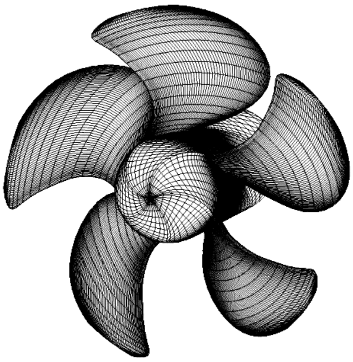

Fig. 8.26: The cavitation mesh for the cavitational analysis

Table 8.4 shows the advance ratio needed to fulfill the non-cavitating thrust identity for each of the three cavitation cases. As can be seen the highest load occurs at case 2.3.1. Case 2.3.3 is past the efficiency top point in the open water diagram, c.f. Fig. 8.5, meaning that pressure side cavitation could be expected.

Table 8.4: Velocities, corresponding J and corresponding $\mathbf{K_T}$ to fulfill the thrust identity of the cavitation free condition for the three cavitation cases.

Case	Va	J	Kt
2.3.1	6.269	1.00	0.387
2.3.2	7.986	1.28	0.245
2.3.3	8.987	1.44	0.167

F_x and PHIW at $\phi = 0$ for case 2.3.1 are shown in Fig. 8.27. The same distributions, but for case 2.3.2 and 2.3.3 are shown in Fig. 8.28 and Fig. 8.29. These distributions vouch for converged and reliable results. The smooth distribution of F_X implies that the load is evenly distributed over the blade radius with a maximal load at approximately $0.7 \leq r/R \leq 0.85$, which is expected, since the pitch is highest in this region. The smooth distribution of PHIW suggests that the wake panels are correctly distributed and well described.

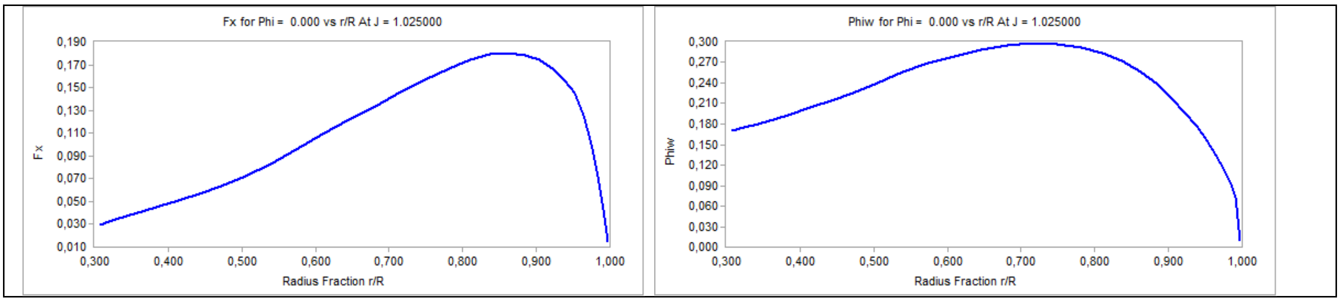

Fig. 8.27: $\mathbf{F_x}$ distribution to the left and PHIW to the right at $\boldsymbol{\phi} = \mathbf{0}$ for case 2.3.1

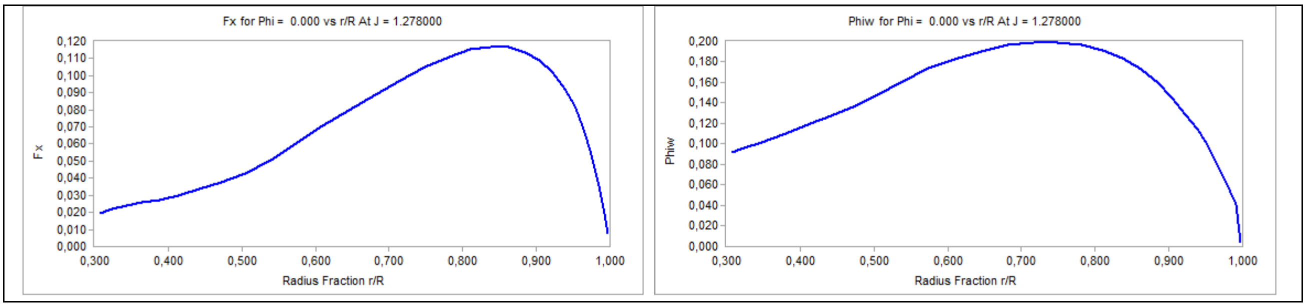

Fig. 8.28: $\mathrm{F_x}$ distribution to the left and PHIW to the right at $\phi = 0$ for case 2.3.2

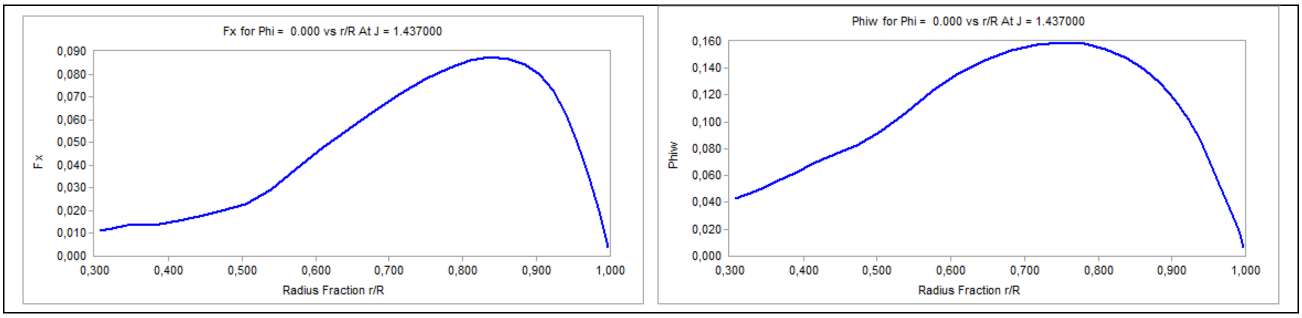

Fig. 8.29: $\mathrm{F_x}$ distribution to the left and PHIW to the right at $\phi = 0$ for case 2.3.3

The zero degree position is characteristic for the rest of the radial results, which hence would be inadequate to include. The cavitation pattern predicted and a sketch of the model test results for case 2.3.1 can be seen in Fig. 8.30. The cavitation pattern along the leading edge is over predicted, a tendency that has been captured before [30]. The blade root cavitation and the free stream cavitation were not captured in the prediction. This could depend on the detachment mode of the solver. In this calculation detachment was possible from leading edge until 0.8 times the chord length. Another approach would be to start searching on the regions of minimum pressure. The cavitating K_T was well predicted.

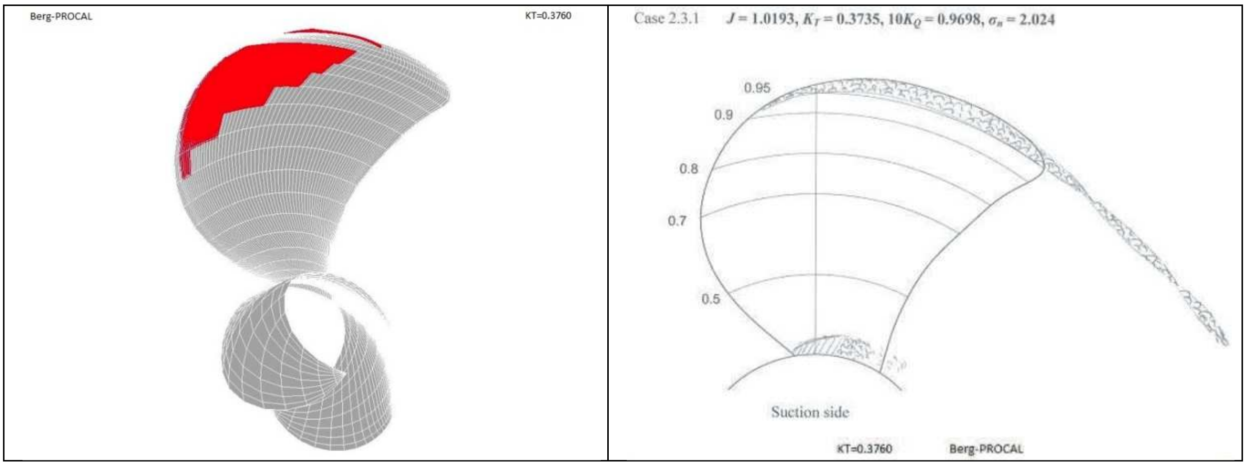

Fig. 8.30: The cavitation pattern on the suction side predicted by PROCAL to the left and model test result to the right for case 2.3.1

The cavitation pattern predicted and a sketch of the model test results for case 2.3.2 can be seen in Fig. 8.31. This is the design point, which occurs at a rather low load. Again, neither the blade root cavitation nor the free stream cavitation was captured. The cavitating K_T was not well predicted.

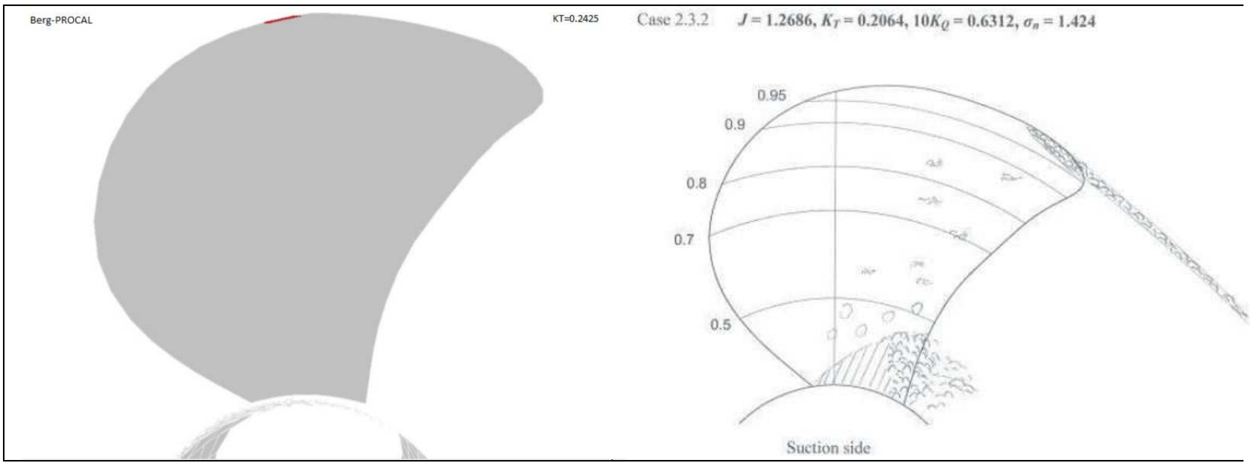

Fig. 8.31: The cavitation pattern on the suction side predicted by PROCAL to the left and model test result to the right for case 2.3.2

It should be noted that Fig. 8.30 and Fig. 8.31 shows only suction side cavitation, since pressure side cavitation didn't occur in the predictions. Case 2.3.3, on the other hand, has a lot of pressure side cavitation. PROCAL recognizes when pressure side cavitation occurs, but cannot calculate it. Therefore case 2.3.3 did not, as expected, show any cavitation at all.

8.2 Open Water Results from CPP1

This section starts by discussing the results of the template setup comparison mentioned in section 4.4.2. After this the validity of the CFD and boundary element method setups are discussed. Further, the predictions from CFD, boundary element method, lifting line method and Wageningen Series are compared to model test results and discussed. Finally results from PROCAL predicted in model scale compared to model test results are shown to validate the viscous correction script.

The comparison between the different setup methods for the CFD-script open water setup template can be seen in Table 8.5. As can be seen, the difference between a MRF zone that is 1.5 times larger and a regular one gives negligible difference. The difference between the short shaft and the long shaft is larger. This should of course depend on that the boundary layer developed over the long shaft is larger, increasing the load at the blade root. This statement is strengthened by the comparison between the long shaft with and without spherical end cap. When the end cap is present the load at the root gets lower, since the boundary layer gets smaller. The long shaft gave the results closest to the model test, suggesting that the development of a proper boundary layer is important for the results. Therefore the pull arrangement, yielding the best results, was introduced.

Table 8.5: A comparison of the results when the open water setups were changed

J=0.499	Kt	Kq	y+ (blades)
Spherical end cap:	0.1579	0.0215	121
Spherical end cap, MRF 1.5 times larger	0.1579	0.0215	121
Long shaft:	0.1639	0.0229	121
Long shaft, spherical end cap	0.1569	0.0214	121
Pull arrangement	0.1616	0.2029	121

The averaged y^+ values at the blades for CPP1 from the open water prediction can be seen in Table 8.6. As can be seen, the y^+ values are reasonable and large enough to yield reliable results with wall functions.

Table 8.6: The averaged y^+ values at the blades for CPP1 from the open water test.

J	0.1	0.2	0.3	0.4	0.5	0.6	0.7	0.8
y^+ OW mesh	133	133	134	135	136	136	137	139

The axial velocity field at J=0.4 is visualized in Fig. 8.32. As can be seen it looks symmetrical and the velocity distribution is intuitive.

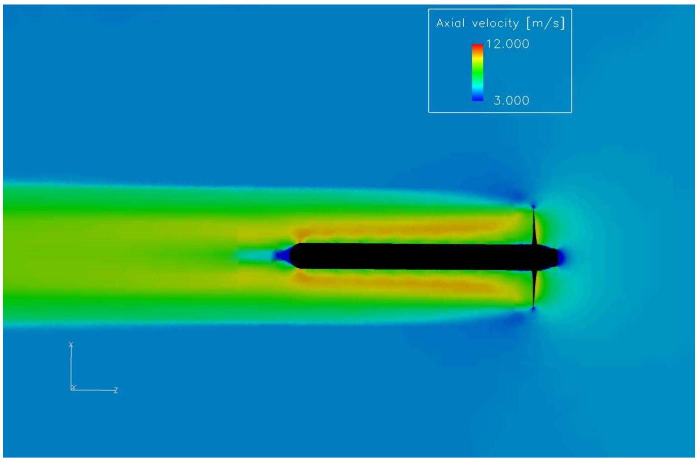

Fig. 8.32: Axial velocity field for CPP1 at J=0.4

The PHIW and F_x distributions of CPP1 at $0.5J_{\eta_{Max}}$ in the PROCAL open water prediction can be seen in Fig. 8.33. As can be seen the distribution is smooth and the highest loads occurs at expected radial sections.

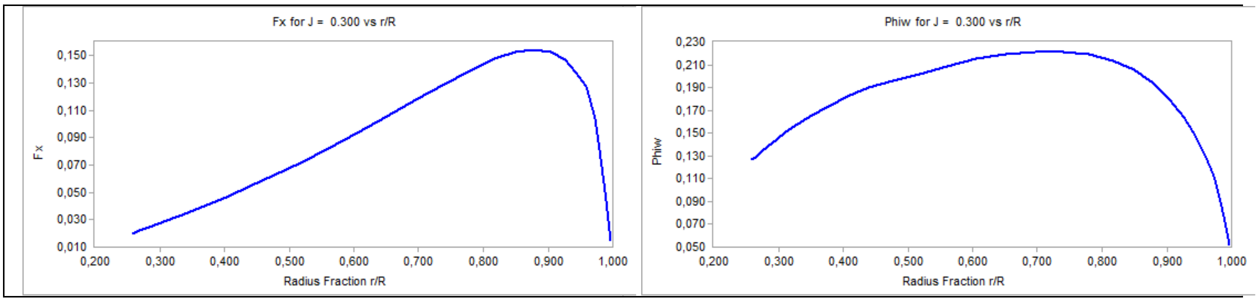

Fig. 8.33: $\mathrm{F_x}$ distribution to the left and PHIW to the right at $0.5J_{\eta_{Max}}$ for CPP1

The results from CFD at full scale compared to the model test results can be seen in Fig. 8.34.

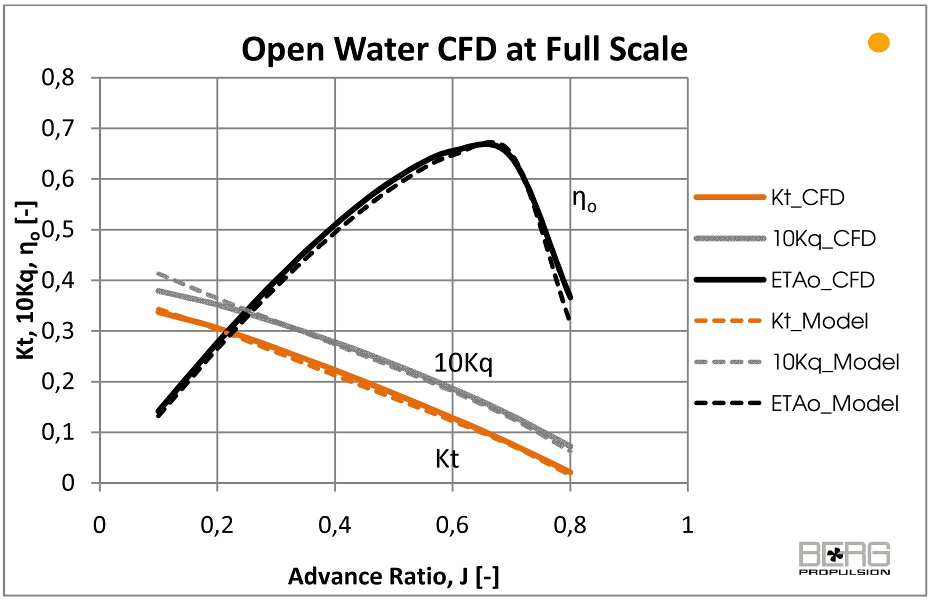

Fig. 8.34: The open water chart predicted by CFD in full scale compared to the model test results scaled to full scale for CPP1

As can be seen, the simulation is very accurate. K_Q differs a little bit in bollard pull, which is discussed further in section 8.3. This also happens after $J_{\eta_{Max}}$, which is discussed further in section 8.1.1.

The results from the boundary element method compared to the model test results scaled to full scale can be seen in Fig. 8.35. As can be seen the approximation is very good. Both K_T and K_Q are slightly over predicted until the design point, resulting in a slightly higher efficiency. Note that this is for CPP1, which is a very smooth propeller.

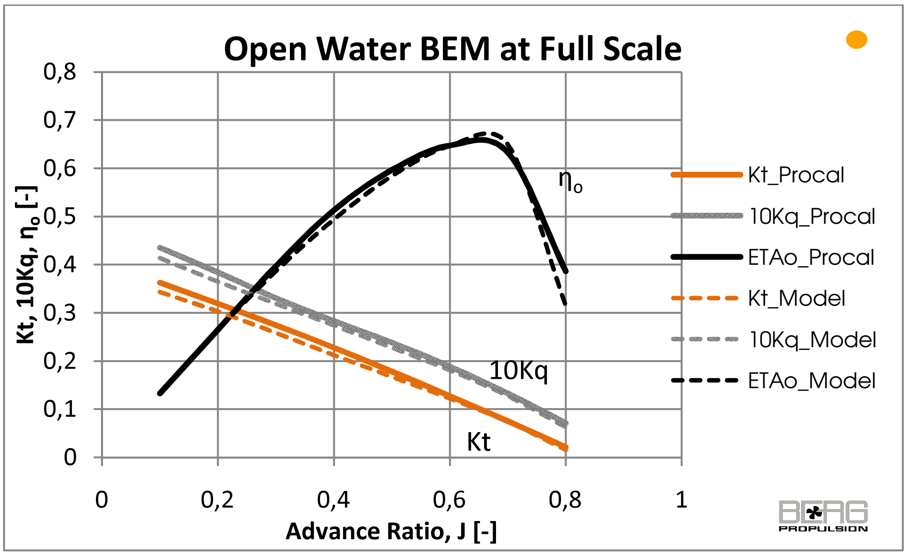

Fig. 8.35: The open water chart predicted by the boundary element method compared to model test results scaled to full scale for CPP1

The results from the lifting line method compared to the model test results scaled to full scale can be seen in Fig. 8.36. These results are significantly better than the results from the SMP'11 propeller. The prediction tends to over predict the efficiency somewhere around the design point. This is a result of a under predicted K_Q. The skew of CPP1 is 34°, which should result in problems for the lifting line method.

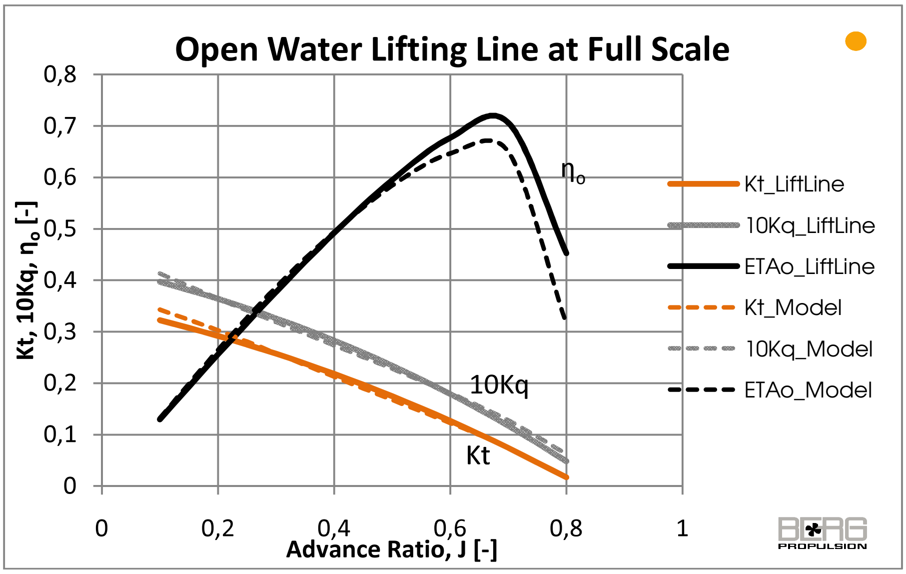

Fig. 8.36: The open water chart predicted by the lifting line method compared to model test results scaled to full scale for CPP1

The results from the Wageningen series compared to the model test results scaled to full scale can be seen in Fig. 8.37. The prediction is quite good. One large difference is the measurement in bollard pull. This could depend on one of the model tests. Recall that the Wageningen Series is based on model tests. One of the model tests could have been performed in a too small basin, resulting in that a too small amount of water could be sucked in the bollard pull condition, c.f. section 8.3. It should be noted that CPP1 is a very Wageningen similar design. Note that it is hard to accurately measure bollard pull characteristics in a model test.

The small difference for the other points probably lies within the larger hub; hub ratio of CPP1 is 25.6% and hub ratio of a Wageningen propeller is 18%. A larger hub gives lower K_T, but also K_Q, and in combination results in a slightly lower efficiency [26]

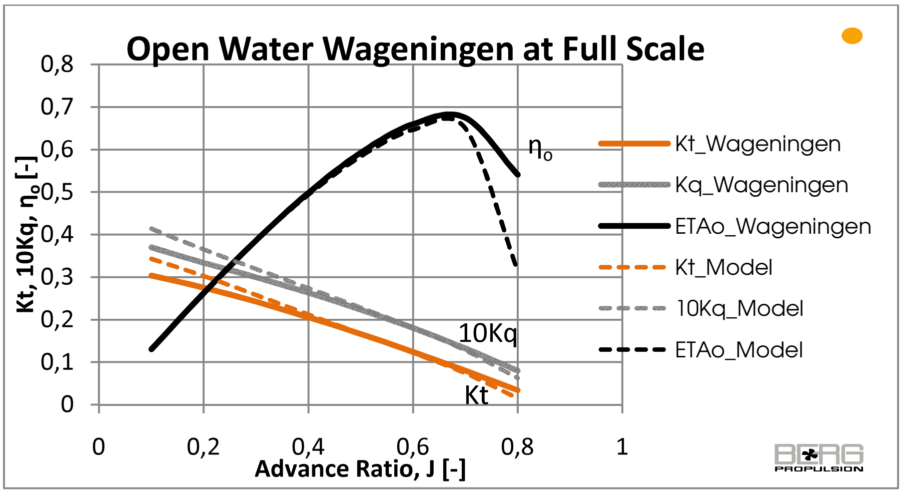

Fig. 8.37: The open water chart predicted by the Wageningen series compared to model test results scaled to full scale for CPP1

The results from the boundary element method at model scale compared to the model test results can be seen in Fig. 8.38. This validates the automated viscous correction method, see section 7.4. The correction seems to follow the built in correction from PROCAL if Fig. 8.38 is compared to Fig. 8.35.

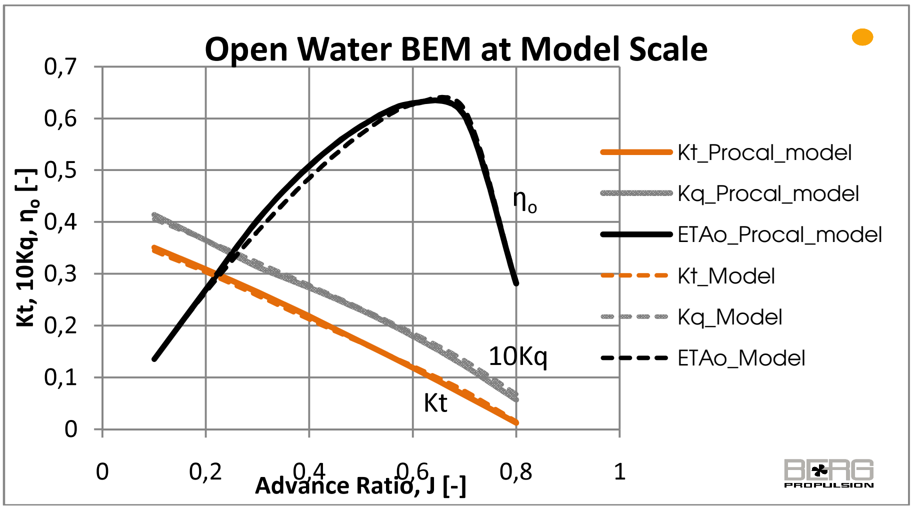

Fig. 8.38: The open water chart predicted by the boundary element method in model scale compared to the model test results for CPP1

8.3 Open Water Results from CPP2

This results section discusses and shows the results of CPP2. First the validity of the boundary element method and CFD setups are discussed. After this the predictions from CFD, boundary element method, lifting line method and Wageningen Series are compared to model test results and discussed. Finally, results from PROCAL predicted in model scale compared to model test results are shown to validate the viscous correction script.

The averaged y^+ values at the blades for CPP1 from the open water prediction can be seen in Table 8.7. As can be seen, the y^+ values are reasonable and large enough to yield reliable results with wall functions.

Table 8.7: The averaged y^+ values at the blades for CPP2 from the open water prediction.

J	**0.0726**	**0.2178**	**0.3636**	**0.5103**	**0.6531**	**0.7988**	**0.9461**
y^+ OW Mesh	148	146	146	148	150	151	155

The axial velocity field at J=0.5103 is visualized in Fig. 8.41. As can be seen it looks symmetrical and the velocity distribution is intuitive.

The PHIW and F_x distributions of CPP2 at $0.5J_{\eta_{Max}}$ in the PROCAL open water prediction can be seen in Fig. 8.39. As can be seen, a small knuckle in the F_x distribution appears. This is a result of the high unloading at the uppermost radial sections of CPP2. Experience says that this should have a small impact on the results.

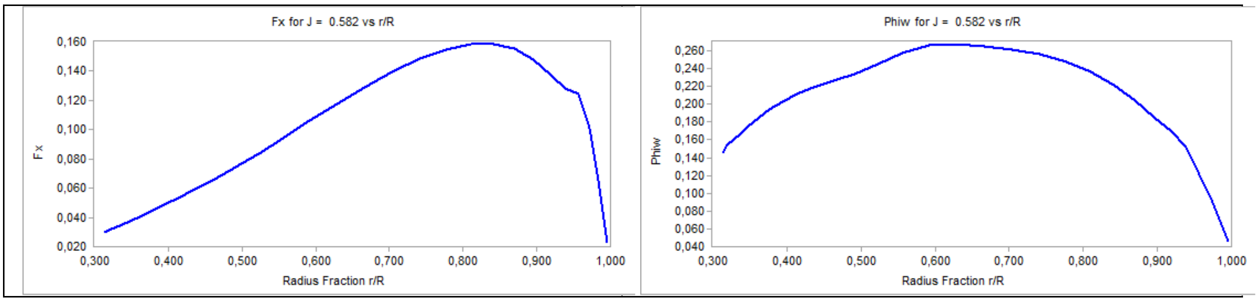

Fig. 8.39: F_x distribution to the left and PHIW to the right at $0.5J_{\eta_{Max}}$ for CPP2

The results from CFD at full scale compared to the model test results can be seen in Fig. 8.40.

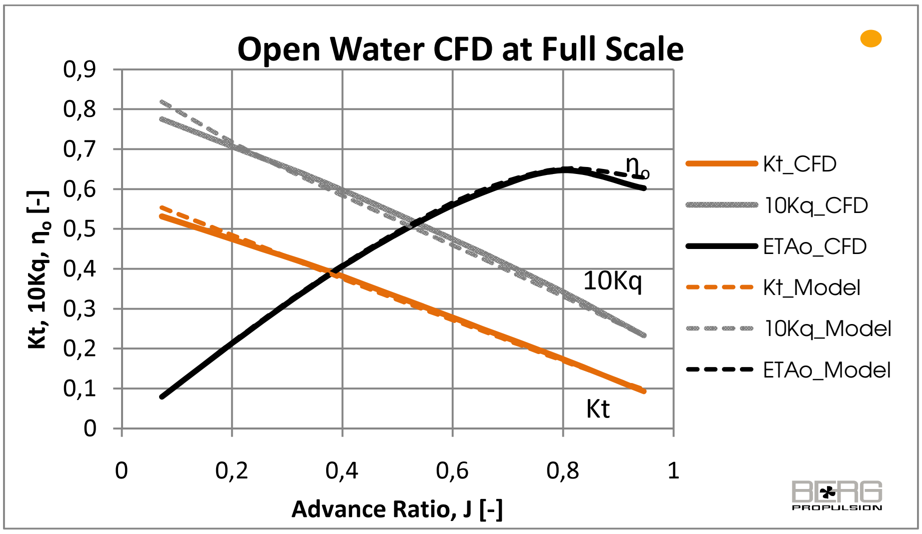

Fig. 8.40: The open water chart predicted by CFD in full scale compared to the model test results scaled to full scale for CPP2

The results are very good except for in bollard pull, as noted for CPP1, and the last point after $J_{\eta_{Max}}$, as noted for both the SMP'11 propeller and CPP1. The problem in bollard pull originates in the domain size. When the domain size was the same as for the other measuring points, i.e. J=0.21278 to J=0.9461, the solution wouldn't converge. The final axial velocity field after several thousand iterations look as in Fig. 8.42

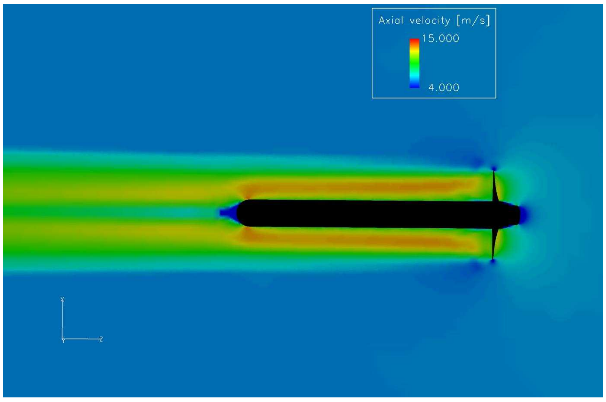

Fig. 8.41: Axial velocity field for CPP2 at J=0.5103

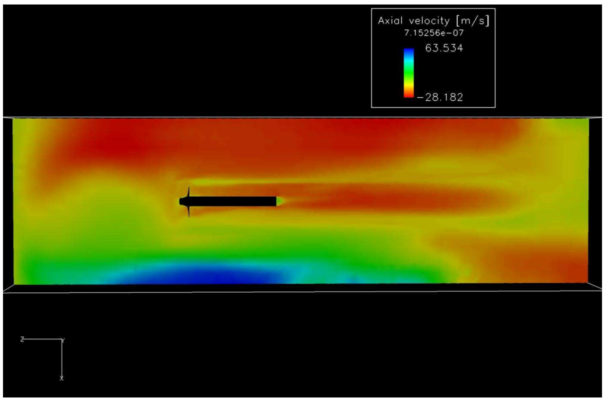

Fig. 8.42: The axial velocity field of an unconverged bollard pull solution of CPP2. Note the unsymmetrical shape and the unrealistic velocities.

The velocity field is unsymmetrical and the velocities indicate a swirling motion in the flow. The velocity on negative x-coordinates has opposite sign to the velocity on positive x-coordinates. (Note that x is in a lateral direction and z is in the axial direction) This is exactly the problem; to operate in bollard pull, the propeller needs a large amount of water to suck in. Since the domain is too small to provide enough water upstream the propeller, it tries to suck water from the rest of the domain, and hence the swirling motion. The remedy was, as mentioned, to significantly increase the size of the domain. This resulted in a more realistic velocity field, see Fig. 8.43.

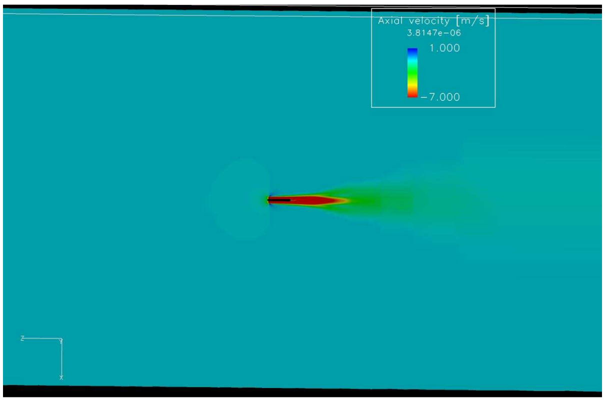

Fig. 8.43: The axial velocity field of a bollard pull solution with increased domain size. Note the large region of water sucked into the propeller

As can be seen, the velocity field looks much more intuitive. The difference in K_Q from the prediction compared to the model test could depend on that the velocity is very low in bollard pull. K_Q is depending on the viscous forces to a large extent, and at low velocities the viscous forces are even more pronounced. Since a lot of flow assumptions are made on the viscous part, a viscous dominated flow might be incorrectly predicted.

The results from the boundary element method at full scale compared to the model test results can be seen in Fig. 8.44. The results are again very accurate. It should be noted that K_Q is slightly over predicted all the way. K_T is slightly under predicted until J=0.4 and then slightly over predicted. The open water characteristics after $J_{\eta Max}$ is well predicted.

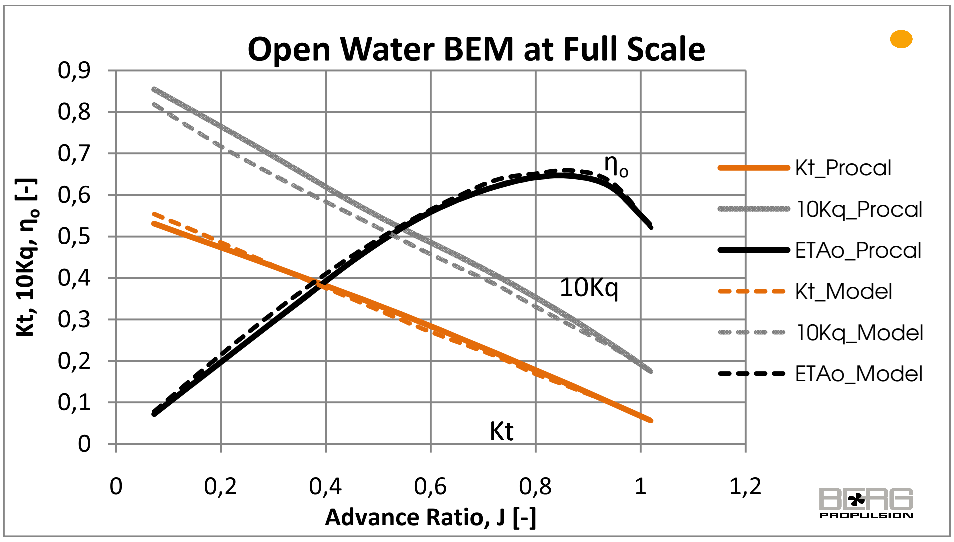

Fig. 8.44: The open water chart predicted by the boundary element method compared to model test results scaled to full scale for CPP2

The results from the lifting line method compared to the model test results scaled to full scale for CPP2 can be seen in Fig. 8.45. The difference is significant. This most probably depends on the high skew of CPP2; the skew is 40°, which is twice as much as the lifting line method should be able to handle.

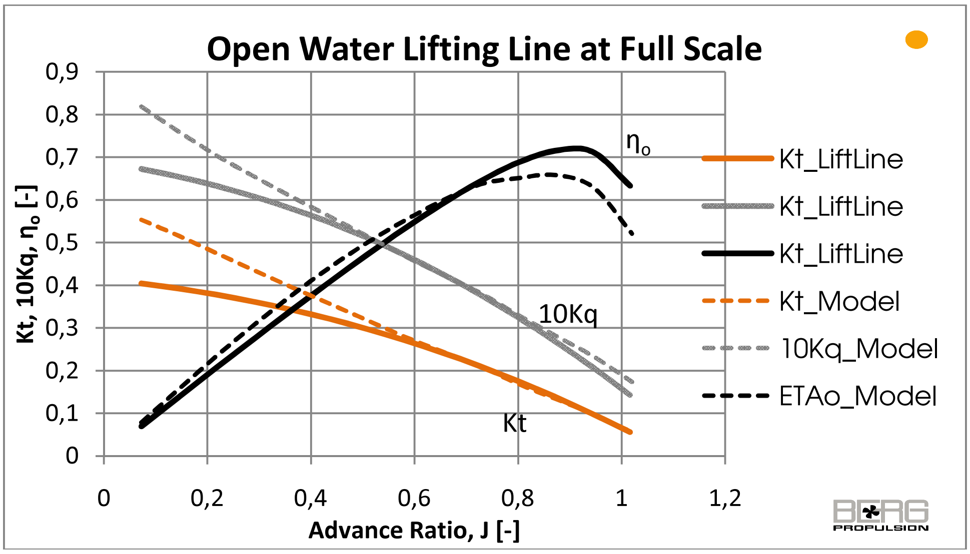

Fig. 8.45: The open water chart predicted by the lifting line method compared to model test results scaled to full scale for CPP2

The results from the Wageningen series compared to the model test results scaled to full scale can be seen in Fig. 8.46. These results suffer from the same problem in bollard pull as for CPP1. The efficiency is over predicted after the design point as an effect of an under predicted K_Q. It should be noted that CPP2 is very different from a Wageningen propeller design.

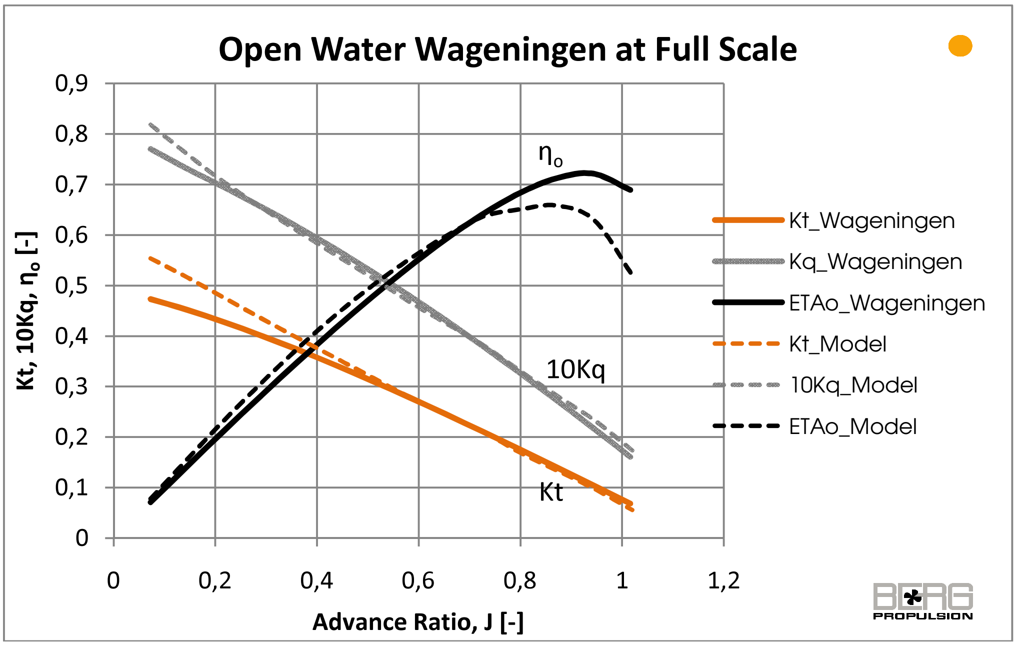

Fig. 8.46: The open water chart predicted by the Wageningen series compared to model test results scaled to full scale for CPP2

The results from the boundary element method at model scale compared to the model test results can be seen in Fig. 8.47. These results do again confirm the validity in the automated viscous correction method in the same way as for CPP1, c.f. Fig. 8.44.

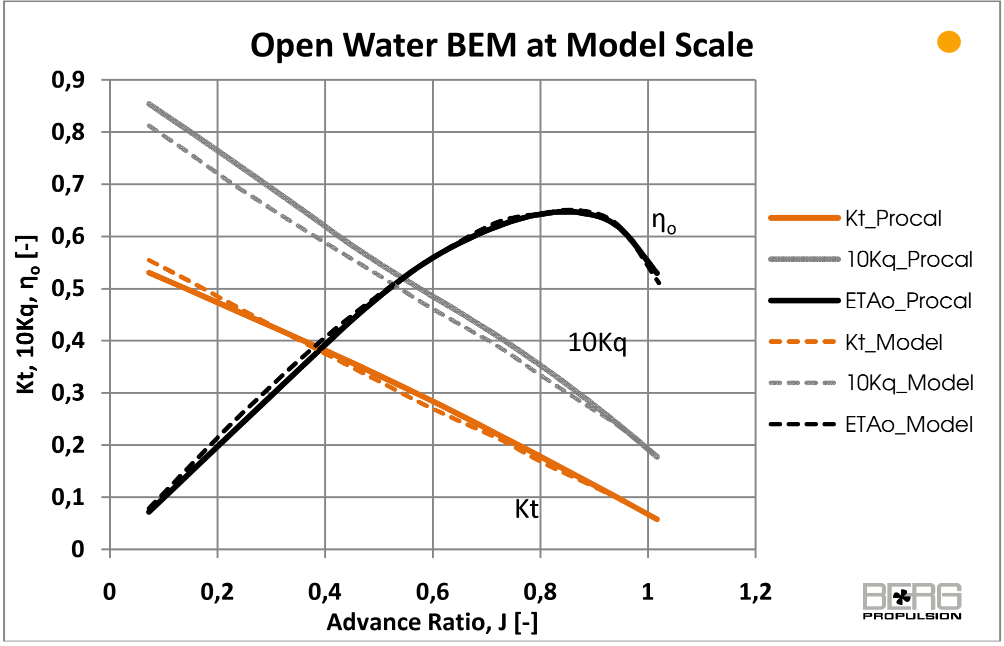

Fig. 8.47: The open water chart predicted by the boundary element method in model scale compared to the model test results for CPP2

8.4 The four Methods in Comparison

This section compares the four open water prediction methods between them based on the results presented in section 8.1 to section 8.3.

An overlay plot of all the four methods with the prediction of K_T plotted against J for all propellers can be seen in Fig. 8.48. As can be seen, CFD is closest to the model test results. The boundary element method (BEM) is quite close as well. This is valid for all three propellers. For the SMP'11 propeller, the lifting line method (LL) is over predicted and the Wageningen Series (WS) is under predicted. For CPP1 and CPP2 both WS and LL are under predicted. The under prediction of them is most significant for CPP2.

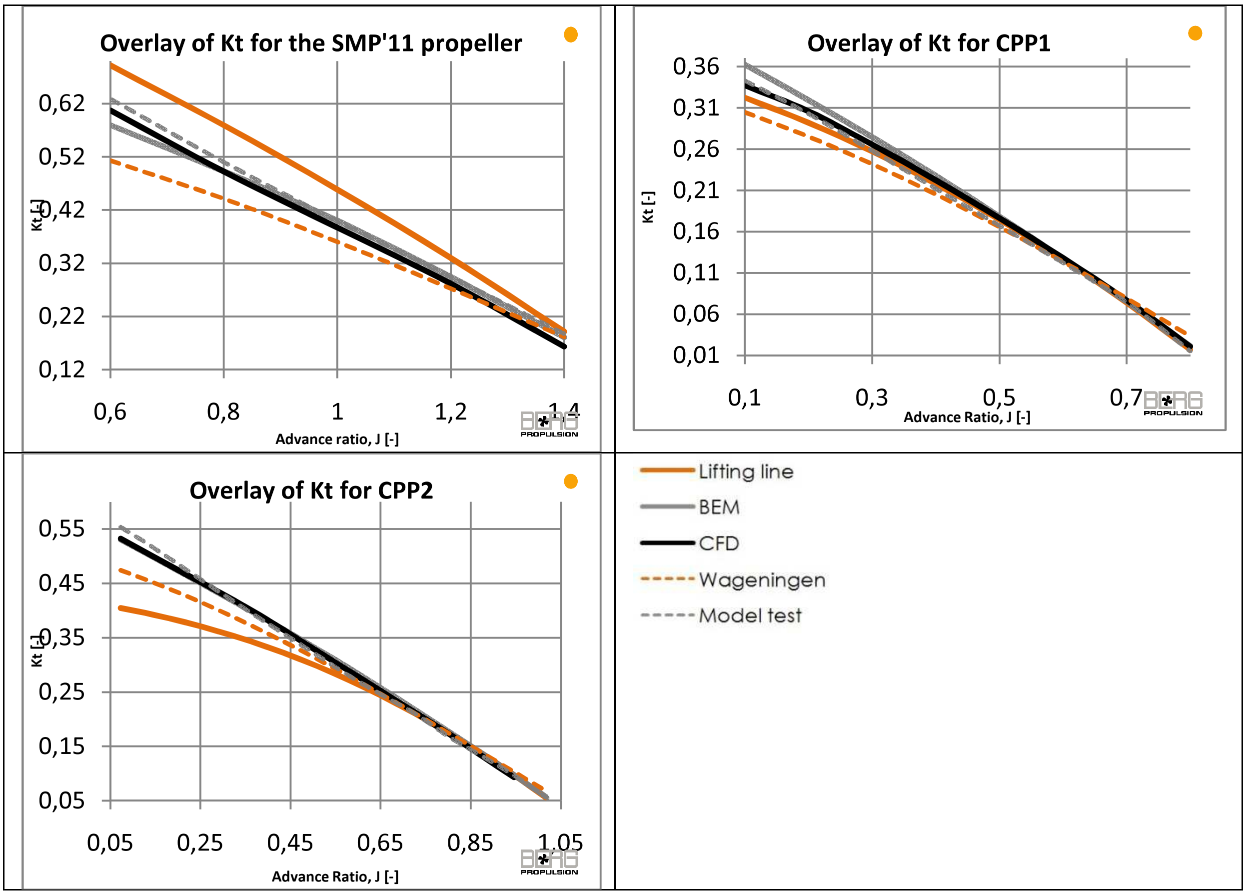

Fig. 8.48: An overlay plot of K_T for all the four prediction methods

An overlay plot of all the four methods with the prediction of $10K_Q$ plotted against J for all propellers can be seen in Fig. 8.49. Again it is noted that CFD gives the most accurate results for all propellers. BEM slightly over predicts for all cases. LL is highly over predicted for SMP'11, quite good for CPP1 and under predicted for CPP2. WS is really good for CPP1 and CPP2 and highly under predicted for SMP'11.

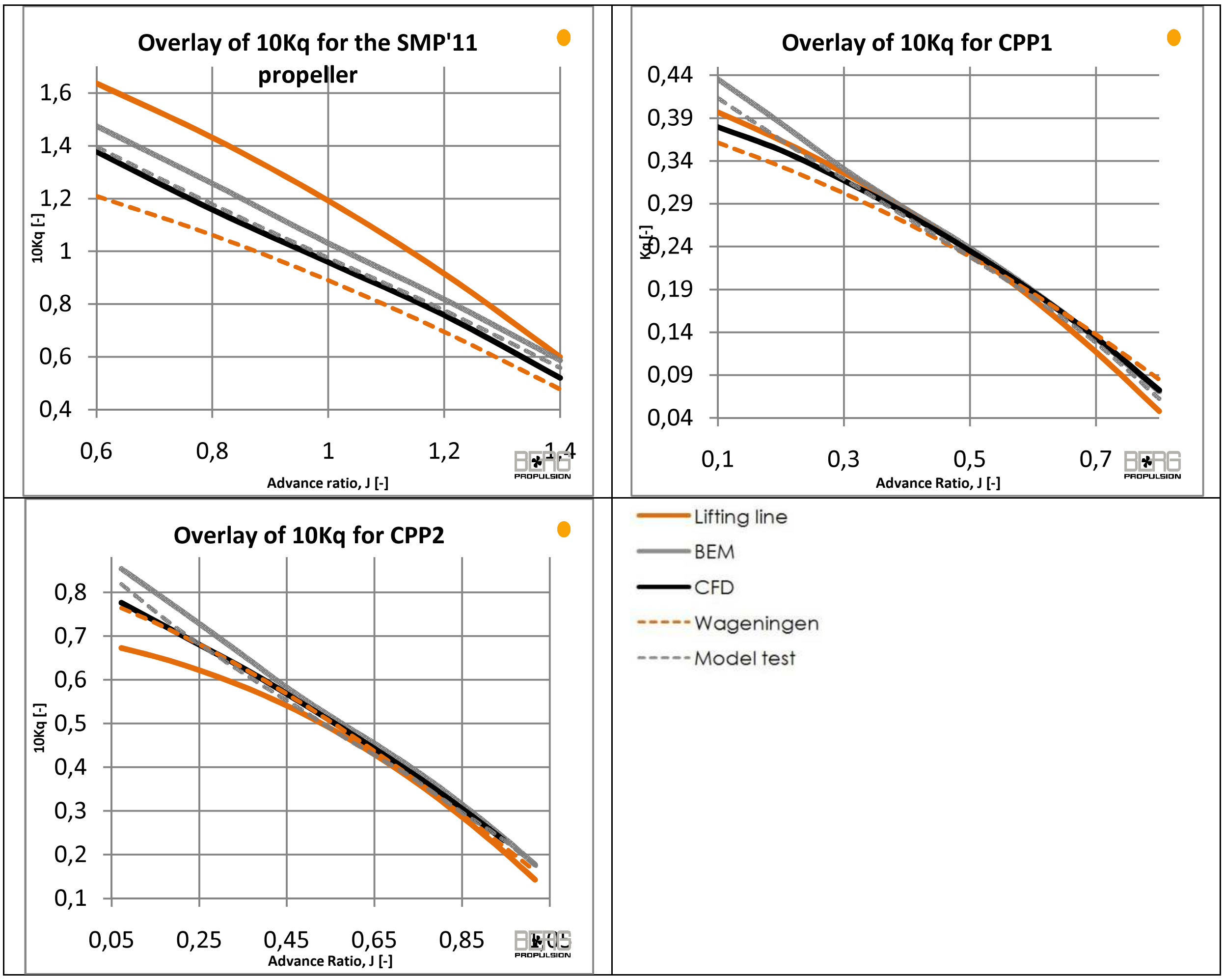

Fig. 8.49: An overlay plot of $\mathbf{10K_Q}$ for all the four prediction methods

An overlay plot of all the four methods with the prediction of η_o plotted against J for all propellers can be seen in Fig. 8.50. Here all methods are quite accurate. It should be noted that $J_{\eta_{Max}}$ is predicted to appear later in LL for all propellers, and a higher maximum efficiency is suggested. This is also true in WS for CPP2.

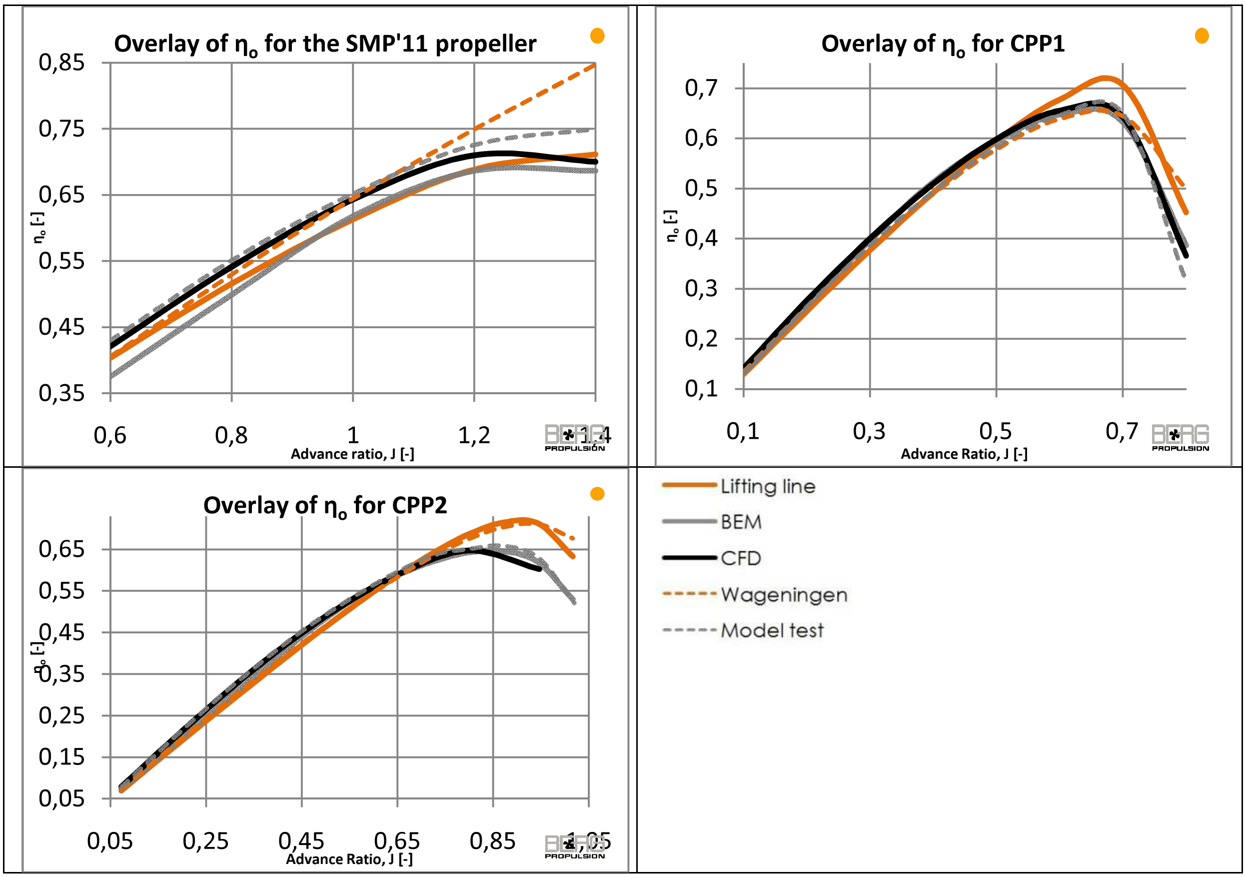

Fig. 8.50: An overlay plot of $\boldsymbol{\eta_o}$ for all the four prediction methods

The CFD method applied in OpenFOAM is very accurate regarding the open water predictions. The only points differing from the model test results were in bollard pull and after $J_{\eta Max}$. It should be noted that OpenFOAM can be used for many other applications than just predicting the open water characteristics, as seen in the SMP’11 results section. A velocity field could be measured with accurate results as an example. It is also always possible to see why the results differ, e.g. the physical explanation of the separation after $J_{\eta Max}$ in section 8.1.1 and the reason for the dissolved tip vortex at x/D=0.2 in section 8.1.2. The largest drawback with CFD is the computational cost. An open water chart with eight advance ratio steps takes about a week to analyse and the setup time can be quite extensive as well.

The boundary element method tool PROCAL is quite accurate. It is not as accurate as CFD in predicting open water characteristics, but it is rather close. One drawback when comparing the open water characteristics predictions is that it was not possible to in a simple way just remove the hub from the results as in the CFD computation in section 8.1.1. This is the major drawback with PROCAL compared to CFD; simulations “outside the box” are not possible. The largest benefit of PROCAL is the low computational cost; an open water chart with eight advance ratio steps takes about two minutes to get. The setup time can be rather extensive sometimes, but not in the near field of CFD.

The reason for that the CFD and BEM methods used in this thesis project was so accurate depends on that the flow was pressure driven. The exact potential flow problem for propellers modelled in PROCAL accurately predicts the pressure forces, since it is derived directly from the Navier-Stokes equations, only neglecting viscosity. The pressure was also well modelled in the CFD method. The major difference between the methods is how viscosity is handled. In

PROCAL it is analytically corrected. In OpenFOAM turbulence models were used. The turbulence models could be seen as a more accurate viscous correction.

The lifting line method program used in this project was not very accurate. For two out of three cases, the differences between the model test results were significant. There was no way to logically explain the difference in the results either. The setup time for the lifting line method was very short and the computational cost was extremely low, on the other hand.

When using the Wageningen method, the computational cost and setup time was extremely low. The results were rather accurate when the propeller was similar to a Wageningen design, but less accurate otherwise. This deficiency could be solved using different corrections for e.g. camber induced pitch, hub ratio and skew.

8.5 The Final Performance of the CFD Automation

This section describes what the CFD-automation script performs when it is used. For a more detailed description of the code, see section 4.4. First a script generated blade from solid works on .IGS-format is provided, see Fig. 8.51.

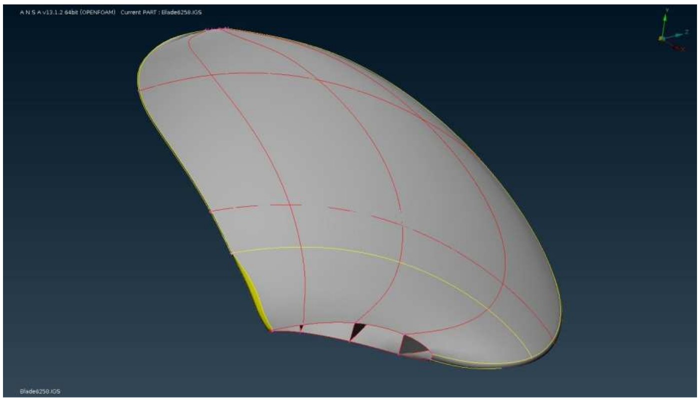

Fig. 8.51: The unclean blade as generated from SW.

The cleanBladeUntilPitchSetting is pushed. The domain, MRF-zone, shaft, hub and blades are fixed. The blade is ready for pitch setting, see Fig. 8.52 for the result.

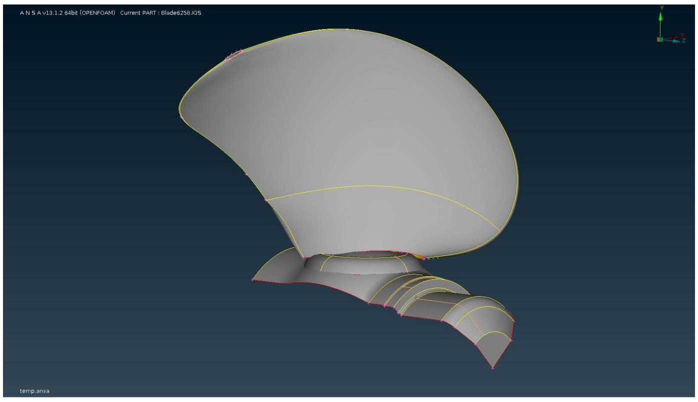

Fig. 8.52: The blade cleaned until pitch setting

The pitch is adjusted manually, perhaps following the procedure in section 4.5. The blade should be intersected to the blade foot and the blade foot to the hub manually as well. As a suggestion the procedure in Appendix D should be used for this. Fig. 8.53 shows a blade intersected to blade foot and hub.

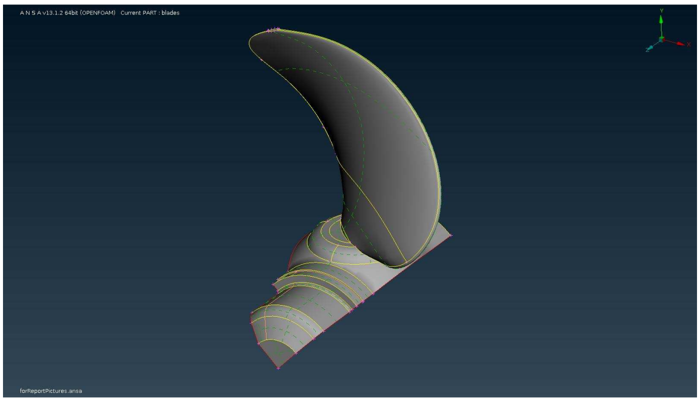

Fig. 8.53: The pitch adjusted blade intersected with the hub.

The surfaceMesh button is pushed. Everything might be surface meshed. The mesh quality could become poor or unmeshed in a few regions. Fig. 8.54 shows the result.

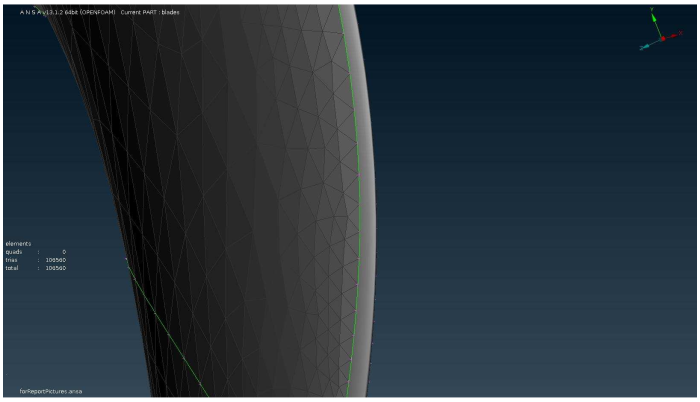

Fig. 8.54: Surface mesh with unmeshed leading edge macro.

The obvious meshing problems or unsatisfactory geometrical descriptions should be fixed manually. If the problem is at leading edge, the recommended procedure in Appendix C might be handy. Fig. 8.55 shows a finished surface mesh.

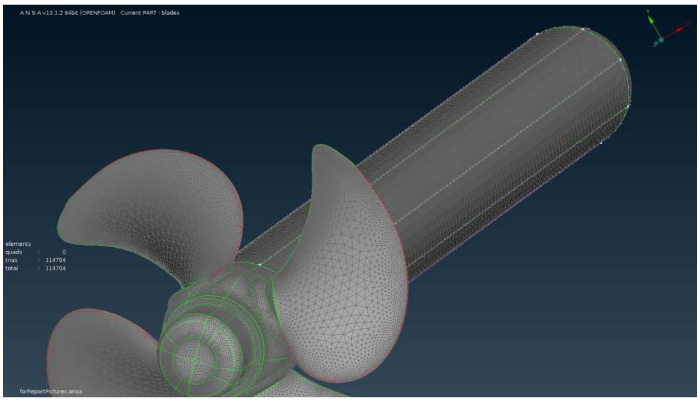

Fig. 8.55: The completed surface mesh, ready for volume mesh and layers

The layersAndVolumeMesh-button is pushed. The last steps of automatic surface mesh cleanup, layer generation and volume meshing is performed. The completed mesh can be seen in Fig. 8.56

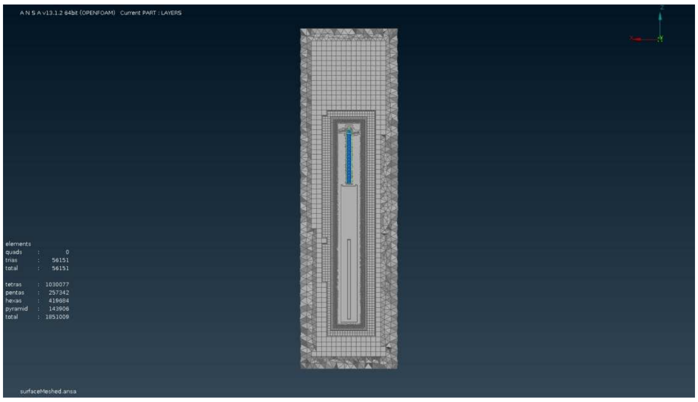

```
A N S A v13.1.2 64bit (OPENFOAM)   Current PART : LAYERS

elements
quads     :        0
trias     :    56151
total     :    56151

tetras    :  1030077
pentas    :   257342
hexas     :   419684
pyramid   :   143906
total     :  1851009

surfaceMeshed.ansa
```

Fig. 8.56: The completed volume mesh

The result could be outputted to e.g. the OpenFOAM template-folder containing the most common boundary conditions. If no pitch setting is needed and the user is familiar with the intersect function in ANSA and no big problems occur when surface meshing is performed, the estimated working time using the script is 5-10 minutes. The whole mesh is completed within 15-25 minutes.

8.6 The Final Performance of the Boundary Element Automation

The propeller design is finished in the design sheet. The user wants to perform a boundary element method analysis. In the PROCAL sheet, the buttons Export Geometry and Export Control File are clicked. PROCAL should be started and file-new-add existing file should be chosen. The User goes to the propeller dialog and hit mesh now and after that output-export. After this it is only to click “procal analysis” and wait. When the analysis is done, the load PROCAL results button has to be clicked from the openWaterResults.

If a full open water chart is wanted, the J_{Max}, J_{Min} and J_{step}values should be set. Then the Export OW Control button should be clicked. The exact same procedure as in the paragraph above should be repeated after this. The complete open water table is tabulated below the “Get PROCAL Results”-button when pressed, see Fig. 8.57.

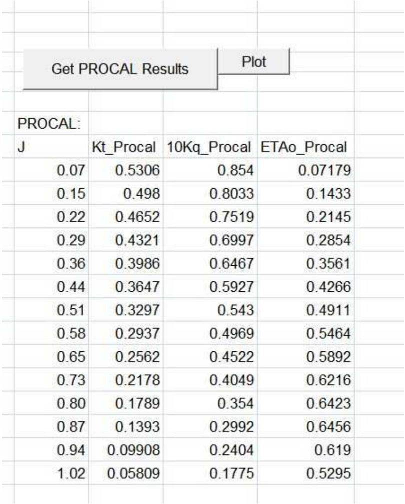

PROCAL:

J	Kt_Procal	10Kq_Procal	ETAo_Procal
0.07	0.5306	0.854	0.07179
0.15	0.498	0.8033	0.1433
0.22	0.4652	0.7519	0.2145
0.29	0.4321	0.6997	0.2854
0.36	0.3986	0.6467	0.3561
0.44	0.3647	0.5927	0.4266
0.51	0.3297	0.543	0.4911
0.58	0.2937	0.4969	0.5464
0.65	0.2562	0.4522	0.5892
0.73	0.2178	0.4049	0.6216
0.80	0.1789	0.354	0.6423
0.87	0.1393	0.2992	0.6456
0.94	0.09908	0.2404	0.619
1.02	0.05809	0.1775	0.5295

Fig. 8.57: The generated table after pushing the Get PROCAL Results-button

If the user wants to plot it, the button plot should be hit. An open water chart is generated, see Fig. 8.58.

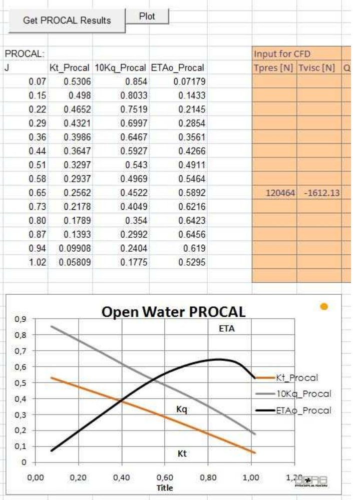

PROCAL:				Input for CFD		
J	Kt_Procal	10Kq_Procal	ETAo_Procal	Tpres [N]	Tvisc [N]	Q
0.07	0.5306	0.854	0.07179			
0.15	0.498	0.8033	0.1433			
0.22	0.4652	0.7519	0.2145			
0.29	0.4321	0.6997	0.2854			
0.36	0.3986	0.6467	0.3561			
0.44	0.3647	0.5927	0.4266			
0.51	0.3297	0.543	0.4911			
0.58	0.2937	0.4969	0.5464			
0.65	0.2562	0.4522	0.5892	120464	-1612.13	
0.73	0.2178	0.4049	0.6216			
0.80	0.1789	0.354	0.6423			
0.87	0.1393	0.2992	0.6456			
0.94	0.09908	0.2404	0.619			
1.02	0.05809	0.1775	0.5295			

Fig. 8.58: The generated open water chart after pressing the plot-button

It should be noted that the mesh performed by the auto generated control files are just good guesses. The results still need to be reviewed in PROCAL. The radial axial force and wake panel distributions should be studied as well as the Kutta condition.

8.7 The Final Performance of the Lift Line Automation

The user has completed the propeller design. In the openWaterResults sheet, the wanted minimum, maximum and step of advance ratio, J, is entered. The lift line workbook is opened and the OW calculation button is pressed. The Get Lift Line Results button is pressed in the design workbook and the results are loaded to the table in the same way as for the PROCAL results. If a plot of the results is wanted, the plot button is pressed and an open water chart appears on the screen.

8.8 The Final Performance of the Wageningen Automation

After insertion of the propeller design in the design workbook, J_{Max}, J_{Min} and J_{step} is inserted in the openWaterResults sheet. The button Get Wageningen Results is pressed. The model test as predicted by Wageningen appears in the table below the button. If the results should be scaled to full scale, the ITTC-78 button is pressed. A table with the full scale Wageningen prediction is outputted below the button.

If any of the results should be plotted, the plot button besides the table generating buttons should be pressed. An open water chart is generated. The final interface for Wageningen, Lift Line, PROCAL, model test and viscous scaling can be seen in Fig. 8.59

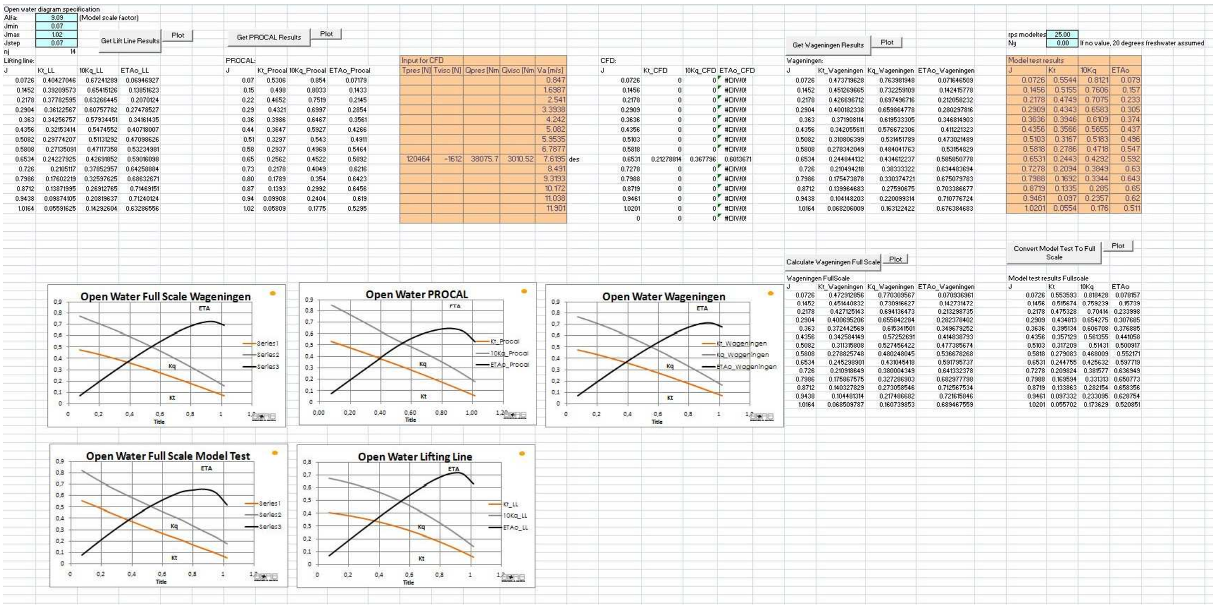

Open water diagram specification

Alfa:	9.09	(Model scale factor)
Jmin	0.07	
Jmax	1.02	
Jstep	0.07	
nj	14	

rps modeltes 25.00
Ny 0.00 If no value, 20 degrees freshwater assumed

Lifting line:

J	Kt_LL	10Kq_LL	ETAo_LL
0.0726	0.40427046	0.67241289	0.06946927
0.1452	0.39209573	0.65415126	0.13851623
0.2178	0.37782595	0.63266445	0.2070124
0.2904	0.36122567	0.60757782	0.27478527
0.363	0.34256757	0.57934451	0.34161435
0.4356	0.32153414	0.5474552	0.40718007
0.5082	0.29774207	0.51131292	0.47098626
0.5808	0.27135091	0.47117358	0.53234981
0.6534	0.24227925	0.42691852	0.59016098
0.726	0.2105117	0.37852957	0.64258884
0.7986	0.17602219	0.32597625	0.68632671
0.8712	0.13871995	0.26912765	0.71469151
0.9438	0.09874105	0.20819637	0.71240124
1.0164	0.05591625	0.14292604	0.63286556

PROCAL:

J	Kt_Procal	10Kq_Procal	ETAo_Procal
0.07	0.5306	0.854	0.07179
0.15	0.498	0.8033	0.1433
0.22	0.4652	0.7519	0.2145
0.29	0.4321	0.6997	0.2854
0.36	0.3986	0.6467	0.3561
0.44	0.3647	0.5927	0.4266
0.51	0.3297	0.543	0.4911
0.58	0.2937	0.4969	0.5464
0.65	0.2562	0.4522	0.5892
0.73	0.2178	0.4049	0.6216
0.80	0.1789	0.354	0.6423
0.87	0.1393	0.2992	0.6456
0.94	0.09908	0.2404	0.619
1.02	0.05809	0.1775	0.5295

Input for CFD

Tpres [N]	Tvisc [N]	Qpres [Nm	Qvisc [Nm	Va [m/s]	
				0.847	
				1.6987	
				2.541	
				3.3938	
				4.242	
				5.082	
				5.9535	
				6.7877	
120464	-1612	38075.7	3010.52	7.6195	des
				8.491	
				9.3193	
				10.172	
				11.038	
				11.901	

CFD:

J	Kt_CFD	10Kq_CFD	ETAo_CFD
0.0726	0	0	#DIV/0!
0.1456	0	0	#DIV/0!
0.2178	0	0	#DIV/0!
0.2909	0	0	#DIV/0!
0.3636	0	0	#DIV/0!
0.4356	0	0	#DIV/0!
0.5103	0	0	#DIV/0!
0.5818	0	0	#DIV/0!
0.6531	0.21278814	0.367796	0.6013671
0.7278	0	0	#DIV/0!
0.7988	0	0	#DIV/0!
0.8719	0	0	#DIV/0!
0.9461	0	0	#DIV/0!
1.0201	0	0	#DIV/0!
0	0	0	#DIV/0!

Wageningen:

J	Kt_Wageningen	Kq_Wageningen	ETAo_Wageningen
0.0726	0.473719628	0.763981948	0.071646509
0.1452	0.451269665	0.732259109	0.142415778
0.2178	0.426696712	0.697496716	0.212058232
0.2904	0.400182338	0.659864778	0.280297816
0.363	0.371908114	0.619533305	0.346814903
0.4356	0.342055611	0.576672306	0.411221323
0.5082	0.310806399	0.531451789	0.473021489
0.5808	0.278342049	0.484041763	0.53154829
0.6534	0.244844132	0.434612237	0.585850778
0.726	0.210494218	0.38333322	0.634483694
0.7986	0.175473878	0.330374721	0.675079783
0.8712	0.139964683	0.27590675	0.703386677
0.9438	0.104148203	0.220099314	0.710776724
1.0164	0.068206009	0.163122422	0.676384683

Model test results

J	Kt	10Kq	ETAo
0.0726	0.5544	0.8121	0.079
0.1456	0.5155	0.7606	0.157
0.2178	0.4749	0.7075	0.233
0.2909	0.4343	0.6583	0.305
0.3636	0.3946	0.6109	0.374
0.4356	0.3566	0.5655	0.437
0.5103	0.3167	0.5183	0.496
0.5818	0.2786	0.4718	0.547
0.6531	0.2443	0.4292	0.592
0.7278	0.2094	0.3849	0.63
0.7988	0.1692	0.3344	0.643
0.8719	0.1335	0.285	0.65
0.9461	0.097	0.2357	0.62
1.0201	0.0554	0.176	0.511

Wageningen FullScale

J	Kt_Wageningen	Kq_Wageningen	ETAo_Wageningen
0.0726	0.472912856	0.770309567	0.070936961
0.1452	0.451440832	0.730916627	0.142731472
0.2178	0.427125143	0.694136473	0.213298735
0.2904	0.400695206	0.655842284	0.282378402
0.363	0.372442569	0.615341501	0.349679252
0.4356	0.342584149	0.57252691	0.414838793
0.5082	0.311315808	0.527456422	0.477385674
0.5808	0.278825748	0.480248045	0.536678268
0.6534	0.245298901	0.431045418	0.591795737
0.726	0.210918649	0.380004349	0.641332378
0.7986	0.175867575	0.327286903	0.682977798
0.8712	0.140327829	0.273058546	0.712567534
0.9438	0.104481314	0.217486682	0.721615846
1.0164	0.068509787	0.160739853	0.689467559

Model test results Fullscale

J	Kt	10Kq	ETAo
0.0726	0.553593	0.818428	0.078157
0.1456	0.515674	0.759239	0.15739
0.2178	0.475328	0.70414	0.233998
0.2909	0.434813	0.654275	0.307685
0.3636	0.395134	0.606708	0.376885
0.4356	0.357129	0.561355	0.441058
0.5103	0.317209	0.51431	0.500917
0.5818	0.279083	0.468009	0.552171
0.6531	0.244755	0.425632	0.597719
0.7278	0.209824	0.381577	0.636949
0.7988	0.169594	0.331313	0.650773
0.8719	0.133863	0.282154	0.658356
0.9461	0.097332	0.233095	0.628754
1.0201	0.055702	0.173629	0.520851

Fig. 8.59: The complete interface for Wageningen, Lift Line, PROCAL, model test and viscous scaling.

(This page is intentionally left blank)

9 Conclusions and Future Work

Firstly the conclusions of this thesis work are listed method for method in this section. If the conclusion only regards the specific method used in the thesis work, this is explicitly mentioned after the conclusion. Finally recommendations regarding future work are presented.

The main conclusions that can be drawn about the CFD-method are that the CFD-method:

- is the most accurate among the compared methods regarding open water characteristics predictions, but has the very highest computational cost
- might have long setup times
- can accurately predict the velocity field downstream the propeller disc if the mesh resolution is high enough
- is good for "out of the box" predictions, such as predicting the characteristics from an odd design or removing the hub from the force results
- gives the possibility to visualize problem areas, such as separation zones
- has problems with predicting bollard pull and efficiency after $J_{\eta_{Max}}$ (assuming that the model test measurements are correct and that the viscous corrections apply in bollard pull, which might be an incorrect assumption). This conclusion only regards the method applied in this thesis.
- could be automated regarding pre-processing for open water predictions, leaving only two manual moments; intersect the blade to the blade foot and hub and check the surface mesh, saving at least five hours of manual work and guaranteeing consequent setups. This conclusion only regards the method applied in this thesis.

The main conclusions that can be drawn from the boundary element method are that the boundary element method:

- is almost as accurate as CFD regarding open water characteristics predictions and has significantly lower computational cost
- has much shorter setup time than CFD
- tends to over predict sheet cavitation at the leading edge at a high load. This conclusion only regards the method applied in this thesis.
- is a good tool for early propeller performance predictions
- could be automated both in regard to pre- and post-processing, saving some time and, more importantly, reducing the risk of setup errors. This conclusion only regards the method applied in this thesis.

The main conclusions that can be drawn from the lifting line method applied in this thesis are that the lifting line method:

- was not very reliable regarding open water characteristics predictions.
- has a very short setup time
- has inaccuracies that do not solely depend on the amount of skew
- has no relationship in whether the method will predict a too light or too heavy propeller
- tends to predict a later $J_{\eta_{Max}}$ and a higher η_{Max}
- could be automated both in regard to pre- and post-processing, which saves some time

Note that all the above conclusions regarding the lifting line method might only be true for the method used in this thesis.

The main conclusions that can be drawn from the Wageningen Series are that the Wageningen Series:

- is accurate for Wageningen similar propeller designs.
- should be corrected if the propeller designs are dissimilar from Wageningen designs
- has an extremely low setup time
- does not need a complete geometry; only pitch, blade area ratio, number of blades and advance ratio are needed to make a prediction
- is very useful at an early design stage due to the low number of inputs
- is useful to get an indication of whether the PROCAL/CFD results are correct
- could be automated both in regard to pre- and post-processing, which saves some time.

The final recommendations of how the tools and specific methods studied in this thesis should be used are that:

- the Wageningen Series should be used for predictions at a very early design stage and to check whether the other predictions are within reasonable values
- the boundary element method should be used when the propeller design is finished and more reliable open water predictions are needed
- the CFD method should be used when more odd designs should be tested or when exact guarantees of open water performance should be leaved.

There are some aspects that should be performed as future work after this thesis. The volume mesh close to the propeller disc in the velocity field measurement should be improved. This could solve the convergence issue at x/D=0.1 and resolve the vortex at x/D=0.2. To get better results in bollard pull and after $J_{\eta_{Max}}$, the wall could be entirely resolved. It would also be interesting to perform an analysis with a fully hexahedral mesh to improve the results. A comparison between the MRF results and results with a sliding mesh would also give better understanding in the level of approximation. The script should be rewritten to handle the periodic boundary condition as soon as the bug in ANSA is fixed. This allows as many more times higher cell resolution as the number of blades of the propeller. It is a qualified approximation as well; the analysis is steady and hence the results won’t be affected by the symmetry assumption.

The cavitation analysis should be tested with a minimum pressure detachment mode in PROCAL. This could solve the issue with the missed blade root and sheet cavitation on the trailing edge. It would also be valuable if a two-phase modeling of the cavitation computation was performed in CFD to get a comparison between the methods in that respect.

The lifting line method should be tested with another software and a deeper investigation should be performed to understand why the results are so unreliable. The Wageningen Series should also be tested with corrections applied for the propellers to get a better insight in the capabilities of the tool.

10 References

[1] Wageningen propeller series program - v2003_1 – A program containing the Wageningen charts

[2] PROCAL v 2.0.2.0 – A boundary element method tool with GUI, post processor, grid generator and solver for the direct formulation of the potential flow problem for propeller. It can also solve for cavitation using the Morino formulation

[3] LiftLine 0.412ges – A lifting line method tool made as an Excel sheet with macros containing the lift line code.

[4] OpenFOAM v1.6 –An open source CFD toolbox. “It can solve anything from complex fluid flows involving chemical reactions, turbulence and heat transfer, to solid dynamics and electromagnetics.” (quoted: http://www.openfoam.com/)

[5] Davidsson L., an Introduction to Turbulence Models. Göteborg, Sweden, Chalmers University of Technology, Department of Thermo and Fluid Dynamics. November 2003.

[6] Davidsson L., Numerical Methods for Turbulent Flow. Göteborg, Sweden, Chalmers University of Technology, Department of Thermo and Fluid Dynamics. January 7, 2005.

[7] Versteeg H.K., Malalasekera W., An Introduction to Computational Fluid Dynamics – The Finite Volume Method 2nd ed., Malaysia 2007

[8] OpenFOAM Wikipedia: http://openfoamwiki.net/index.php/See_the_MRF_development

[9] Volker Bertram, “Practical Ship Hydrodynamics”, Madras, 2000

[10] Bosschers J., PROCAL v2.0 Theory Manual, MARIN, Report 20834-7-RD, Wageningen, June 2009

[11] Bosschers J., PROCAL v2.0 User’s Guide, MARIN, Report 20834-6-RD, Wageningen, June 2009

[12] ANSA v13.1.2 – A meshing program for CFD and FEM including CAD tools.

[13] Andersson, B. et al, Computational Fluid Dynamics for Chemical Engineers 6th ed, Göteborg, March 2010

[14] ANSA v13.1.x Online Reference Manual, BETA CAE Systems S.A., January 2011

[15] Hally D., Generation of Panels for CRS PROCAL, DRDC Atlantic, External Client Report, Canada, October 2004

[16] PROCAL discussion forum website: http://wiki.crships.org/index.php/Special:Search?search=idiots&go=Go

[17] Kupier G., The Wageningen Propeller Series, Netherlands, May 1992

[18] Dyne G., Bark G., Ship Propulsion, Chalmers University of Technology division of hydromechanics, Göteborg 2005

[19] SMP’11 Workshop case 2 general description: http://www.sva-potsdam.de/assets/images/smp11/case2_PPTC_geometry.pdf

[20] SMP’11 Workshop case 2 open water test case: http://www.sva-potsdam.de/assets/images/smp11/case2-1_PPTC_owt.pdf

[21] SMP’11 Workshop case 2 velocity field measurement case: http://www.sva-potsdam.de/assets/images/smp11/case2-2_PPTC_vel.pdf

[22] SMP’11 Workshop case 2 cavitation tests case: http://www.sva-potsdam.de/assets/images/smp11/case2-3_PPTC_cav.pdf

[23] FieldView v12.2 – A CFD post-processing and rendering tool

[24] Nijland M., Lift-Line Beta Release User Manual, Wärtsilä Ship Power Technology, 2009

[25] White F. M., Fluid Mechanics, 5th ed., University of Rhode Island, New York 2003

[26] Klerebrant Klasson O., Huuva T., The Development of a Correction Formula from Wageningen BSeries Reference Hub Size to Any Other Hub Size, Berg Propulsion Technology AB, May 2011

[27] Visual Basic v6.5.1053 – A BASIC-based programming language linked with excel

[28] Lloyd’s Register, Procal Task 4.1e, Panelling Procedure, Department of Consultancy Services Group, Technical Investigations, Report no. 6517, 2010

[29] Magnus Pettersson, Berg Propulsion Technology AB, verbally

[30] Klerebrant Klasson O., Pettersson M., Validation study of AMG_STERN and CRS_PIF, Berg Propulsion Technology AB, September 2010